European Cells and Materials Vol. 42 2021 (pages 334-374) DOI: 10.22203/eCM.v042a22 ISSN 1473-2262

# CURRENT OSTEOMYELITIS MOUSE MODELS, A SYSTEMATIC REVIEW

C. Guarch-Pérez, M. Riool and S.A.J. Zaat*

Department of Medical Microbiology and Infection Prevention, Amsterdam UMC, University of Amsterdam, Amsterdam Institute for Infection and Immunity, Amsterdam, the Netherlands

**Abstract**

Osteomyelitis is an inflammatory bone disease caused by an infecting microorganism leading to a gradual bone loss. Due to the difficulty in studying osteomyelitis directly in patients, animal models allow researchers to investigate the pathogenesis of the infection and the development of novel prophylactic, anti-inflammatory and antimicrobial treatment strategies. This review is specifically focused on the *in vivo* mouse osteomyelitis studies available in literature. Thus, a systematic search on Web of Science and PubMed was conducted using the query "(infection) AND (mice OR mouse OR murine) AND (model OR models) AND (arthroplasty OR fracture OR (internal fixator) OR (internal fixation OR prosthesis OR implant OR osteomyelitis)". After critical assessment of the studies according to the inclusion and exclusion criteria, 135 studies were included in the detailed analysis. Based on the model characteristics, the studies were classified into five subject groups: haematogenous osteomyelitis, post-traumatic osteomyelitis, bone-implant-related infection, peri-prosthetic joint infection, fracture-related infection. In addition, the characteristics of the mice used, such as inbred strain, age or gender, the characteristics of the pathogens used, the inoculation methods, the type of anaesthesia and analgesia used during surgery and the procedures for evaluating the pathogenicity of the infecting micro-organism were described. Overall, the mouse is an excellent first step *in vivo* model to study the pathogenesis, inflammation and healing process of osteomyelitis and to evaluate novel prophylaxis and treatment strategies.

**Keywords**: Osteomyelitis, *in vivo*, model, mouse, staphylococci, bone, infection.

***Address for correspondence**: Sebastian A.J. Zaat, Department of Medical Microbiology and Infection Prevention, Amsterdam UMC, Meibergdreef 9, 1105 AZ, Amsterdam, the Netherlands.
Telephone number: +31 205664863 Email: s.a.zaat@amsterdamumc.nl



**List of Abbreviations**

| | |
|---|---|
| *A. baumannii* | *Acinetobacter baumannii* |
| AP | alkaline phosphatase |
| ATCC | American type culture collection |
| BLI | bioluminescence imaging |
| *C. acnes* | *Cutibacterium acnes* |
| *C. albicans* | *Candida albicans* |
| CCR2 | C-C chemokine receptor type 2 |
| CFU | colony-forming unit |
| Cna | collagen-binding adhesin |
| CRP | C-reactive protein |
| *E. coli* | *Escherichia coli* |
| ELISA | enzyme-linked immunosorbent assay |
| FnbA/B | fibronectin-binding proteins A and B |
| FISH | fluorescence *in situ* hybridisation |
| FLI | fluorescence imaging |
| GM | genetically modified |
| Ig | immunoglobin |
| IL | interleukin |
| IL-1R | IL 1 receptor |
| IMHC | immunohistochemistry |
| IMF | immunofluorescence |
| IVIS | *in vivo* imaging system |
| *K. pneumoniae* | *Klebsiella pneumoniae* |
| MCP | monocyte chemoattractant protein |
| MRI | magnetic resonance imaging |
| MRSA | methicillin-resistant *S. aureus* |
| NET | neutrophil extracellular trap |
| *P. aeruginosa* | *Pseudomonas aeruginosa* |
| PET | positron emission tomography |
| PINP | procollagen type I propeptide |
| PJI | peri-prosthetic joint infection |
| PMMA | polymethylmethacrylate |

| | |
|---|---|
| PMN | polymorphonuclear leukocytes |
| PNA-FISH | peptide nucleic acid fluorescent *in situ* hybridisation |
| PSM | phenol-soluble modulin |
| qRT-PCR | real-time quantitative reverse transcription PCR |
| RNA-Seq | RNA sequencing |
| *S. agalacticae* | *Streptococcus agalacticae* |
| *S. aureus* | *Staphylococcus aureus* |
| *S. epidermidis* | *Staphylococcus epidermidis* |
| SACs | *S. aureus* abscess communities |
| Sar*A* | staphylococcal accessory regulator A |
| SCV | small colony variant |
| SigB | staphylococcal sigma factor B |
| SPF | specified-pathogen free |
| SEM | scanning electron microscopy |
| T1D | type 1 diabetes |
| T2D | type 2 diabetes |
| TEM | transmission electron microscopy |
| Th1 | T helper 1 cell |
| Th2 | T helper 2 cell |
| TNF | tumour necrosis factor |
| TRAP | tartrate-resistant acid phosphatase |
| μCT | micro-computed tomography |

## Introduction

### General introduction of osteomyelitis

Osteomyelitis is an inflammatory bone disease caused by an infecting microorganism leading to a gradual bone loss (Kavanagh *et al.*, 2018). The disease can affect a localised bone section or several parts such as cortex, periosteum and even the surrounding soft tissue. These infections can be caused by a contamination through the bloodstream (known as haematogenous infections), by direct seeding of an open fracture related to trauma or surgery or by a contiguous spread from nearby tissue or a prosthetic device (Kavanagh *et al.*, 2018; Lew and Waldvogel, 2004; Zimmerli and Trampuz, 2011). In fact, the main risk factors associated with osteomyelitis are trauma, orthopaedic devices and diabetic foot infection (Berendt *et al.*, 2008).

### Pathophysiology of the disease

Osteomyelitis begins with the bacterial attachment and subsequent biofilm formation on the bone tissue and/or orthopaedic device. Biofilms consist of a community of bacteria attached to a biological or inert surface that are embedded in a matrix of exopolysaccharide, protein and extracellular DNA (Crabbé *et al.*, 2019). The biofilm structure provides an increased tolerance to antibiotics and immune defences, for instance, due to the presence of bacterial phenotypes with low metabolic activity and SCV (Crabbé *et al.*, 2019).

Osteomyelitis is mainly caused by staphylococci, especially by *S. aureus* and *S. epidermidis*, but can also be caused by other Gram-positive pathogens such as streptococci, by Gram-negative pathogens such as *P. aeruginosa* and even by a mixture of pathogens (Bernthal *et al.*, 2010; Horst *et al.*, 2012; Inzana *et al.*, 2015b). Furthermore, bacterial infections can find other ways to persist despite treatment (Kavanagh *et al.*, 2018). For example, staphylococci can survive intracellularly in human cells such as macrophages, osteoblasts or even osteocytes causing a chronic persistent osteomyelitis extremely difficult to treat (Boelens *et al.*, 2000; Ellington *et al.*, 2006; Valour *et al.*, 2015; Yang *et al.*, 2018). *S. aureus* can also form SACs, small but highly persistent microcolonies in the bone and soft tissue (Guggenberger *et al.*, 2012; Hofstee *et al.*, 2020; Tuchscherr *et al.*, 2017), and can hide in canaliculi within the bone, out of reach of phagocytic cells (de Mesy Bentley *et al.*, 2017). In addition, the worldwide increase in antibiotic resistance leaves fewer treatment options available (O'Neill, 2014). Consequently, patients require prolonged antibiotic treatment and longer hospitalisation and re-operation, resulting in longer disability and in a dramatic clinical and economic burden for the society. Therefore, it is crucial to develop new prevention, diagnosis and treatment strategies for osteomyelitis (Masters *et al.*, 2019; Moriarty *et al.*, 2016).

### Clinical translation and the need for animal models

Novel strategies for prevention, diagnosis and treatment should be properly evaluated to ensure their effectiveness before use in patients. However, the diverse incidence rate of osteomyelitis ranging from 1 to 30 %, depending on the clinical situation and presence of a device (Metsemakers *et al.*, 2015), the diversity in the anatomical locations affected and the wide range of patients age make it difficult to study the disease within the human population (Lazzarini *et al.*, 2006). Moreover, osteomyelitis can be caused by a broad variety of microorganisms, which may necessitate specific treatment for each pathogen (Arciola *et al.*, 2005b).

To overcome these obstacles, animal models have been developed to study the pathology and pathogenesis of osteomyelitis and the efficacy of prophylactic and treatment regimes. These animal

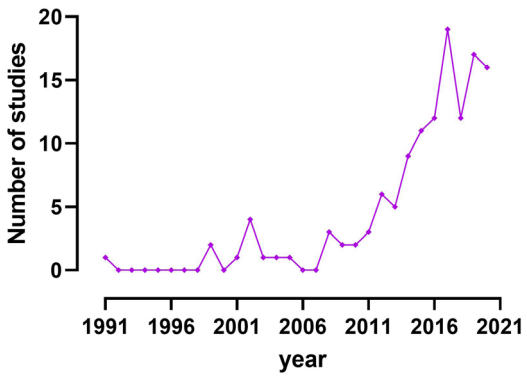


**Fig. 1. Number of studies using mouse osteomyelitis models per year between 1991 and 2020.** The number of mouse osteomyelitis models steadily increased from 2010 to 2020.

models should meet specific features to most accurately model the clinical situation in patients, such as a similar bone anatomy, gender influence or susceptibility to infection (Wancket, 2015). Therefore, only research conducted with well-established animal models will contribute to a better understanding of the pathogenesis of the disease and will advance the progress of novel preventive and treatment strategies towards the clinic (Coenye *et al.*, 2018). Although different animal species such as sheep, rabbit, dog and rats have been used for this purpose, the use of mouse models to study osteomyelitis has rapidly increased during the last decade (Fig. 1; Reizner *et al.*, 2014).

**Mouse models: advantages and limitations**

Mouse models for osteomyelitis gained popularity particularly with the unravelling of the mouse genome by the Mouse Genome Sequencing Consortium in 2002 (Mouse Genome Sequencing Consortium *et al.*, 2002). The general advantages of mice as models for osteomyelitis studies are their reproducibility (*i.d.* development of the infection within the mouse strain and availability of the mouse strains to reproduce and continue an experimental approach), their bone physiological and structural similarity to humans, the diversity of genetic and molecular tools available to study them and their relatively low costs. This enables extensive experimental designs, tailored to solve a wide variety of research questions. Furthermore, the mouse has a relatively short life cycle, providing the advantage of a rapid development of the pathological features of osteomyelitis.

Mouse bone is similar in its physiology and structure to human bone, with the presence of trabecular and cortical bone and with similar cell types. However, mice lack a haversian system (osteon) but instead use resorption cavities for bone remodelling that have a similar function to the haversian system (Holstein *et al.*, 2009). This results in a similar physiological control of bone remodelling (Holstein *et al.*, 2009). Compared to larger animals, mice have much smaller bones, making surgical manipulation more challenging (Muschler *et al.*, 2010). This limitation has been successfully solved with high level technology for small rodents that allows the establishment of highly standardised bone surgical procedures. Even the techniques for the insertion of devices such as intramedullary nails or the placement of fixation plates on the bone have been properly standardised, allowing a closer translation to the clinical situation in human patients (Haffner-Luntzer *et al.*, 2016; Histing *et al.*, 2011).

Mice and humans share more than 90 % genetic homology (Mouse Genome Sequencing Consortium *et al.*, 2002). A recent study has demonstrated that gene expression responses of mice and humans to trauma, burns and endotoxemia are significantly correlated

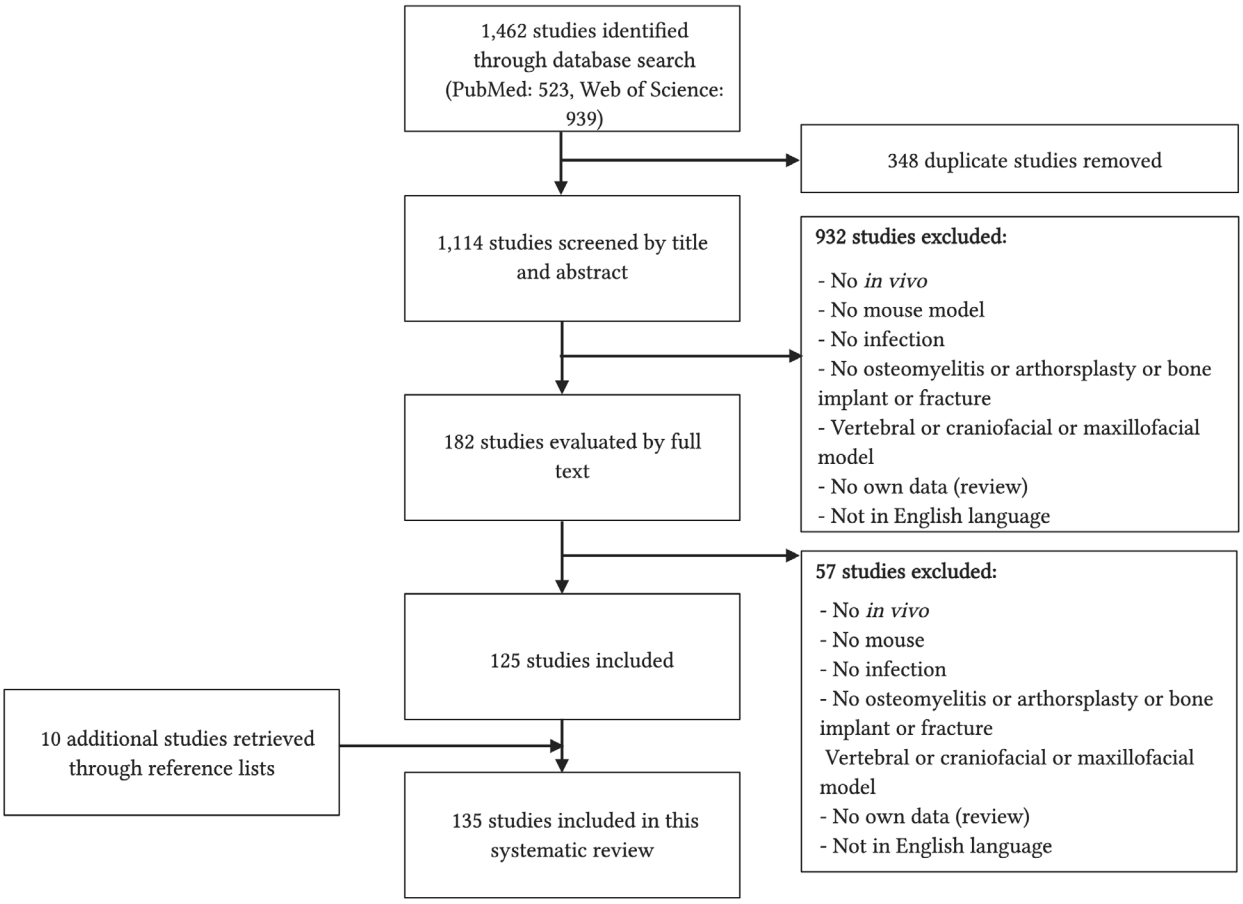


**Fig. 2. Schematic flow chart of the steps followed to obtain the collection of studies included in the present systematic review.**

(Takao and Miyakawa, 2015). The immune response to osteomyelitis also shows resemblance between mice and humans. For example, pro-inflammatory cytokines involved in the immune response against bacterial infection such as TNF-$\alpha$, IL-6, IL-1$\beta$ and IL-17A are upregulated in mouse as well as in human patients in the presence of osteomyelitis (Lüthje *et al*., 2020; Yoshii *et al*., 2002b). There are also differences. For example, the chemokine CXCL8, which has a central role in the early defence against infection in humans, has not been identified in mice (Lüthje *et al*., 2020). On the other hand, anti-inflammatory cytokines such as IL-4 are upregulated in both mice and humans during bone repair after infection (Lüthje *et al*., 2020). Despite the differences, if the detailed course of the immune responses in mice is known, it is possible to compare the results to the human situation.

Regarding osteomyelitis and pathogenesis, numerous studies have successfully established an infection in the bone, bone fractures and bone with an implant (Bernthal *et al*., 2010; Horst *et al*., 2012; Inzana *et al*., 2015b). The present review discusses the major models described in the literature and their most important characteristics.

### Aim of the review

The aim of the present systematic review is to discuss the different types of mouse osteomyelitis models available, to study the pathophysiology and immune response of the disease and the evaluation of the efficacy of novel preventive and treatment strategies. Based on the model characteristics, the published papers were classified into five subject groups: haematogenous osteomyelitis, post-traumatic osteomyelitis, bone-implant-related infection, PJI and fracture-related infection. In addition, the characteristics of the mice used, such as inbred strain, age or gender, the characteristics of the pathogens used, the inoculation methods, the type of anaesthesia and analgesia used during surgery and the procedures for evaluating the infection are described.

## Materials and Methods

### Search strategy

Two databases, Web of Science (Web ref. 1) and PubMed (Web ref. 2), were used to systematically identify studies exploring osteomyelitis in mouse models. The two databases were strategically searched using the search strategy shown in Fig. 2. The search query used for PubMed was (infection[MESH] OR infection[TIAB]) AND (mice[MESH] OR mice[TIAB] OR mouse[TIAB] OR murine[TIAB]) AND (model[TIAB] OR models[TIAB]) AND (arthroplasty[MESH] OR arthroplasty[TIAB] OR fracture[MESH] OR fracture[TIAB] OR (internal fixator)[MESH] OR (internal fixator)[TIAB] OR (internal fixation)[TIAB] OR prosthesis[MESH] OR prosthesis[TIAB] OR implant[TIAB] OR osteomyelitis[MESH] OR osteomyelitis[TIAB]). A simpler query was used for Web of Science: (infection) AND (mice OR mouse OR murine) AND (model OR models) AND (arthroplasty OR fracture OR (internal fixator) OR (internal fixation OR prosthesis OR implant OR osteomyelitis). The final search was conducted on the 15th of March 2021. In addition, other relevant studies found through the reference lists that met the eligibility criteria were included (Fig. 2).

### Inclusion and exclusion criteria

The inclusion criteria were: (1) *in vivo* mouse experimental study, (2) bacterial or fungal osteomyelitis studies, (3) long bones. The exclusion criteria were: (1) no osteomyelitis, (2) no bone infection vertebral osteomyelitis, (3) craniofacial or maxillofacial osteomyelitis, (4) non-infection osteomyelitis, (5) no mouse model, (6) no *in vivo* study, (7) no full-text literature, (8) not written in English language.

### Summary of literature search

Fig. 2 shows the systematic search procedure. A total of 1,462 articles were identified (523 from PubMed and 939 from Web of Science). From those, 348 duplicates were removed. 932 articles were excluded during the initial screening of titles and abstract and 57 during the secondary screening by full reading. 10 additional articles that met the eligibility criteria were retrieved from the reference lists of the papers collected. At the end, 135 studies were included in the present systematic review.

### Model design characteristics

All the studies discovered following the systematic search have in common that they use the mouse as a model to evaluate different aspects of osteomyelitis infection including pathogenesis, prophylaxis and treatment strategies. *S. aureus* was the main bacterial species used in the experimental studies but also other species, such as *A. baumannii* and *E. coli*, were found and are described in the review. A section discussing the main model design characteristics in detail, such as mouse strain, bacterial species, inoculum methods, surgical procedures and evaluation methods, was also included.

The experimental studies were organised into five different categories, each with corresponding tables listing the surgical procedure and bacterial inoculation method used. These categories were haematogenous osteomyelitis, post-traumatic osteomyelitis, bone-implant-related infection, PJI and fracture-related infection (Table 1-6). Each table provides the major details of the published procedure: (1) reference; (2) title; (3) microbiological status of the mice (*e.g.* SPF), gender and strain; (4) age; (5) time points; (6) bacterial strain, inoculum size and volume; (7) inoculation method; (8) evaluation methods. In Table 2, the size and location of the

**Table 1. Classification of haematogenous osteomyelitis mouse models.**

| Reference | Title | Microbiological status, gender, and strain | Age | Time points | Bacterial strain, inoculum size and volume | Inoculation method | Evaluation methods |
|---|---|---|---|---|---|---|---|
| Ji *et al.*, 2020 | EGFR/FAK and c-Src signalling pathways mediate the internalisation of *Staphylococcus aureus* by osteoblasts | Male C57BL/6 | 10 weeks | 14 d | *S. aureus* clinical isolate, $10^6$ CFU in 100 μL | Intravenous injection | IMHC, IMF |
| Potter *et al.*, 2020 | Host nutrient milieu drives an essential role for aspartate biosynthesis during invasive *S. aureus* infection | Female C57BL/6J | 7 weeks | 1, 4 and 7 d | *S. aureus* AH1263, $5 \times 10^7$ CFU | Retro-orbital vein injection | CFU counts (femur) |
| Hou *et al.*, 2019 | G-CSF partially mediates bone loss induced by *S. aureus* infection in mice | C57BL/6 | | 7 and 35 d | *S. aureus* clinical isolate, $10^6$ CFU/mL, 100 μL | Intravenous injection | μCT, histology, qRT-PCR, IMHC, IMF |
| Tuchscherr *et al.*, 2019 | Clinical *S. aureus* isolates vary in their virulence to promote adaptation to the host | Female C57BL/6 | 10 weeks | 3 and 42 d | *S. aureus*, $10^6$ CFU in 200 μL | Injection *via* lateral tail vein | CFU counts (tibia) |
| Tuchscherr *et al.*, 2017 | *S. aureus* regulator sigma B is important to develop chronic infections in hematogenous murine osteomyelitis model | Female C57BL/6 | 10 weeks | - | *S. aureus* LS1, LS1 AsigB, $10^6$ CFU in 150 μL | Injection *via* lateral tail vein | CFU counts (tibia and femur) |
| Wang *et al.*, 2017 | Mouse model of hematogenous implant-related *S. aureus* biofilm infection reveals therapeutic targets | SPF male C57BL/6 | 10-12 weeks | 1, 3, 7, 14, 21 and 28 d | *S. aureus* SAP231, $10^6$, $5 \times 10^6$ and $10^7$ CFU | Retro-orbital vein injection, femoral intramedullary nail protruding in the joint (1 mm) | BLI, CFU counts (implant), histology, SEM |
| Tuchscherr *et al.*, 2016 | *S. aureus* develops increased resistance to antibiotics by forming dynamic small colony variants during chronic osteomyelitis | SPF female C57BL/6 | 10 weeks | 5 and 35 d | *S. aureus* 6850, $10^6$ CFU in 200 μL | Injection *via* lateral tail vein | MRI, CFU counts (tibia), percentage of SCV |
| Szafranska *et al.*, 2014 | High-resolution transcriptomic analysis of the adaptive response of *S. aureus* during acute and chronic phases of osteomyelitis | SPF C57BL76 | 10 weeks | 7 and 28 d | *S. aureus* 6850, $10^6$ *CFU in* 150 μL | Injection *via* lateral tail vein | RNA-Seq analysis |
| Horst *et al.*, 2012 | A novel mouse model of *S. aureus* chronic osteomyelitis that closely mimics the human infection | SPF female C57BL/6 | 10 weeks | 3, 7, 14, 22, 35, 49 and 63 d | *S. aureus* ATCC 53657, $10^6$ CFU, $5 \times 10^5$ CFU and $2 \times 10^5$ CFU in 150 μL | Injection *via* lateral tail vein | CFU counts, ELISA, histology, X-ray, TEM, MRI |
| Blevins *et al.*, 2003 | Role of sarA in the pathogenesis of *S. aureus* bone infection | Male NIH-Swiss | 5-8 weeks | 1, 7 and 14 d | *S. aureus* UAMS-1 and sarA mutant, $5 \times 10^7$ CFU | Injection *via* lateral tail vein | CFU counts (femur), histology |
| Elasri *et al.*, 2002 | *S. aureus* collagen adhesin contributes to the pathogenesis of osteomyelitis | Male NIH-Swiss | 5-8 weeks | 14 d | *S. aureus* UAMS-1 and UAMS-237, $10^8$ CFU in 100 μL | Injection *via* lateral tail vein | CFU counts (femur), histology |
| Lee *et al.*, 2002 | The *S. aureus* Map protein is an immunomodulator that interferes with T cell–mediated responses | SPF female BALB/c, C3H/Hen, nu/nu (nude) and nu/+ | 8-10 weeks | 0.5, 1, 2 and 4 d | *S. aureus* Newman, $10^7$ CFU in 0.5 mL | Intravenous injection | CFU counts (heart, blood, kidney and joint), histology |
| Chadha *et al.*, 1999 | Experimental acute hematogenous osteomyelitis. Histopathological and immunological findings | C3H/HeJ | 8-10 weeks | 7 d | *S. aureus* LS-1, $5 \times 10^7$ CFU in 1 mL | Injection *via* lateral tail vein | Flow cytometry, histology, molecular analysis |
| Yoon *et al.*, 1999 | Experimental acute hematogenous osteomyelitis: Influence of *S. aureus* on T-cell immunity | C3H/HeJ | 8-10 weeks | 1, 3, 6, 8, 10, 14, 21 and 29 d | *S. aureus* LS-1, $10^7$ CFU in 200 μL | Injection *via* lateral tail vein | Histology, flow cytometry, qRT-PCR, ELISA |
| Ashman and Papadimitriou, 1991 | Chronic osteomyelitis as a consequence of systemic *Candida albicans* infection | SPF female BALB/c and CBA/CaH | 8 weeks | 180 d | *C. albicans* 3630, $10^5$ CFU | Intravenous injection | Histology |

**Table 2a. Classification of the post-traumatic osteomyelitis mouse models.**

| Reference | Title | Microbiological status, gender, and strain | Age | Time points | Bacterial strain, inoculum size, volume | Inoculation method | Defect type and hole size (G) | Evaluation |
|---|---|---|---|---|---|---|---|---|
| Ford *et al.*, 2020 | Diflunisal-loaded poly (propylene sulfide) nanoparticles decrease *S. aureus*-mediated bone destruction during osteomyelitis | Female C57BL/6J, FNB/NJ and BALB/c | 7-8 weeks | 14 d | *S. aureus* USA300 LAC (AH1263), $10^6$ CFU in 2 μL | Inoculation in intramedullary canal | Unicortical defect in the lateral midshaft of the femur, diameter of 1 mm (21 G) | μCT, BLI, histology |
| Isogai *et al.*, 2020 | Potential osteomyelitis biomarkers identified by plasma metabolome analysis in mice | SPF male BALB/c | 12 weeks | 3 d | *S. aureus* Xen 29 ATCC 12600, $10^8$ CFU in 1 μL | Inoculation in intramedullary canal | Perforation in the distal end of the femur using a drill with 0.5 mm burr | Serology, BLI |
| Ramirez *et al.*, 2020 | Exploiting correlations between protein abundance and the functional status of saeRs and sarA to identify virulence factors of potential importance in the pathogenesis of *S. aureus* osteomyelitis | Female C57BL/6 | 6-8 weeks | 14 d | *S. aureus* LAC, *ΔsarA*, *ΔsaeRS*, $10^6$ *CFU in* 2 μL | Inoculation in intramedullary canal | Unicortical defect in the lateral midshaft of the femur | CFU counts (femur) and μCT |
| Wagner *et al.*, 2020 | Local Wnt3a treatment restores bone regeneration in large osseous defects after surgical debridement of osteomyelitis | Male and female C57BL/6 | 12 weeks | 17 and 21 d | *S. aureus*, $10^3$ CFU in 1 μL | Injected into the medullary cavity of the tibia | Perforation in the tibia of 1 mm of diameter | Western blot, histology, IMHC, IMF, μCT |
| Rom *et al.*, 2019 | The impacts of msaABCR on sarA-associated phenotypes are different in divergent clinical isolates of *S. aureus* | C57BL/6 | 8-10 weeks | 14 d | *S. aureus* USA300 LAC and UAMS-1 and mutants, $10^6$ CFU in 2 μL | Inoculation in intramedullary canal | Unicortical defect at lateral midshaft of the femur, diameter of 1 mm (21 G) | μCT, staphyloxantin production |
| Spoonmore *et al.*, 2020 | Concurrent local delivery of diflunisal limits bone destruction but fails to improve systemic vancomycin efficacy during *S. aureus* osteomyelitis | Female C57BL/6J | 7-8 weeks | 7 and 14 d | *S. aureus* USA300 LAC, $10^6$ CFU in 2 μL | Inoculation in the femur | Unicortical defect at lateral midshaft of the femur, diameter of 1 mm (21 G) | CFU counts (femur) |
| Lu *et al.*, 2019 | High-resolution bimodal imaging and potent antibiotic/photodynamic synergistic therapy for osteomyelitis with a bacterial inflammation-specific versatile agent | ICR/JCL | 4 weeks | 0, 14 and 28 d | *S. aureus* ATCC 6538, $10^6$ CFU in 2 μL | Inoculation in intramedullary canal | Unicortical defect at the tibia, diameter of 1.5 mm | BLI, histology, μCT |
| Putnam *et al.*, 2019 | MyD88 and IL-1R signalling drive antibacterial immunity and osteoclast-driven bone loss during *S. aureus* osteomyelitis | C57BL/6J Myd88$^{-/-}$ and IL1r1$^{-/-}$ | 5-8 weeks | 1, 4, 7, 10 and 14 d | *S. aureus* AH1263 LAC, $10^6$ CFU in 2 μL | Inoculation in intramedullary canal | Unicortical defect at lateral midshaft of the femur, diameter of 1 mm (21 G) | μCT, histology, shitomorphometric analysis, double calcein label, CFU counts (femur), cytokines, flow cytometry, osteoclastogenesis assay |
| Wagner *et al.*, 2019 | Adipose-derived stromal cells are capable of restoring bone regeneration after post-traumatic osteomyelitis and modulate B-cell response | Male and female C57BL/6J | 12 weeks | 3 and 7 d | *S. aureus* clinical isolate | Inoculation in intramedullary canal | Defect at the proximal medial tibia, diameter of 1 mm | Flow cytometry, μCT, western-blot, histology, IMHC, IMF |

**Table 2b. Classification of the post-traumatic osteomyelitis mouse models.**

| Reference | Title | Microbiological status, gender, and strain | Age | Time points | Bacterial strain, inoculum size, volume | Inoculation method | Defect type and hole size (G) | Evaluation |
|---|---|---|---|---|---|---|---|---|
| Zhu *et al.*, 2019 | Inhibition of pyroptosis attenuates *S. aureus* bone injury in traumatic osteomyelitis | Male C57BL/6 | 6 weeks | 3 and 7 d | *S. aureus* 6850 (ATCC 53657), $10^8$ CFU in 1 μL | Inoculation in intramedullary canal | Perforation at the fossa intercondyloid, diameter of 23 G | μCT, qRT-PCR, ELISA |
| Tuohy *et al.*, 2018 | Assessment of a novel nanoparticle hyperthermia therapy in a murine model of osteosarcoma | Female C3H-HeN | 8-10 weeks | | *S. aureus* Xen 36 | Pre-incubation of silk suture | Defect at the tibia, diameter of 25 G and 23 G | Histology, qRT-PCR, flow cytometry |
| Wu *et al.*, 2018 | Baicalin alleviates osteomyelitis by regulating TLR-2 in the murine model | SPF male BALB/c | 12 weeks | 1, 3 and 7 d | *S. aureus* ATCC 43300, $10^8$ CFU in 1 μL | Inoculation in intramedullary canal | Defect at the distal end of the femur, diameter of 23 G | RT-PCR, ELISA for IL-6, IL-1B and CRP, μCT, Western blot, ALP assay |
| Chen *et al.*, 2017 | CHI3L1 regulation of inflammation and the effects on osteogenesis in a *S. aureus*-induced murine model of osteomyelitis | C57BL/6J | 7-8 weeks | 14 d | *S. aureus* 6850 (ATCC 53657), $10^6$ CFU in 2 μL | Inoculation in intramedullary canal | Perforation of the femur, diameter of 1 mm | μCT, qRT-PCR, Western blot, ELISA; histology, IMHC |
| Qadri *et al.*, 2017 | Metallic nanoparticles to eradicate bacterial bone infection | Female BALB/c | 8-12 weeks | 7 d | *S. aureus* Xen36 ATCC 49525 | Pre-inoculation of silk suture in the tibia | Perforation in the tibia of 0.25 mm of diameter | CFU counts (tibia), histology, protein quantification, reduced glutathione (GSH) measurement for oxidative stress |
| Wagner *et al.*, 2017b | Diminished bone regeneration after debridement of posttraumatic osteomyelitis is accompanied by altered cytokine levels, elevated b cell activity, and increased osteoclast activity | Male and female C57BL/6 | 12 weeks | 17 and 21 d | *S. aureus*, $10^3$ CFU in 1 μL | Injected into the medullary cavity | Perforation in the tibia of 1 mm of diameter | Western blot, cytokines, histology, IMH, IMF, flow cytometry |
| Xiao *et al.*, 2017 | Detecting chronic post-traumatic osteomyelitis of mouse tibia via an IL-13Rα2 targeted metallofullerene MRI probe | Female BALB/c | 8-10 weeks | 28 d | *S. aureus* ATCC 25923, $10^7$ CFU in 150 μL | Pre-inoculation of a vircryl suture for 30 min | Defect in the proximal end of tibia, diameter of 27 G | Luminol-bioluminescence imaging of myeloperoxidase, MRI, histology, IMHC |
| Loughran *et al.*, 2016 | Impact of sarA and phenol-soluble modulins on the pathogenesis of osteomyelitis in diverse clinical isolates of *S. aureus* | Female C57BL/6 | 8-10 weeks | 14 d | *S. aureus* USA300 strain LAC, USA200 UAMS-1, and sarA or alpha class of PSMs mutants, $10^5$ CFU in 2 μL | Inoculation in intramedullary canal | Defect in the lateral midshalft of the femur, diameter of 21 G | μCT, proteomics |
| Mendoza Bertelli *et al.*, 2016 | *S. aureus* protein A enhances osteoclastogenesis via TNFR1 and EGFR signalling | BALB/c | 10 weeks | 14 d | *S. aureus* FPR3757 and the isogenic SpA-mutant, (1-2) × $10^6$ CFU in 2.5 μL | Inoculation in fibrin | Perforation in the tibia with a diameter of 1 mm | CFU counts (tibia), histology, μCT |
| Wagner *et al.*, 2016 | Surgical debridement is superior to sole antibiotic therapy in a novel murine posttraumatic osteomyelitis model | Male and female C57BL/6 | - | 7 and 14 d | *S. aureus* Rosenbach 1884, 2 × $10^3$ CFU in 0.5 μL | Inoculation in intramedullary canal | Unicortical defect in the proximal medial tibia, diameter of 1 mm | CFU counts, histology, Gram staining, qRT-PCR |

**Table 2c. Classification of the post-traumatic osteomyelitis mouse models.**

| Reference | Title | Microbiological status, gender, and strain | Age | Time points | Bacterial strain, inoculum size, volume | Inoculation method | Defect type and hole size (G) | Evaluation |
|---|---|---|---|---|---|---|---|---|
| Wilde *et al.*, 2015 | Bacterial hypoxic responses revealed as critical determinants of the host-pathogen outcome by TnSeq analysis of *S. aureus* invasive infection | Female C57BL/6J | 7-8 weeks | | *S. aureus* HG003, $10^6$ CFU in 2 μL | Inoculation in femur | Unicortical defect, diameter of 1 mm (21 G) | BLI, transposon seq analysis, qPCR |
| Cassat *et al.*, 2013 | A secreted bacterial protease tailors the *S. aureus* virulence repertoire to modulate bone remodelling during osteomyelitis | C57BL/6J | 7-8 weeks | 14 d | *S. aureus* USA300 LAC, $10^6$ CFU in 2 μL | Inoculation in intramedullary canal | Unicortical defect in the lateral midshaft of the femur, diameter of 1 mm (21 G) | μCT, histopathology |
| Funao *et al.*, 2012 | Establishment of a real-time, quantitative, and reproducible mouse model of *Staphylococcus* osteomyelitis using bioluminescence imaging | Male BALB/c | 12 weeks | 3, 7, 21 and 28 d | *S. aureus* Xen-29 (ATCC 12600), $10^8$ CFU in 1 μL | Inoculation in intramedullary canal | Perforation at the distal end of the femur, diameter of 23 G | Flow cytometry, histology, BLI, serology |
| Sottnik *et al.*, 2010 | Chronic bacterial osteomyelitis suppression of tumour growth requires innate immune responses | Female C3H-HeN, BALB/c, C57BL/6 | 8-10 weeks | 10 d | *S. aureus* Xen 36 (ATCC 49525), $10^6$ CFU in 1 mL | Pre-inoculation of silk suture | Perpendicular hole in the proximal tibia, diameter of 23 G | Flow cytometry, CFU counts (tibia) |
| Varoga *et al.*, 2009 | Osteoblasts participate in the innate immunity of the bone by producing human β defensin-3 | Male BALB/c | 8-12 weeks | 12 h | *S. aureus*, $10^6$ CFU/mL in 10 μL | Injection in the intraosseous cavity | | RT-qPCR and ELISA |
| Takahashi *et al.*, 2008 | Bone-targeting of quinolones conjugated with an acidic oligopeptide | Female ddY | 8-10 weeks | | *S. aureus* JCM 2413, $10^5$ CFU in 1 μL | Inoculation in intramedullary canal | Perforation at the proximal third portion of the tibia, diameter of 26 G | CFU counts (tibia) |
| Varoga *et al.*, 2008 | The role of human β-defensin-2 in bone | Male BALB/c | 8-12 weeks | 12 h | *S. aureus*, $10^6$ CFU/mL in 10 μL | Injection into the intraosseous cavity | | RT-qPCR and IMHC |
| Marriott *et al.*, 2005 | Osteoblasts produce monocyte chemoattractant protein-1 in a murine model of *S. aureus* osteomyelitis and infected human bone tissue | BALB/c | - | 1 and 2 d | *S. aureus* ATCC 49230, $10^3$ CFU | Agarose beads | Perforation in the bone cortex | IMHC, RT-PCR |
| Marriott *et al.*, 2004 | Osteoblasts express the inflammatory cytokine interleukin-6 in a murine model of *S. aureus* osteomyelitis and infected human bone tissue | BALB/c | - | 2 and 4 d | *S. aureus* ATCC 49230, $10^3$ CFU | Agarose beads | Perforation in the bone cortex | IMHC, RT-PCR |
| Yoshii, 2002a | Inhibitory effect of roxithromycin on the local levels of bone-resorbing cytokines in an experimental model of murine osteomyelitis | Female ICR | 5 weeks | 1, 3, 5, 7, 14, 21 and 28 d | *S. aureus* E-31461, $10^8$ CFU/mL | Pre-inoculation of silk suture | Perforation of the tibia, diameter of 23 G | ELISA of IL-1B, IL-6, TNF-α |
| Yoshii *et al.*, 2002b | Local levels of interleukin-1beta, -4, -6, and tumour necrosis factor in an experimental model of murine osteomyelitis due to *S. aureus* | Female ICR | 5 weeks | 1, 3, 5, 7, 14, 21 and 28 d | *S. aureus* E-31461, $10^8$ CFU/mL | Pre-inoculation of silk suture | Perforation of the tibia, diameter of 23 G | CFU counts (tibia), bone histology, ELISA of cytokines |

**Table 3a. Classification of the bone-implant infection mouse models.**

| Reference | Title | Microbiological status, gender, strain | Age | Time points | Bacterial strain, inoculum size, volume | Inoculation method, placement of the device | Evaluation |
|---|---|---|---|---|---|---|---|
| Lin *et al.*, 2021 | mRNA transcriptome analysis of bone in a mouse model of implant-associated *Staphylococcus aureus* osteomyelitis | Male, C57BL/6 | 10-12 weeks | 14 and 28 d | *S. aureus* clinical strain, $10^6$ CFU/mL in 2 μL | Inoculation at the bone cavity, femoral intramedullary pin | μCT, X-ray, CFU counts (bone and implant), histology, immunohistochemistry, immunofluorescence, qRT-PCR |
| Masters *et al.*, 2021 | Distinct vasculotropic versus osteotropic features of *S. agalactiae versus S. aureus* implant-associated bone infection in mice | Female BALB/c | 6 weeks | 14 d | *S. aureus* USA300 and *S. agalacticae* COH1, $5 \times 10^5$ CFU/mL | Pre-inoculation of the implants, transcortical tibia pin | CFU counts (bone, implant and tissue), μCT, X-ray, histology, TEM, TRAP |
| Tomizawa *et al.*, 2021 | The limitations of mono- and combination antibiotic therapies on immature biofilms in a murine model of implant-associated osteomyelitis cefazolin, gentamicin and vanco with or not rifampicin | Female BALB/c | 6-8 weeks | 0, 3, 7 and 14 d | *S. aureus* UAMS-1 $2.5 \times 10^5$ CFU | Pre-inoculation of the implants, transcortical tibia pin | CFU counts (implant and tissue), SEM, histology (Brown and Brenn) |
| Aguilera-Correa *et al.*, 2020 | A new antibiotic-loaded Sol-Gel can prevent bacterial prosthetic joint infection: from *in vitro* studies to an *in vivo* model (moxifloxicin) | Male CD1 | 16 weeks | 35 d | *S. aureus* and *E. coli* clinical strains | Injection in femoral canal, femoral intramedullary implant | CFU count (bone and implant), histology, μCT |
| Masters *et al.*, 2020 | Identification of penicillin binding protein 4 (PBP4) as a critical factor for *S. aureus* bone invasion during osteomyelitis in mice | Female BALB/c | 6-8 weeks | 14 d | *S. aureus* USA300 or Δpbp4, $5 \times 10^5$ CFU/mL | Pre-inoculation of the pins for 20 min, transcortical tibia pin | CFU counts (bone, tissue, implant), μCT, X-ray, histology (Brown and Brenn), TRAP, TEM |
| Tomizawa *et al.*, 2020 | Biofilm producing *Staphylococcus epidermidis* inhibits osseous integration without osteolysis and histopathology in a murine septic implant model | Female BALB/c | 6-8 weeks | 7, 14 and 42 d | *S. epidermidis* RP62a $1.6 \times 10^5$ CFU and *S. aureus* USA300 LAC $2.1 \times 10^5$ CFU | Pre-inoculation of pins, transcortical tibia pin | CFU counts (tissue and implant), histology, μCT, SEM, qPCR biomechanical test |
| Wang *et al.*, 2020b | NF-κB/TWIST1 mediates migration and phagocytosis of macrophages in the mice model of implant-associated *S. aureus* osteomyelitis | Male C57BL/6 | 8 weeks | 3 d | *S. aureus*, $10^6$ CFU in 2 μL | Inoculation in intramedullary cavity, femoral intramedullary implant | RT-qPCR, Western blot, histology, IMHC |
| Zhang *et al.*, 2019 | Significant suppression of *S. aureus* colonization on intramedullary Ti6Al4V implants surface-grafted with vancomycin- bearing polymer brushes | Male and female CL57BL/6 | 8-12 weeks | 7, 14 and 21 d | *S. aureus* Xen29, $10^4$ CFU in 4 μL | Inoculation in intramedullary cavity, femoral intramedullary pin | μCT, BLI, blood counts, CFU counts (pin), histology |
| Boles *et al.*, 2018 | Local delivery of amikacin and vancomycin from chitosan sponges prevent polymicrobial implant-associated biofilm | C57BL/6 | 8-12 weeks | 7 d | *S. aureus* UAMS-1, $10^4$ CFU and *E. coli* ATCC 25922, $10^2$ CFU | Pre-inoculation of the K-wire, femoral intramedullary K-wire | CFU counts (femur and K-wire) |
| Jiang *et al.*, 2019 | Aspirin alleviates orthopaedic implant-associated infection | Female C57BL/6J | 8 weeks | 11 d | *S. aureus* ATCC 43300, $10^6$ CFU in 1.5 mL | Pre-inoculation of pin, transcortical tibia pin | μCT, histology, immunohistochemistry |
| Wells *et al.*, 2018 | Ciprofloxacin and rifampin dual antibiotic-loaded biopolymer chitosan sponge for bacterial inhibition | C57BL/6 | 8-12 weeks | 7 d | Polymicrobial mixture: *S. aureus* UAMS-1, $10^4$ CFU and *E. coli* ATCC 25922, $10^2$ CFU | Pre-inoculation of pin, femoral intramedullary pin | CFU counts (pin and femur) |

**Table 3b. Classification of the bone-implant infection mouse models.**

| Reference | Title | Microbiological status, gender, strain | Age | Time points | Bacterial strain, inoculum size, volume | Inoculation method, placement of the device | Evaluation |
|---|---|---|---|---|---|---|---|
| Harris *et al.*, 2017 | Phosphatidylcholine coatings deliver local antimicrobials and reduce infection in a murine model: a preliminary study | C57BL/6 | 8-12 weeks | 7 d | *S. aureus* UAMS-1, $10^4$ CFU | Wound inoculation, femoral intramedullary nail | CFU counts (femur and implant) |
| Ishikawa *et al.*, 2017 | Surface topography of silicon nitride affects antimicrobial and osseointegrative properties of tibial implants in a murine model | Female BALB/c | 8 weeks | 1, 3, 5, 7, 10 and 14 d | MRSA USA300 LAC, $10^5$ CFU | Pre-inoculation of implants for 20 min, transcortical pin in the tibia | CFU counts (implant), SEM |
| Jørgensen *et al.*, 2017 | Hyperbaric oxygen therapy is ineffective as an adjuvant to daptomycin with rifampicin treatment in a murine model of *S. aureus* in implant-associated osteomyelitis | Female C57BL6/J | 8-10 weeks | 14 d | *S. aureus* ATCC 12600, $10^6$ CFU/mL | Pre-incubation of implant for 24 h, transcortical pin in the tibia | CFU counts (tibia and implant), serological biomarkers |
| Funao *et al.*, 2016 | A novel hydroxyapatite film coated with ionic silver via inositol hexaphosphate chelation prevents implant-associated infection | SPF male BALB/c | 12 weeks | 28 d | *S. aureus* Xen29 ATCC 12600, $10^8$ CFU in 1 μL | Inoculation in intramedullary cavity, intramedullary nail in the femur | BLI, serology, histology |
| Jørgensen *et al.*, 2016 | Rifampicin-containing combinations are superior to combinations of vancomycin, linezolid and daptomycin against *S. aureus* biofilm infection *in vivo* and *in vitro* | Female C57BL/6J | 6-8 weeks | 11 and 14 d | *S. aureus* ATCC 12600, $10^6$ CFU/mL | Pre-incubation of implant for 24 h, transcortical pin in the tibia | CFU counts (implant and tibia) |
| Shiono *et al.*, 2016 | Delayed *Propionibacterium acnes* surgical site infections occur only in the presence of an implant | Male BALB/c | 12 weeks | 1, 3, 7, 14, 28, 56 and 84 d | *P. acnes* ATCC 51277, $10^6$ CFU in 1 μL | Inoculation at the implant tip, femoral intramedullary nail | Histology, optical imaging, SEM, genetic analysis |
| Choe *et al.*, 2015 | Immunomodulatory peptide IDR-1018 decreases implant infection and preserves osseointegration | Female C57BL/6 J and macrophage Fas-induced apoptosis | 6 to 8 weeks | 1 and 15 d | *S. aureus* Xen36, 100 μL of $3 \times 10^{10}$ CFU/mL | Pre-incubation of implant for 20 min, implant in the mid-diaphysis of the femur | TNF-α, MCP-1, IL-6, FLI counts of macrophages, IL-1β, CFU counts (implant and femur), BLI, ultimate force, stiffness, work to maximum load for osseointegration |
| Nishitani *et al.*, 2015 | Quantifying the natural history of biofilm formation *in vivo* during the establishment of chronic implant-associated *S. aureus* osteomyelitis in mice to identify critical pathogen and host factors | Female C57BL/6 and BALB/c | - | 1, 3, 7, 14 and 28 d | *S. aureus* SH100, UAMS-1 and USA300 LAC | Pre-inoculation of the implant, transcortical tibia pin | BLI, SEM, CFU counts (implant, tibia, soft tissue), RNA analysis, percentage of biofilm area |
| Nishitani *et al.*, 2015 | A diagnostic serum antibody test for patients with *S. aureus* osteomyelitis | Female BALB/c and C57BL/6 | 6-8 weeks | 14 and 42 d | *S. aureus, S. epidermidis, Staphylococcus lugdunensis* and *E. coli*, $5 \times 10^5$ CFU/pin | Pre-inoculation of the pins, transcortical tibia pin | ELISA |
| Jørgensen *et al.*, 2014 | A modified chronic infection model for testing treatment of S. *aureus* biofilms on implants | Female C57BL/6J | 6-8 weeks | 4, 6, 8, 11 and 15 d | *S. aureus* Xen31 $3.2 \times 10^4$ CFU/pin and *S. aureus* Xen 29 $1.7 \times 10^4$ CFU/pin | Pre-incubation of the implant in 50 ml with $10^6$ CFU for 24 h, transcortical tibia pin | Epifluorescence microscopy, confocal microscopy, CFU counts (implant and tibia) |

**Table 3c. Classification of the bone-implant infection mouse models.**

| Reference | Title | Microbiological status, gender, strain | Age | Time points | Bacterial strain, inoculum size, volume | Inoculation method, placement of the device | Evaluation |
|---|---|---|---|---|---|---|---|
| Zhu *et al.*, 2014 | The potential role of increasing the release of mouse b-defensin-14 in the treatment of osteomyelitis in mice: a primary study | Male BALB/c | 8-12 weeks | 1, 4 and 7 d | *S. aureus* ATCC 43300, $10^3$ CFU in 10 µL | Inoculation in intramedullary cavity, tibial intramedullary nail | Body weight and temperature, CFU counts (tibia), histology, ELISA, IMHC, interfacial membrane preparation, RT-PCR, Western blot |
| Varrone *et al.*, 2014 | Passive immunisation with anti-glucosaminidase monoclonal antibodies protects mice from implant-associated osteomyelitis by mediating opsonophagocytosis of *S. aureus* megaclusters | Female BALB/cJ | 8-10 weeks | 0, 3, 5, 7, 10 and 14 d | *S. aureus* Xen29 UAMS-1 | Pre-incubation of pin for 20 min, transcortical pin in the tibia | TEM, SEM, BLI, µCT, histology |
| Walton *et al.*, 2014 | Comparison of 3 real-time, quantitative murine models of Staphylococcal biofilm infection by using *in vivo* bioluminescent imaging | Female ICR | 6-8 weeks | 1, 4, 8 and 35 d | *S. aureus* Xen36 | Pre-incubation of pins, transcortical pin in the tibia | BLI and histology |
| Gedbjerg *et al.*, 2013 | Anti-glucosaminidase IgG in sera as a biomarker of host immunity against *S. aureus* in orthopaedic surgery patients | Female BALB/c | 6-8 weeks | 42 d | *S. aureus* clinical strain | Pre-incubation of pin for 20 min, transcortical pin in the tibia | Serum collection for functional titer percentage inhibition |
| Shandley *et al.*, 2012 | Hyperbaric oxygen therapy in a mouse model of implant-associated osteomyelitis | Male C57BL/6 | 7-9 weeks | 0, 12 and 19 d | *S. aureus*, $2.7 \times 10^4$ CFU, *P. aeruginosa*, $6 \times 10^4$ CFU, *K. pneumoniae* $1.1 \times 10^4$ CFU in 200 µL | Pre-inoculation of pin for 5 min, transcortical pin in the tibia | PCR, ELISA |
| Prabhakara *et al.*, 2011 | Suppression of the inflammatory immune response prevents the development of chronic biofilm infection due to MRSA | C57BL/6 and BALB/c | 6-8 weeks | 7, 14, 21, 28 and 49 d | MRSA-M2, $3 \times 10^5$ CFU/pin | Pre-incubation of pin for 20 min, transcortical pin in the tibia | CFU counts (tibia), PNA-FISH, cytokines |
| Prabhakara *et al.*, 2011 | Murine immune response to a chronic *S. aureus* biofilm infection | C57BL/6 | 6-8 weeks | 4, 7, 14, 21, 28 and 49 d | MRSA-M2 and UAMS-1, $2 \times 10^5$ CFU/pin | Pre-incubation of pin for 20 min, transcortical pin in the tibia | ELISA for cytokine level, IgG, flow cytometry, CFU counts(tibia), PNA-FISH of pin |
| Crane *et al.*, 2009 | Efficacy of colistin impregnated beads to prevent multi-drug resistant *A. baumannii* implant-associated osteomyelitis | Female C57BL/6 | 6-8 weeks | 19 d | *A. baumannii* and *S. aureus* Xen29, $2.5 \times 10^5$ CFU | Pre-inoculation of the pin, transcortical pin in the tibia | µCT, histology, serology |
| Li *et al.*, 2008 | A quantitative mouse model of implant-associated osteomyelitis and the kinetics of microbial growth, osteolysis and humoral immunity | Female C57BL/6 | 6-8 weeks | 0, 4, 7, 11, 14 and 18 d | *S. aureus* ATCC 49230, $9.5 \times 10^5$ CFU; Xen29 (ATCC 12600), $4.2 \times 10^5$ CFU | Pre-incubation of pin for 20 min, transcortical pin in the tibia | IVIS, µCT, histology, qRT-PCR, serology |
| Johansson *et al.*, 2001 | Collagen and fibronectin binding in experimental Staphylococcal osteomyelitis | CBA | 6 weeks | 28-32 d | *S. aureus* Phillips and PH100, $10^9$ CFU/mL in 500 µL | Injected in the bone hole, intramedullary tibial steel cerclage | CFU counts (tissue), histology |

**Table 4. Classification of diabetes and bone-implant infection mouse models.**

| Reference | Title | Microbiological status, gender, strain | Age | Time points | Bacterial strain, inoculum size, volume | Inoculation method, placement of the device | Evaluation | Diabetes induction |
|---|---|---|---|---|---|---|---|---|
| Farnsworth *et al.*, 2018 | Obesity/type 2 diabetes increases inflammation, periosteal reactive bone formation, and osteolysis during *S. aureus* implant-associated bone infection | Male C57BL/6J | | 1, 3, 7, 14 and 21 d | *S. aureus* USA300 LAC, $2 \times 10^5$ CFU/pin | Pre-inoculation of the pins, transcortical tibia pin | Histology, RNAseq, μCT, CFU counts (tibia) | High-fat (60 % kcal) or low-fat (10 % kcal) diet for 3 months |
| Farnsworth *et al.*, 2017 | Adaptive upregulation of ClfA by *S. aureus* in the obese, T2D host mediates increased virulence | Male C57BL/6J | 12 weeks | 14 and 21 d | *S. aureus* JE2 and ClfA mutant strain | Pre-incubation of the pin for 20 min, transcortical tibia pin | CFU counts (tissue and tibia), RT-PCR, histology, immunofluorescence, coagulation assays | High-fat diet (60 % kcal) |
| Wang *et al.*, 2017b | Chronic osteomyelitis increases the incidence of T2D in humans and mice | Female C57BL/6 | 10 weeks | | *S. aureus* | Pre-inoculation of the pin, transcortical tibia pin | X-ray, fasting blood glucose measure | Not mentioned |
| Farnsworth *et al.*, 2015 | A humoral immune defect distinguishes the response to *S. aureus* infections in mice with obesity and T2D from that in mice with T1D | Male C57BL/6J | 12 weeks | 7 and 14 d | *S. aureus* Xen36, $2 \times 10^5$ CFU | Pre-inoculation of the wire for 20 min, transcortical tibia pin | CFU counts (tibia and tissue), BLI, ELISA | Streptozotozin for T1D and high-fat diet for T2D |
| Lovati *et al.*, 2014 | Does PGE1 vasodilator prevent orthopaedic implant-related infection in diabetes? preliminary results in a mouse model | Female NOD/ShiLtJ mice type I diabetic | 14 weeks | 7, 14 and 28 d | *S. aureus* ATCC 25923, $1 \times 10^3$ CFU in 3 μL | Injection in femoral canal, femoral intramedullary pin | μCT, histology, blood analysis, CFU count (femur) | Transgenic mice |
| Lovati *et al.*, 2013 | Diabetic mouse model of orthopaedic implant-related *S. aureus* infection | NOD/ShiLtJ mice and non-diabetic CD1 | | 28 d | *S. aureus* ATCC 25923, $1 \times 10^3$ CFU in 3 μL | Injection in femoral canal, femoral intramedullary pin | μCT, histology, blood analysis, CFU count (femur) | Transgenic mice |

**Table 5a. Classification of the peri-prosthetic joint-implant infection mouse models.**

| Reference | Title | Microbiological status, gender, strain | Age | Time points | Bacterial strain, inoculum size, volume | Inoculation method, placement of the device | Evaluation |
|---|---|---|---|---|---|---|---|
| Wang *et al.*, 2021 | CCR2 contributes to host defence against *S. aureus* orthopaedic implant-associated infections in mice | Male C57BL/6J | 8-12 weeks | 7, 14 and 21 d | *S. aureus* USA 300 SAP231 $10^3$ CFU in 2 μL | Inoculation on the implant surface, femoral intramedullary implant protruding in the joint (1 mm) | IVIS, CFU counts (bone and implants), flow cytometry |
| Sosa *et al.*, 2020 | The antimicrobial potential of bacteriophage-derived lysin in a murine debridement, antibiotics, and implant retention model of prosthetic joint infection | Female C57BL/6J | 16 weeks | 10 d | *S. aureus* Xen36, $10^4$ CFU | Injection in the knee, press-fit insertion of tibial component | CFU counts (tissue and implants), X-ray |
| Wang *et al.*, 2020a | IL-1β and TNFα are essential in controlling an experimental orthopaedic implant-associated infection | Male C57BL/6 | 8-12 weeks | 0, 3, 7 and 14 d | *S. aureus* Xen36 ATCC 49525, $10^3$ CFU in 2 μL | Inoculation in joint cavity, femoral intramedullary implant protruding in the joint (1 mm) | Flow cytometry |
| Yamada *et al.*, 2020 | Monocyte metabolic reprogramming promotes pro-inflammatory activity and *S. aureus* biofilm clearance | Male and female C57BL/6NCrl | 8 weeks | 7, 14 and 21 d | *S. aureus* USA300 LAC 13c, $10^3$ CFU in 2 μL | Inoculation on the K-wire, femoral intramedullary implant protruding in the joint (1 mm) | CFU counts (tissue, knee, femur, implant), IVIS, flow cytometry |
| Sheppard *et al.*, 2020 | Novel *in vivo* mouse model of shoulder implant infection | Male C57BL/6 | 12 weeks | 1, 3, 5, 7, 10, 14, 18, 21, 28, 35, and 42 d | *S. aureus* Xen36 (ATCC 49525) $10^3$ and $10^4$ CFU in 2 μL | Inoculation at the implant tip, humerus nail protruding in the joint | IVIS, histology, confocal microscopy, X-ray, CFU counts (tissue and implant) |
| Zhang *et al.*, 2020 | Surface grafted zwitterionic polymers improve the efficacy of a single antibiotic injection in suppressing *S. aureus* periprosthetic infections | C57BL/6 | 8-12 weeks | 21 d | *S. aureus* Xen29, $10^4$ CFU/mL in 4 μL | Injection in the femoral canal, femoral intramedullary nail | IVIS, histology, μCT |
| Hernandez *et al.*, 2019 | Disruption of the gut microbiome increases the risk of periprosthetic joint infection in mice | Male C57BL/6 | 16 weeks | 5 d | *S. aureus* Xen36 ATCC 49525, $10^2$ CFU in 2 μL | Inoculation in joint cavity, press-fit insertion of tibial component | CFU counts (joint and implant), flow cytometry |
| Peng *et al.*, 2019 | Curcumin μP promising anti-bacterial and anti-inflammatory agent for treating periprosthetic joint infections | Male C57BL/6 | 12 weeks | 7 d | *S. aureus* ATCC 43300, $2 \times 10^3$ CFU | Inoculation in intramedullary cavity, femoral intramedullary nail | Inflammatory index score, μCT, histology |
| Stavrakis *et al.*, 2019 | Controlled release of vancomycin and tigecycline from an orthopaedic implant coating prevents *S. aureus* infection in an open fracture animal model | Male C57BL/6 | Male 12 weeks | 3, 14, 28 and 42 d | *S. aureus* Xen 36 ATCC 49525, $10^8$ *CFU in* 2 μL | Inoculation in fracture site, femoral intramedullary nail protruding in the joint | X-ray, BLI, CFU counts (tissue and pin) |
| Carli *et al.*, 2018 | Vancomycin-loaded polymethylmethacrylate spacers fail to eradicate PJI in a clinically representative mouse model | C57BL/6 | 12 weeks | 14 d | *S. aureus* Xen36 ATCC 49525, $3 \times 10^5$ CFU in 2 μL | Inoculation in joint space, press-fit insertion of tibial component | X-ray, SEM |
| Heim *et al.*, 2018 | Heterogeneity of $Ly6G^+$ $Ly6C^+$ myeloid-derived suppressor cell infiltrates during *Staphylococcus aureus* biofilm infection | Male and female C57BL/6 | 8 weeks | 3, 7, 14 and 28 d | *S. aureus* USA300 LAC 13c, $10^3$ CFU | Inoculation at the implant tip, femoral intramedullary nail protruding in the joint | Flow cytometry |
| Thompson *et al.*, 2018 | Mouse model of Gram-negative prosthetic joint infection reveals therapeutic targets | Male C57BL/6 | 6-8 weeks | 1, 3, 7, 14 and 21 d | *P. aeruginosa* Xen41 (PAO1) and *E. coli* Xen14 (WS2572) | Inoculated in the knee joint, femoral intramedullary K-wire protruding in the joint (0.5 mm) | μCT, histology, CFU counts (implant and tissue), cytokines |
| Pickett *et al.*, 2018 | Molecularly specific detection of bacterial lipoteichoic acid for diagnosis of prosthetic joint infection of the bone | Male C57BL/6 | 6 weeks | 3, 7, 14 and 21 d | *S. aureus* FPR3757 and its isogenic SpA-mutant, $10^3$ CFU in 2 μL | Inoculated in the knee joint, femoral intramedullary K-wire protruding in the joint (0.5 mm) | Flow cytometry, BLI, PET imaging |

**Table 5b. Classification of the peri-prosthetic joint-implant infection mouse models.**

| Reference | Title | Microbiological status, gender, strain | Age | Time points | Bacterial strain, inoculum size, volume | Inoculation method, placement of the device | Evaluation |
|---|---|---|---|---|---|---|---|
| de Mesy Bentley *et al.*, 2017 | Evidence of *S. aureus* deformation, proliferation, and migration in canaliculi of live cortical bone in murine models of osteomyelitis | Female BALB/c J | 8-10 weeks | 14 d | *S. aureus* UAMS-1, $5 \times 10^5$ CFU | Pre-inoculation of pins | TEM, SEM |
| Carli *et al.*, 2017 | Quantification of peri-implant bacterial load and *in vivo* biofilm formation in an innovative, clinically representative mouse model of periprosthetic joint infection | C57BL/6 | 12 weeks | 7, 14, 21, 28, 35 and 42 d | *S. aureus* Xen36, $3 \times 10^5$ CFU, 2 μL | Inoculation in joint space, press-fit insertion of tibial component | X-ray, SEM, weight, crystal violet, serum amyloid |
| Hedge *et al.*, 2017 | Single-dose, preoperative vitamin-D supplementation decreases infection in a mouse model of periprosthetic joint infection | Male C57BL/6J | 4 weeks | | *S. aureus* Xen36 ATCC 49525, $10^3$CFU in 2 μL | Pipetted in the joint space, femoral intramedullary nail protruding in the joint (1 mm) | IVIS |
| Mandell *et al.*, 2017 | Elimination of antibiotic resistant surgical implant biofilms using an engineered cationic amphipathic peptide WLBU2 | Female C57BL/6J | 12 weeks | 3 d | *S. aureus* SH1000, $10^6$ CFU in 10 μL | Inoculation at the joint, femoral intramedullary nail protruding in the joint (1 mm) | CFU counts (femur and implant) |
| Peng *et al.*, 2017 | *S. aureus* biofilm elicits the expansion, activation, and polarisation of myeloid-derived suppressor cells *in vivo* and *in vitro* | Male C57BL/6J-Tg | 12 weeks | 8 d | *S. aureus* ATCC 43300, $2 \times 10^3$ CFU | Inoculation in joint space, femoral intramedullary nail | SEM, flow cytometry, RT-PCR, immunofluorescence staining, confocal microscopy |
| Thompson *et al.*, 2017 | Oral-only linezolid-rifampin is highly effective compared with other antibiotics for periprosthetic joint infection | Male C57BL/6 | 6-8 weeks | 0, 7, 14, 21, 28, 35 and 42 d | *S. aureus* SAP23, $10^3$ CFU in 2 μL | Inoculation in intramedullary cavity, femoral intramedullary nail protruding in the joint (1 mm) | BLI, CFU counts (tissue and implant), X-ray, μCT |
| Wang *et al.*, 2017a | Preclinical evaluation of photoacoustic imaging as a novel non-invasive approach to detect an orthopaedic implant infection | Male C57BL/6 | 10 weeks | 1, 2, 3 and 4 d | *S. aureus* Xen36 ATCC 49525, $10^3$ CFU in 2 μL | Inoculation in intramedullary cavity, femoral intramedullary nail protruding in the joint (1 mm) | BLI, FLI |
| Ashbaugh *et al.*, 2016 | Polymeric nanofiber coating with tunable combinatorial antibiotic delivery prevents biofilm-associated infection *in vivo* | Male C57BL/6 | 10 weeks | 3, 7 and 14 d | *S. aureus* Xen36, $10^3$ CFU in 2 μL | Pipetted in the top of the implant, femoral intramedullary nail protruding in the joint (1 mm) | BLI, CFU counts (tissue and implant), SEM, X-ray, μCT |
| Kaur *et al.*, 2016 | *In vivo* assessment of phage and linezolid-based implant coatings for treatment of MRSA mediated orthopaedic device related infections | Female BALB/c | 4-6 weeks | 1, 3, 5, 7, 10, 15 and 20 d | *S. aureus* 43300, 10 μL of $10^5$, $10^6$, $10^7$, $10^8$ CFU/mL | Injection at the joint space, femoral intramedullary nail protruding in the joint | Histopathology, CFU counts (tissue and implant), cytokines levels, screening of resistant mutants, healing parameters |
| Stavrakis *et al.*, 2016 | *In vivo* efficacy of a "smart" antimicrobial implant coating | Male C57BL/6 | 12 weeks | 0, 1, 3, 5, 7, 10, 14 and 21 d | *S. aureus* Xen36, $10^3$ CFU in 2 μL | Inoculation in intramedullary cavity, intramedullary nail in the femur | BLI, CFU counts (tissue and implant), X-ray |
| Vidlak and Kielian, 2016 | Infectious dose dictates the host response during *S. aureus* orthopaedic-implant biofilm infection | Male IL-12p40 KO and C57BL/6 WT | 8 to 12 weeks | 7 and 14 d | *S. aureus* USA300 LAC, $10^3$ or $10^5$ CFU | Inoculation at the implant tip, femoral intramedullary nail protruding in the joint (1 mm) | CFU counts (tissue, joint, femur and implant), flow cytometry, multianalyte microbead arrays |
| Heim *et al.*, 2015a | IL-10 production by MDS cells contributes to bacterial persistence during *S. aureus* orthopaedic biofilm infection | Male IL10GFP, IL-10 KO and C57BL/6 | 8 weeks | 3, 7 and 14 d | *S. aureus* USA300, $10^3$ CFU | Inoculation at implant tip, femoral intramedullary nail protruding in the joint (1 mm) | ELISA IL-10, flow cytometry, CFU count (tissue, joint and femur), multianalyte microbead, qRT-PCR |

**Table 5c. Classification of the peri-prosthetic joint-implant infection mouse models.**

| Reference | Title | Microbiological status, gender, strain | Age | Time points | Bacterial strain, inoculum size, volume | Inoculation method, placement of the device | Evaluation |
|---|---|---|---|---|---|---|---|
| Heim *et al.*, 2015b | IL-12 promotes MDS cell recruitment and bacterial persistence during *S. aureus* orthopaedic implant infection | Male C57BL/6NCr | 8 weeks | 7, 14, 21 and 28 d | *S. aureus* USA300 LAC, $10^3$ CFU | Inoculation at the implant tip, femoral intramedullary nail protruding into the joint (1 mm) | Flow cytometry, CFU counts (tissue, joint and femur), qRT-PCR, μCT, histology, ELISA |
| Young *et al.*, 2015 | Regional intraosseous administration of prophylactic antibiotics is more effective than systemic administration in a mouse model of TKA | Female CD1 | 7-9 weeks | 1, 2, 3 and 4 d | *S. aureus* Xen36 ATCC 49525, $5 \times 10^6$ CFU in 2 μL | Inoculation in intramedullary cavity, femoral intramedullary nail protruding into the joint (1 mm) | CFU counts (tissue), BLI |
| Scherr *et al.*, 2015 | *S. aureus* biofilms induce macrophage dysfunction through leukocidin AB and alpha-toxin | Male C57BL/6 | 8 weeks | 3 and 7 d | *S. aureus* USA LAC 13c, Δhla, ΔlukAB, or ΔlukAB Δhla, $10^3$ CFU | Inoculation at the implant tip, femoral intramedullary nail protruding into the joint (1 mm) | Flow cytometry, CFU counts (tissue, joint, femur) |
| Bernthal *et al.*, 2014 | Combined *in vivo* optical and μCT imaging to monitor infection, inflammation, and bone anatomy in an orthopaedic implant infection in mice | Male LysEGFP mice | 12 weeks | 2, 5, 14, 19, 28 and 48 d | *S. aureus* Xen29 ATCC 12600, $10^3$ CFU in 2 μL | Inoculation in intramedullary cavity, femoral intramedullary nail protruding into the joint (1 mm) | μCT, BLI |
| Heim *et al.*, 2014 | Myeloid-derived suppressor cells contribute to *S. aureus* orthopaedic biofilm infection | Male C57BL/6 | 8 weeks | 7 and 14 d | *S. aureus* USA300 LAC, $10^3$ CFU | Pre-incubation of the implant, femoral intramedullary nail protruding into the joint (1 mm) | SEM, flow cytometry, μCT, histology, milliplex multianalyte bead array, qRT-PCR, T-cell proliferation assay |
| Niska *et al.*, 2013 | Vancomycin-rifampin combination therapy has enhanced efficacy against an experimental *S. aureus* PJI | Male C57BL/6J | 8 weeks | 0, 7, 14, 21, 28, 35, 42 and 49 d | *S. aureus* Xen36 ATCC 49525, $10^4$ CFU in 2 μL | Inoculation in joint space, femoral intramedullary nail protruding into the joint (1 mm) | BLI, X-ray, CFU counts (tissue and implant), histology |
| Niska *et al.*, 2012a | Monitoring bacterial burden, inflammation and bone damage longitudinally using optical and μCT imaging in an orthopaedic implant infection in mice | Male LysEGFP mice with green myeloid cells | 12 weeks | 0, 7, 14, 21, 28, 35 and 49 d | *S. aureus* Xen29 ATCC 12600, $10^3$ CFU in 2 μL | Inoculation in joint space, femoral intramedullary nail protruding into the joint (1 mm) | CFU counts (femur and implant), histology, μCT imaging, X-ray, BLI |
| Niska *et al.*, 2012b | Daptomycin and tigecycline have broader effective dose ranges than vancomycin as prophylaxis against a *S. aureus* surgical implant infection in mice | Male C57BL/6 | 12 weeks | 0, 3 and 7 d | *S. aureus* Xen36 ATCC 49525 and *S. aureus* USA300, $10^4$ CFU in 2 μL | Inoculation in joint space, femoral intramedullary nail protruding into the joint (1 mm) | BLI, X-ray, CFU counts (joint tissue and implant), SEM |
| Pribaz *et al.*, 2012 | Mouse model of chronic post-arthroplasty infection: non-invasive *in vivo* bioluminescence imaging to monitor bacterial burden for long-term study | Male C57BL/6 and male LysEGFP with eGFP myeloid cells | 12 weeks | 0, 3, 7, 14, 21, 28, 35 and 42 d | *S. aureus* ALC290614, Xen2915, Xen4016 and Xen36, $10^2$, $10^3$, $10^4$ CFU in 2 μL | Inoculation in joint space, femoral intramedullary nail protruding into the joint (1 mm) | BLI, SEM, CFU counts (implant) |
| Bernthal *et al.*, 2010 | Protective role of IL-1b against post-arthroplasty *S. aureus* infection | Male C57BL/6J, IL-1b-deficient and TLR2-deficient | 12 weeks | 7 and 42 d | *S. aureus* Xen36, $10^3$ CFU in 2 μL | Pipetted in the joint, femoral intramedullary nail protruding into the joint (1 mm) | BLI, SEM, histology, myeloperoxidase activity |
| Bernthal *et al.*, 2010 | A mouse model of post-arthroplasty *S. aureus* joint infection to evaluate *in vivo* the efficacy of antimicrobial implant coatings | Male C57BL/6 and LysEGFP | 12 weeks | 0, 1, 3, 5, 7 and 10 d | *S. aureus* SH1000, $5 \times 10^2$, $5 \times 10^3$, $5 \times 10^4$ CFU in 2 μL | Inoculation in joint space, femoral intramedullary nail protruding into the joint (1 mm) | IVIS, histology, SEM |

**Table 6a. Classification of bone-fracture-related infection mouse models.**

| Reference | Title | Microbiological status, gender, strain | Age | Time points | Bacterial strain, inoculum size, volume | Inoculation method, defect size, placement of the device | Evaluation |
|---|---|---|---|---|---|---|---|
| Cahill *et al.*, 2021 | Locally delivered adjuvant biofilm-penetrating antibiotics rescue impaired endochondral fracture healing caused by MRSA infection | Male C57BL/6 | 10-12 weeks | 3, 7, 14 and 28 d | *S. aureus*, $10^6$ CFU in 2 μL | Inoculation in the fracture gap, not mentioned, intramedullary nail in the tibia | CFU counts (tissue and implant), X-ray, histology, μCT |
| Lindsay *et al.*, 2021 | MnTE-2-PyP disrupts *S. aureus* biofilms in a novel fracture model | Male C57BL/6 | 25-30 weeks | 14 d | *S. aureus* ATCC 29213, $10^4$ CFU in 10 μL | Inoculation in the fracture gap, not mentioned, intramedullary nail in the femur | CFU counts (tibia and implant) |
| Büren *et al.*, 2019 | Histological score for degrees of severity in an implant-associated infection model in mice | Female BALB/c | 10-12 weeks | 7, 14 and 28 d | *S. aureus* ATCC 29213, $10^3$ CFU in 1 μL | Inoculation in intramedullary cavity, diameter of 0.22 mm, 4-holes fixation plate next to the femur | Histology |
| Johnson *et al.*, 2019 | Lysostaphin and BMP-2 co-delivery reduces *S. aureus* infection and regenerates critical-sized segmental bone defects | Male C57BL/6 | 10-12 weeks | | *S. aureus* UAMS-1 (ATCC 49230) and Xen29 | Pre-inoculation of the radial scaffold, fracture gap of 2.5 mm, 4 mm scaffold in the radius | μCT, histology, flow cytometry, cytokines, mechanical test, CFU counts (implant and tissue), X-ray |
| Rochford *et al.*, 2019 | Infection burden and immunological responses are equivalent for polymeric and metallic implant materials in vitro and in a murine model of fracture-related infection | SPF female C57BL/6 and BALB/c | 20-28 weeks | 1, 3 and 7 d | *S. aureus* JAR 06.01.31, $9 \times 10^5$ CFU/pin | Pre-inoculation of plate, diameter of 0.44 mm, 4-holes fixation plate next to the femur | Histology, CFU counts (implant, femur, soft tissue), cytokines, qRT-PCR |
| Trombetta *et al.*, 2019a | Calcium phosphate spacers for the local delivery of sitafloxacin and rifampin to treat orthopaedic infections: efficacy and proof of concept in a mouse model of single-stage revision of device-associated osteomyelitis | Female BALB/cJ | 13-15 weeks | 0, 7, 14, 21, 28 and 70 d | *S. aureus* Xen36 ATCC 49525, $2.5 \times 10^6$ CFU/mL | Pre-incubation of titanium screw, diameter of 0.67 mm, 6-holes fixation plate next to the femur | BLI, CRP, SEM, X-ray, CFU counts (femur, tissue, device) |
| Trombetta *et al.*, 2019b | A murine femoral osteoctomy model with hardware exchange to assess antibiotic-impregnated spacers for implant associated osteomyelitis | Female BALB/cJ | 23-25 weeks | 0, 7, 14 and 19 d | *S. aureus* Xen36 ATCC 49525, $2.5 \times 10^6$ CFU/mL | Pre-incubation of the titanium screw for 20 min, diameter of 0.67 mm, 6-holes fixation plate next to the femur | BLI, X-ray, CFU counts (femur, tissue, and device), SEM |
| Oezel *et al.*, 2019 | Effect of antibiotic infused calcium sulfate/hydroxyapatite (CAS/HA) insets on implant- associated osteitis in a femur fracture model in mice | Female BALB/cJ | 10-12 weeks | 7 and 42 d | *S. aureus* ATCC 29213, $1.35 \times 10^5$ CFU in 1 μL | Inoculation in the fracture gap, diameter of 0.22 mm, 6-holes fixation plate next to the femur | CFU count (tissue), IL-6 quantification, PMN, AP levels |

**Table 6b. Classification of bone-fracture-related infection mouse models.**

| Reference | Title | Microbiological status, gender, strain | Age | Time points | Bacterial strain, inoculum size, volume | Inoculation method, defect size, placement of the device | Evaluation |
|---|---|---|---|---|---|---|---|
| Büren *et al.*, 2018 | Effect of hyperbaric oxygen therapy (HBO) on implant-associated osteitis in a femur fracture model in mice | Female BALB/c | 10-12 weeks | 7 and 14 d | *S. aureus* ATCC 29213, $1.94 \times 10^3$ CFU in 1 μL | Inoculation in the fracture gap, diameter of 0.22 mm, 4-holes fixation plate next to the femur | CFU counts (lavage), X-ray, IL-6, NETs, AP, PINP |
| Johnson *et al.*, 2018 | Hydrogel delivery of lysostaphin eliminates orthopaedic implant infection by *S. aureus* and supports fracture healing | Male C57BL/6 | 10-12 weeks | 7 d | *S. aureus* USA300 and UAMS-1, $1.5 \times 10^8$ CFU/mL | Pre-inoculation of implant, fracture at femoral mid-diaphysis, femoral intramedullary nail | μCT, histology, CFU counts (tissue, femur, nail), cytokines |
| Yokogawa *et al.*, 2018 | Immunotherapy synergises with debridement and antibiotic therapy in a murine 1-stage exchange model of MRSA implant-associated osteomyelitis | Female BALB/cJ | 10 weeks | 7 and 14 d | *S. aureus* USA300 LAC:*lux*, $10^5$ CFU | Pre-incubation of screw, 4-holes fixation plate next to the femur | CFU counts (device), μCT, histology, X-rays |
| Sabaté Brescó *et al.*, 2017 | Influence of fracture stability on *S. epidermidis* and *S. aureus* infection in a murine femoral fracture model | SPF female C57BL/6 and BALB/c | 20-28 weeks | 3, 7, 14 and 30 d | *S. epidermidis* Epi 103.1, $10^4$ CFU in 2.5 μL; *S. aureus* JAR06.01.31, $10^3$ CFU in 2.5 μL | Inoculation in the fracture gap, diameter of 0.44 mm, 4-holes fixation plate next to the femur | CFU counts (femur, tissue, implant), histology, SEM, light microscopy BB stained, weight |
| Rochford *et al.*, 2016 | Monitoring immune responses in a mouse model of fracture fixation with and without *S. aureus* osteomyelitis | SPF female C57BL/6 | 20-28 weeks | 1, 3, 7, 14, 21, 28 and 35 d | *S. aureus* JAR 06.01.31, $4 \times 10^8$ CFU/mL | Pre-incubation of plate for 20 min, diameter of 0.44 mm, 4-holes fixation plate next to the femur | CFU counts (femur, tissue, implant), flow cytometry assay, RT-PCR, cytokines, X-ray, histology |
| Inzana *et al.*, 2015a | 3D printed bioceramics for dual antibiotic delivery to treat implant-associated bone infection | Female BALB/c J | 13-15 weeks | 0, 1, 4, 7, 10, 13, 16, 19, 22, 25 and 28 d | *S. aureus* Xen36 ATCC 49525, $8 \times 10^4$ CFU/mL | Incubation of collagen sheet for 2 h, diameter of 0.67 mm, 6-holes fixation plate next to the femur | BLI, X-ray, SEM, CFU counts (femur, tissue, implant) |
| Inzana *et al.*, 2015b | A novel murine model of established staphylococcal bone infection in the presence of a fracture fixation plate to study therapies utilizing antibiotic-laden spacers after revision surgery | Female BALB/cJ | 13-15 weeks | 0, 1, 5, 7, 10 and 14 d | *S. aureus* Xen36 ATCC 49525, $8 \times 10^4$ CFU/mL | Incubation of collagen sheet for 2 h, diameter of 0.67 mm, 6-holes fixation plate next to the femur | BLI, X-ray, decalcified histology, SEM, μCT, CFU counts (femur, tissue, implant) |
| Windolf *et al.*, 2014 | Lysostaphin-coated titan-implants preventing localized osteitis by *S. aureus* in a mouse model | Female BALB/c | 10-12 weeks | 7 and 14 d | *S. aureus* ATCC 29213, $1.94 \times 10^3$ CFU in 1 μL | Inoculation in the fracture gap, diameter of 0.22 mm, 4-holes fixation plate next to the femur | CFU counts, X-ray, flow cytometry, ELISA (IL-6) |
| Windolf *et al.*, 2013 | Implant-associated localized osteitis in murine femur fracture by biofilm forming *S. aureus*: a novel experimental model | Female BALB/c | 10-12 weeks | 0, 7, 14 and 21 d | *S. aureus* ATCC 29213, $10^3$ CFU in 1 μL | Inoculation in the fracture gap, diameter of 0.22 mm, 4-holes fixation plate next to the femur | Histology, SEM, ELISA (IL-6), CFU counts, flow cytometry, X-ray |

unicortical defect are also included. Tables 3, 4 and 5 also list the type of device and placement of the device. In Table 5, the type of diabetes induced is also included. Table 6 also includes the size of the fracture, type of device and placement of the device.

## Analysis of the data

### Characteristics of the mouse

The studies retrieved in the systematic search have used mice with different characteristics such as inbred strain, age and gender. Differences in mouse strain, age, gender, microbiome composition and the use of conventional or SPF animals could influence the osteomyelitis and fracture healing process. Therefore, it is important to take these characteristics into account to properly choose the animal model.

Inbred mouse strains harbour differences in bone density and bone length. Bone composition differs among inbred mouse strains. For instance, the femur density of C57BL/6J mice (0.45 mg/mm$^3$) is significantly lower than that of C3H/HeJ mice (0.69 mg/mm$^3$) and of BALB/c mice (0.55 mg/mm$^3$). Interestingly, the femur of C3H/HeJ mice is significantly shorter than that of BALB/c and C57BL/6J mice at all ages measured (Beamer *et al.*, 1996; Kohler *et al.*, 2005). Most researchers selected C57BL/6 (59 %) or BALB/c (28 %) mice for osteomyelitis studies (Fig. 3**a**). Regarding infection development, in a fracture-related infection study using *S. epidermidis*, BALB/c mice showed larger bacterial counts and formation of larger abscesses compared to C57BL/6 mice (Sabaté Brescó *et al.*, 2017). In cases of infection with *S. aureus*, opposite results were observed regarding the ability of C57BL/6 and BALB/c mice to clear the infection in a bone-implant-related infection study (Nishitani *et al.*, 2015b; Prabhakara *et al.*, 2011b). The authors observed that 58 %, 50 % and 75 % of the BALB/c mice cleared the infection at 21, 28 and 49 d post-infection, respectively; while 100 % of the C57BL/6 mice were unable to clear the infection even 49 d post-infection (Prabhakara *et al.*, 2011b). Moreover, a study comparing *S. aureus* infection, using a bioluminescent *S. aureus* strain, in C57BL/6 and BALB/c mice only showed a brief peak of high intensity bioluminescence at 3 d in the BALB/c strain, characterising active infection, while the C57BL/6 showed high bioluminescence intensity that extended from day 3 through day 7 (Nishitani *et al.*, 2015b). The immune system of C57BL/6 and BALB/c mice differs (Sellers *et al.*, 2012), with C57BL/6 mice being more differentiated towards a Th1-like phenotype

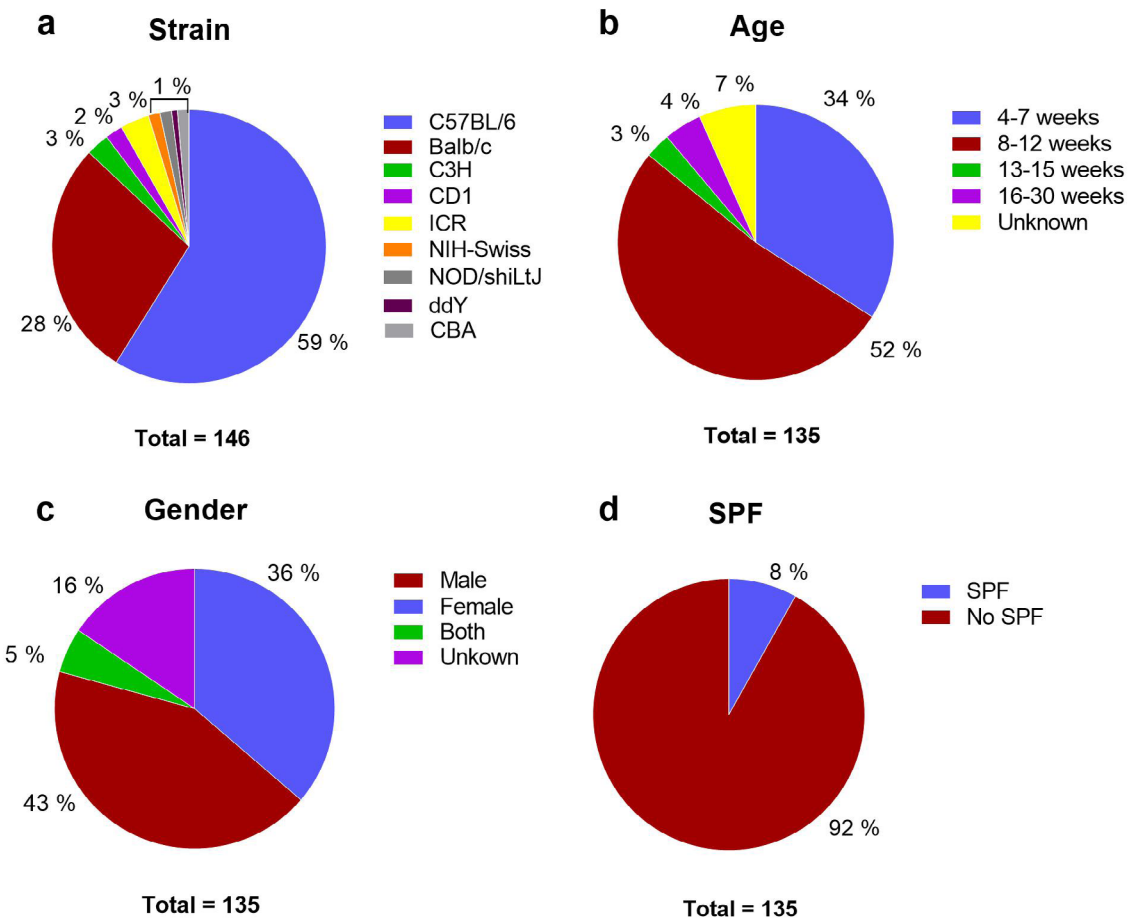


**Fig. 3. Classification of the osteomyelitis mouse models by (a) mouse strain, (b) age, (c) gender and (d) SPF.** 135 studies were included in the graphs. In panel **a**, some studies included more than one inbred strain. Therefore, there is a total number of 146 studies.

and BALB/c mice towards a Th2-like phenotype in the presence of an *S. aureus* infection (Prabhakara *et al*., 2011b). This needs to be further investigated to understand the response in each mouse strain and allow the researcher to choose the proper mouse strain for a study.

The animal ages determines to the quality of their bones and the time required for complete healing of a fracture (Ferguson *et al*., 2003; Haffner-Luntzer *et al*., 2016). A faster healing process will reduce the risk and period of the infection. Mice are sexually mature at 6-8 weeks of age (Jilka, 2013). Therefore, mice of this age (34 %) or slightly older (9-12 weeks, 52 %) are often selected for osteomyelitis studies because their bones are no longer growing (Fig. 3**b**). Some authors emphasise the importance of using older mice, 16-30 weeks old, when the animals reach skeletal maturity (Rochford *et al*., 2016; Sabaté Brescó *et al*., 2017); however, those are less often used (7 %). The skeletal maturity is characterised by the larger size and greater strength of the bones but also by the degree of mineralisation (Ferguson *et al*., 2003). The peak of mineralisation is not achieved until an age of 20 weeks in C57BL/6 mice (Brodt *et al*., 1999; Ferguson *et al*., 2003).

The animal gender may also influence the healing of the bone and development of infection. For example, hormonal cycles in the females can have a significant influence on bone repair. On the other hand, males are more territorial and may require separate cages to avoid fighting, making them more labour-intensive and expensive to keep (Mills and Simpson, 2012). Of the osteomyelitis *in vivo* studies collected in the present review, 36 % used male mice, 43 % used female mice, 5 % used both genders and 16 % did not mention the gender (Fig. 3**c**).

The gut microbiome is composed of a wide range of species of microorganisms, including bacteria, yeast and viruses, and provides essential health benefits to its host, particularly by regulating the immune homeostasis (Vlasova *et al*., 2019). A recent study has revealed that changes in the gut microbiome can influence the development of bone infections in mice (Hernandez *et al*., 2019). Mice with a disrupted microbiome are more likely to develop a bone infection than mice with a non-modified microbiome; moreover, mice with a disrupted microbiome also show a reduced immune response to the infection (Hernandez *et al*., 2019). However, more research is necessary to better understand how the gut microbiome influences the response to the infection and help researchers to decide on the optimal features of the mouse strain to select for an *in vivo* study (Hernandez *et al*., 2019). Moreover, to reduce the presence of unwanted infections affecting the experiments, some researchers prefer to use SPF animals. The use of SPF animals has the additional benefits of being cost-saving as it minimises the number of animals used for a study (Letson *et al*., 2019). However, SPF animals may have undesired changes in their immune system that may be linked to modifications in their gut microbiome (Letson *et al*., 2019). 8 % of the studies analysed in the present review chose SPF mice for their *in vivo* osteomyelitis studies (Funao *et al*., 2016; Horst *et al*., 2012; Isogai *et al*., 2020; Rochford *et al*., 2016; Sabaté Brescó *et al*., 2017; Szafranska *et al*., 2014) but in 92 % of studies conventional mice were used (Fig. 3**d**).

**Bacterial species related to osteomyelitis**

*S. aureus* has been the main bacterial species chosen (90 %) for *in vivo* experiments because it is the most common pathogen causing osteomyelitis (Kavanagh *et al*., 2018; Fig. 4**a**). Its ability to cause osteomyelitis is related to the presence of features, known as virulence factors, that allow the bacteria to attach to bones and foreign bodies and form biofilms, to evade the immune system and to cause harmful toxic effects. These virulence factors can be classified by their function as adherence factors, immunomodulatory factors, enzymes and toxins. In the present review, relevant virulence factors were identified and further described below.

Adherence virulence factors such as bacterial adhesins or coagulase can be crucial for bacterial attachment and establishment of an infection. Bacterial adhesins are proteins present on the bacterial surface that can interact with and bind to eukaryotic extracellular (matrix) proteins. Among these adhesins, Cna, FnbA and FnbB are relevant for tissue colonisation and development of bone infections. FnbA and FnbB are present in 98 % and 99 % of clinical isolates from osteomyelitis, respectively (Arciola *et al*., 2005a). An *in vivo* mouse study has shown the essential role of Cna in the bone colonisation by comparing the infectivity of the *S. aureus* UAMS-1 (ATCC 49230) strain expressing Cna and FnbA and its isogenic Cna mutant known as *S. aureus* UAMS-237 (Elasri *et al*., 2002). The strain UAMS-1 is an isolate derived from the clinical strain USA200 and is one of the most widely used *S. aureus* strains in osteomyelitis research (Li *et al*., 2008). Only the Cna positive bacterial strain was able to colonise the murine tibia (Elasri *et al*., 2002). Thus, to be able to establish an infection in the bone it is necessary to use a Cna positive strain.

Immune evasion is also an important virulence factor for bacteria to establish and maintain the infection in the bone. *S. aureus* has developed strategies to persist and evade clearance by the immune system and establish a chronic bone infection (Tuchscherr *et al*., 2017). For example, SigB is an important transcription factor contributing to the avoidance of bacterial clearance by the immune response (Tuchscherr *et al*., 2017). *S. aureus* lacking SigB induces large numbers of small abscesses, which contributes to the elimination of the bacteria in murine osteomyelitis (Tuchscherr *et al*., 2017). The study also showed that a deletion of *sigB* results in a reduced production of SarA (Tuchscherr *et al*.,

2017). SarA plays a key role in the establishment of the osteomyelitis in a haematogenous murine model (Blevins *et al*., 2003). A deletion of *sarA* in *S. aureus* UAMS-1 and *S. aureus* RN6390 results in a significantly reduced number of CFU compared to the wild-type strains (Blevins *et al*., 2003).

The extent of bone destruction caused by the infection is also related to virulence factors such as toxins, *e.g.* PSMs. PSMs are amphipathic peptides with functions as cytotoxins and pro-inflammatory inducers (Cassat *et al*., 2013). The role of PSMs was studied in an osteomyelitis mouse model indicating that PSMs cause osteoblast cell death and contribute to the destruction of the bone (Cassat *et al*., 2013; Loughran *et al*., 2016).

Although antimicrobial resistance is not a virulence factor, in certain situations it is a key factor in the development of an infection and it may be considered to be a virulence-like factor. Antimicrobial resistance plays a key role in persistent osteomyelitis due to the fast development of resistance to multiple antibiotics and the difficulty in treating these infections, causing a persistent osteomyelitis. MRSA is responsible for 40-60 % of all *S. aureus* infections. Therefore, several authors chose MRSA strains for the osteomyelitis mouse model (Jørgensen *et al*., 2014; Loughran *et al*., 2016). In addition, it is important to consider the antimicrobial resistance profile of the bacterial strain when testing antimicrobial strategies. Nevertheless, the resistant strain needs to be virulent enough, with the presence of virulence factors such as adhesins, to establish an infection in the first place.

90 % of the mouse osteomyelitis studies included in the present review were focused on *S. aureus* infections (Fig. 4**a**). However, other bacterial pathogens can cause osteomyelitis and can also be used to establish an infection and further understand the pathophysiology of the disease. For example, Sabaté Brescó *et al.* (2017) compared the development of fracture-related infection caused by *S. aureus* JAR 06.01.31 and *S. epidermidis* 103.1. Compared to *S. aureus*, *S. epidermidis* infection was less intense, leading to fewer bacteria, causing less bone damage and affecting less the animals' weight. Tomizawa *et al.* (2020) compared the pathogenic potential of an *S. epidermidis* strain RP62a *versus S. aureus* strain USA300, both methicillin-resistant strains, in a bone-implant-related infection mouse model. As expected, *S. aureus* caused a more aggressive and damaging osteomyelitis than *S. epidermidis*. Nevertheless, *S. epidermidis* formed a large biofilm on the implant and caused less inflammation than *S. aureus*.

Shandley *et al*. (2012) aimed to establish a bone-implant-related infection in mice with *S. aureus*, *P. aeruginosa* and *K. pneumoniae* to evaluate the antimicrobial activity of hyperbaric oxygen therapy. Their results showed that *P. aeruginosa* and *S. aureus* are equally capable of establishing the infection in the bone. However, *K. pneumoniae* was not able to infect the bone well and was cleared before infection

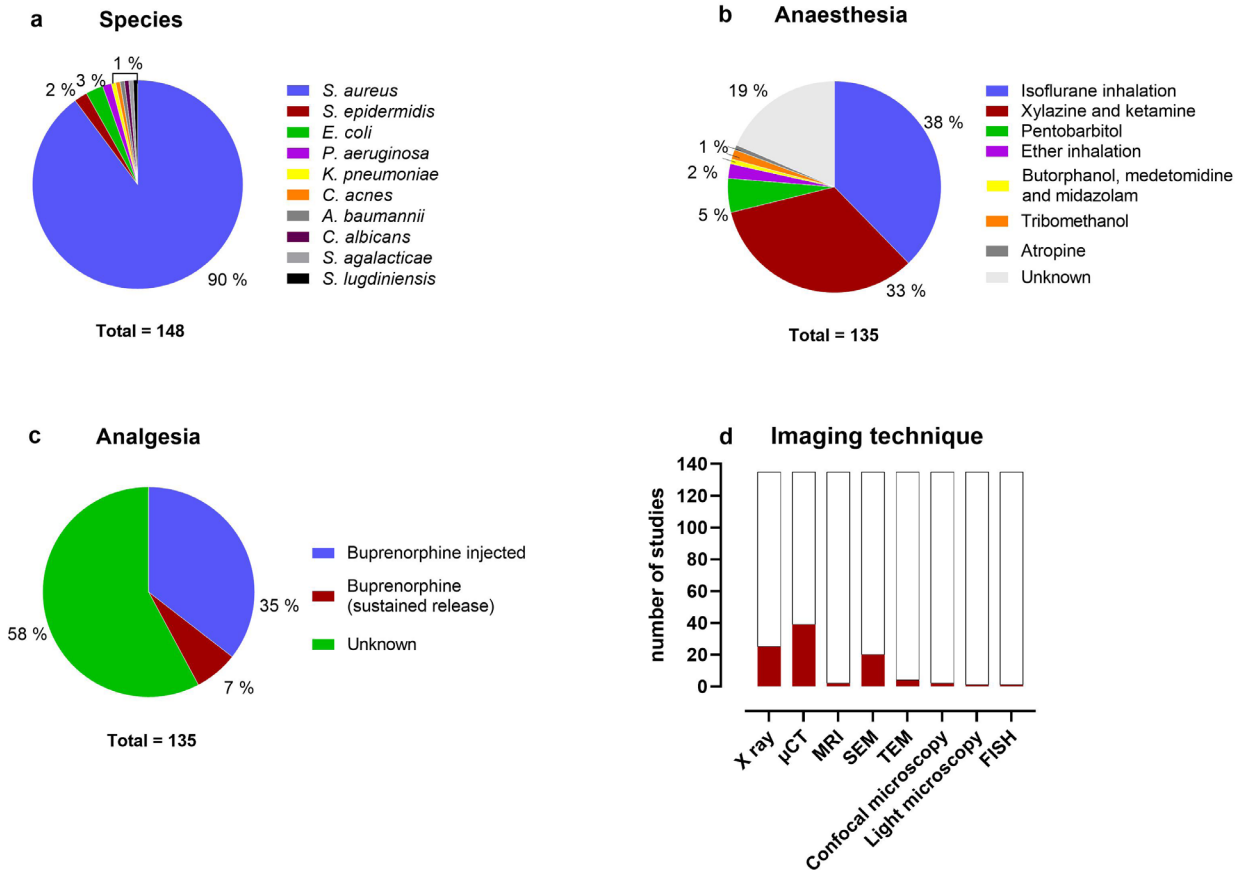


**Fig. 4. Classification of the osteomyelitis mouse models by (a) bacterial or fungal pathogen used to infect the animals, (b) image technique used to assess the infection, (c) anaesthesia used to perform the surgery and (d) analgesia used after the surgery.** 135 studies were included in the graphs.

was established. Boles *et al*. (2018) established a polymicrobial infection with *S. aureus* UAMS-1 and *E. coli* ATCC 25922 in a mouse implant infection model. *E. coli* was not found either in bones or on implants after 7 d.

Crane *et al*. (2009) studied the efficacy of colistin beads in an implant-related osteomyelitis mouse model infected with *S. aureus* or *A. baumannii* clinical isolates. In contrast to the osteolytic response in the presence of *S. aureus*, *A. baumannii* caused an osteoblastic bone formation response around the infected devices. *S. aureus* was also associated with the presence of biofilm in necrotic bone sections, whereas no biofilm was found in the necrotic tissue in the animals infected with *A. baumannii* (Crane *et al*., 2009). Shiono *et al*. (2016) studied the development of osteomyelitis by *C. acnes* with and without a titanium bone implant. *C. acnes* survived attached to the implant for 6 months, causing a delayed infection, while it only survived 28 d in the control group without an implant (Shiono *et al*., 2016). Masters a *et al*. (2021) studied the pathogenesis of *S. agalacticae versus S. aureus* in a bone implant infection model. Their results showed that *S. agalacticae* colonies were only retrieved from the soft tissue and bone but not from the implant after 14 d of infection. *S. agalacticae* caused less osteolysis and no loss of weight compared to *S. aureus*. Moreover, their TEM images revealed the vasculotropic pathogenesis of *S. agalacticae* compared to the osteotropic behaviour of *S. aureus* (Masters *et al*., 2021).

To summarise, it is advisable to consider all of these bacterial features (*e.g.* bacterial species, virulence factors and antimicrobial resistance profile) when choosing the appropriate bacterial strain for the intended *in vivo* osteomyelitis mouse studies. In addition, the use is recommended of a strain with a well-documented origin, phenotypic and genotypic profile (and to ensure availability of the strain in view of repeatability and reproducibility of the experiments), proved pathogenicity of the strain and strain characteristics (*e.g.* biofilm formation, panel of adhesins, bacterial toxins and antimicrobial resistance) (Moriarty *et al*., 2019).

**Inoculation method and dose**

Depending on the research question, the bacterial inoculum can be administered in different ways. To mimic a contamination during trauma or surgery, the inoculum can be administered during implantation or defect/fracture formation by pipetting it onto the wound site or applying it using an injector along or in the vicinity of the implant, bone defect or fracture (Thompson *et al*., 2017). It is advisable to use a low volume for the inoculum to prevent dispersion of the inoculum to other tissues. Therefore, 56 of the studies analysed in the present review used a small inoculum between 1 and 5 μL (Tables 2-6).

To mimic a device contamination, the devices are pre-inoculated with the bacterial strain overnight or briefly before surgery (de Mesy Bentley *et al*., 2017; Ishikawa *et al*., 2017; Li *et al*., 2008; 2017; Pribaz *et al*., 2012; Thompson *et al*., 2017). This method can be applied to evaluate the antimicrobial efficacy of contact-killing or antifouling surfaces (Ishikawa *et al*., 2017). Moreover, the pre-inoculation of the device can be used to create established biofilms to study an advanced stage of the infection and to evaluate more challenging antimicrobial treatment regimes. Nevertheless, it is advisable to not use a pre-inoculation method to evaluate the antimicrobial activity of a drug delivery system because the device may release the drug before the surgical implantation and the bacteria may be killed prior to implantation.

The injury can also be contaminated from the insertion of a surgical material into the wound such as a pre-inoculated silk suture (Yoshii, 2002a; Yoshii *et al*., 2002b), pre-inoculated agarose beads (Marriott *et al*., 2004; Marriott *et al*., 2005) or a pre-inoculated collagen sheet (Inzana *et al*., 2015b).

To mimic a late infection or haematogenous infection, the inoculum is injected into the bloodstream at a later point, for example, *via* the lateral tail vein (Blevins *et al*., 2003; Chadha *et al*., 1999; Elasri *et al*., 2002; Horst *et al*., 2012; Szafranska *et al*., 2014; Tuchscherr *et al*., 2017; Yoon *et al*., 1999) or the retro-orbital sinus (Potter *et al*., 2020; Wang *et al*., 2017c). In these models, a larger inoculum volume, between 100 and 1,000 μL, is used to allow the inoculum to distribute throughout the bloodstream thus mimicking the haematogenous model.

In general, to create an osteomyelitis mouse model, it is advisable to perform dose-determining studies to establish the dose required to initiate a bone infection. The data collected in the present review show that a certain range of both injection volumes and numbers of CFU are used to establish a bone infection (Tables 1-6).

**Anaesthesia and analgesia in osteomyelitis models**

The discomfort of the animals must be maximally reduced for ethical reasons but also because of the potentially adverse influence on experimental outcomes (Moriarty *et al*., 2019). Mouse anaesthesia demands a thorough knowledge of the mouse physiology and of the pharmacology of the anaesthetics and analgesics in the animals. Depending on the objectives of the experimental procedure, anaesthetics and analgesics can be administered through injection or inhalation (Adams and Pacharinsak, 2015; Gargiulo *et al*., 2012). In this section, the anaesthetics and analgesics that have been used for these osteomyelitis mouse models will be discussed.

In 40 % of the 135 studies considered in the present review, mice were anaesthetised by inhalation and in 60 % by injection. Inhaled anaesthetics, such as isoflurane, require the use of nose-cone ventilation during surgery, limiting the possibility of adjusting the mouse position, which usually is necessary to create a bone defect or fracture. Inhalation anaesthesia provides greater safety for prolonged

procedures than injectable anaesthetics to maintain the animals in an anaesthesia of sufficient depth. Moreover, inhaled anaesthetics provide more control on the dose administered to the animal and are associated with a quicker recovery compared to injectable anaesthetics (Buitrago *et al*., 2008). In the osteomyelitis mouse studies, 38 % of the studies used isoflurane and only 2 studies (2 %) used ether as inhaled anaesthetic (Yoshii *et al*., 2002a; 2002b, Fig. 4**b**). Injectable anaesthetics permit an easier manipulation of the animals during the surgical procedure, where the animals can undergo various positional changes during the process of creation of bone defect or fracture, which may be required for the placement of a fixation device (nail or plate). However, for longer surgical procedures, the use of inhaled anaesthetics is recommended to avoid the animals awakening during surgery. The most common injectable anaesthetics used within the osteomyelitis mouse models were the combination of xylazine and ketamine (33 %), which are inexpensive, easy to administer and pose no health risks to the researchers (Fig. 4**b**). Moreover, this combination provides good immobilisation with, additionally, a certain degree of analgesia. Unfortunately, the injectable anaesthetics may present a higher risk of overdose and cardiovascular and respiratory depression that may lead to an increased animal mortality (Buitrago *et al*., 2008).

Regarding the analgesics, they are administered before and after the surgical procedure. 35 % of the studies injected between 0.01 and 0.05 mg/kg of buprenorphine (Pribaz *et al*., 2012; Shandley *et al*., 2012). In several studies (7 %), a polymeric matrix with buprenorphine was inserted into the wound to provide a sustained release of the drug for 72 h to minimise any additional distress (Niska *et al*., 2012a; Stavrakis *et al*., 2016; Wang *et al*., 2017a; Fig. 4**c**). However, in most of the studies (58 %), the analgesic procedure used was not specified.

**Osteomyelitis evaluation assays**

The development of an infection in the bone and surrounding tissue and its effects on the tissue can be evaluated using different techniques. Most authors performed similar assays to analyse the development of infection in the osteomyelitis mouse models. These techniques were classified into three categories: (i) quantification of the infection development, (ii) image analysis and (iii) histomorphological analysis.

*Quantification of the infection development*

To evaluate how the infection develops over time, it is advisable to perform a quantification of the number of bacteria present at different time points. 80 of the studies (59 %) evaluated the infection development by euthanising the animals at different time points, collecting bones, implants, surrounding tissues and/or organs and performing microbial culture to quantify the numbers of CFU (Kaur *et al*., 2016; Nishitani *et al*., 2015b; Niska *et al*., 2012a; Tomizawa *et al*., 2020a; Young *et al*., 2015).

The quantification of infection can also be performed by qRT-PCR (Crane *et al*., 2009; Li *et al*., 2008; Wagner *et al*., 2016). This method allows distinguishing and quantifying between different bacterial species and is even considered to discriminate metabolically active and dormant bacteria.

Other authors used a non-invasive *in vivo* quantification method with BLI of bacteria to follow the infection development in single animals over time. The use of bioluminescent bacteria means that fewer animals are needed because the same animal can, in principle, be used to assess the degree of the infection at every time point over the course of the experiment (Bernthal *et al*., 2010; Li *et al*., 2008; Pribaz *et al*., 2012). One limitation of the bioluminescence technique is the loss of signal during the experiment due to the possible loss of the plasmid that carries the bioluminescence *lux* in the bacterial strain. Therefore, the use of a bacterial strain with *lux* inserted in the chromosome is advisable to not lose the bioluminescence signal over time. However, the bioluminescent signal can also disappear due to metabolic inactivity of the bacteria, which may be the consequence of biofilm formation. This will also happen with strains carrying *lux* in their chromosome. Therefore, this limitation should always be kept in mind when using bioluminescence monitoring of infections. The number of CFU, as derived from the bioluminescence readings at the last time point, should always be confirmed by comparison with the actual numbers of cultured CFU obtained from the specimens following animal sacrifice.

The following examples illustrate the possible difficulty in interpreting bioluminescence signals. The *S. aureus* ALC 2906 strain, which carries the bioluminescence construct on a chloramphenicol-resistance-gene-containing plasmid, had a detectable bioluminescence signal at 10 d in a PJI mouse model. Then, the plasmid was lost due to the lack of pressure for antibiotic selection by chloramphenicol (Pribaz *et al*., 2012). On the other hand, *S. aureus* Xen 36 strain (ATCC 45925 as genetic background) had higher bioluminescence signals than Xen 40 strain (UAMS-1 as genetic background) but there were no differences in biofilm formation between the strains nor in numbers of CFUs cultured from the implant at 42 d post-infection (Pribaz *et al*., 2012). It is also important to consider that the bioluminescence signal intensity has been reported to be up to 10-fold higher in BALB/c mice than in C57BL/6 mice due to the differences in light absorption in the respective white *versus* black pigmented skin and hairs of these mouse strains (Nishitani *et al*., 2015b).

A novel imaging modality based on ultrasound, known as photoacoustic imaging, was also used to follow the development of an infection (Wang *et al*., 2017a). In this technique, laser pulses are

directed into the body at a specific wavelength to excite a photoacoustic tracer molecule present in the target tissue. The authors conjugated the tracer molecule indocyanine green to beta-cyclodextrin, a polysaccharide taken up by bacteria but not by host cells. Photoacoustic imaging provided significantly deeper tissue penetration (30-50 mm) than BLI (10-20 mm) (Wang *et al*., 2017a).

*Image analysis*

Advanced imaging techniques such as conventional radiography (Carli *et al*., 2018; Rochford *et al*., 2016), μCT (Niska *et al*., 2012a) and MRI (Horst *et al*., 2012) provide three-dimensional images of the bone structure. In most cases, these techniques were used to evaluate the structural effects of the infection in the bone (*e.g.* bone destruction and inflammation) and on the fracture healing process (Fig. 4**d**). These methods of visualisation were also used to check proper placement of the orthopaedic device upon implantation (Trombetta *et al*., 2019a). In addition, μCT scans can reveal detailed information about tissue mineral density, total callus volume and bone volume fraction of the callus, allowing for evaluation of the bone regeneration process after trauma or fracture. Although μCT scans can also be applied *in vivo*, *ex vivo* μCT scans provide a significantly higher resolution because *ex vivo* a higher dose of X-ray irradiation can be used (Bernthal *et al*., 2014; Laperre *et al*., 2011; Niska *et al*., 2012a).

MRI is one of the imaging modalities of choice for osteomyelitis diagnosis in humans because it provides excellent anatomical detail and it is non-invasive and highly sensitive for detecting an early infection. Horst *et al*. (2012) used MRI to monitor the development of the osteomyelitis during the acute phase of the infection in mice and its progression into a chronic infection. MRI allowed studying the presence of inflammation as well as the bone thickness and deformation in the mouse tibia (Horst *et al*., 2012).

Other imaging techniques used on *ex vivo* samples are SEM (16 %), TEM (3 %) and confocal microscopy (1 %). Several authors have used SEM to evaluate the bacterial biofilm formation on the surface of the bone tissue or/and inserted devices (Carli *et al*., 2018; Sabaté Brescó *et al*., 2017; Trombetta *et al*., 2019a; Windolf *et al*., 2013). TEM can also be used to obtain bone tissue images with a higher magnification and resolution than SEM. For example, de Mesy Bentley *et al.* (2017) used TEM to assess and analyse the invasion of *S. aureus* into the bone and the remodelling of the bone tissue. Moreover, the use of TEM has shown the formation of *S. aureus* colonies within the non-mineralised collagen matrix and located intracellularly within neutrophils (Masters *et al*., 2021).

*Histomorphological analysis*

Histological staining methods were developed to assess and analyse the progression of infection in the bone and the remodelling process of the bone fracture and surrounding tissues (Rochford *et al*., 2016; Sabaté Brescó *et al*., 2017; Windolf *et al*., 2013; Yokogawa *et al*., 2018). This technique can identify bacteria and distinguish between different cell types such as osteoblasts, osteoclasts and neutrophils as well as between structural features of the infected tissue. These structural changes in the tissues are well-established for humans and are used to diagnose osteomyelitis in clinical practice.

The histological examination of the osteomyelitis mouse model developed by Horst *et al*. (2012) was performed during the acute and chronic phase of the osteomyelitis and compared to histological tissue samples from a patient with acute osteomyelitis and a patient with chronic osteomyelitis. The histological sections revealed a massive influx of granulocytes, with an intense bacterial colonisation and necrosis, during acute infection at 7 d that was similar to that seen in the human acute osteomyelitis sections. At 21 d, in the stage of chronic infection, the mouse sections revealed osteoclastic resorption with new bone formation similar to the human chronic osteomyelitis sections (Horst *et al*., 2012). Another osteomyelitis mouse study, that used histological staining, included a scoring system of the sections according to the level of cells infiltration, with scores of 0 for no osteomyelitis, 1 for minimal or rare (< 10 % tissue involvement), 2 for mild (10-20 %) and 3 for frequent (20-50 %) osteomyelitis (Lee *et al*., 2002). Haematoxylin and eosin straining was performed to stain tissue and cells, Gram staining for bacteria. Similarly, Büren *et al.* (2019) developed a standardised histological score system for a bone-fracture-related infection model to evaluate the severity of the infection in the mouse. Their score system evaluated 4 independent histological parameters: (i) presence of callus, (ii) consolidation of the osteotomy, (iii) structural changes of the medullary cavity, (iv) number of bacteria. The presence of callus and the consolidation of the osteotomy were evaluated using haematoxylin-eosin staining and the quantification of bacteria was performed following Giemsa staining (Büren *et al*., 2019). These examples illustrate the usefulness of histological scoring systems for a semi-quantitative evaluation of histology in mouse osteomyelitis models.

**Literature review of osteomyelitis mouse models**

135 osteomyelitis infection mouse studies were collected, analysed and classified into the following 5 categories: (i) haematogenous osteomyelitis (11 %), (ii) post-traumatic osteomyelitis (22 %), (iii) bone-implant-related infection (28 %), (iv) PJI (26 %), (v) fracture-related infection (13 %) (Fig. 5**a**). The haematogenous osteomyelitis models are characterised by the bacterial or fungal colonisation of the bone through the bloodstream. The post-traumatic osteomyelitis models represent the local infection of the bone following unicortical defect or trauma. The bone-implant-related infection models

mimic the development of an infection in the presence of a foreign body in the bone. The PJI models mimic the development of an infection in the presence of a device in the bone and synovial fluid. The fracture-related infection models represent the development of an infection in a bone fracture. The authors studied the course of the infection either in the femur (58 %), tibia (37 %), femur and tibia (2 %), humerus (1 %) or radius (1 %) (Fig. 5**b**). The mouse femur was selected more often than the tibia, for several reasons. The femur is tubular, larger and thicker than the tibia, thus facilitating the insertion of large devices. Moreover, the curvature of the tibia may complicate the insertion of longer devices. Lastly, the proximity of the fibula to the tibia can influence the development of the infection and the healing of the bone.

*Haematogenous osteomyelitis mouse models*

Haematogenous osteomyelitis takes place following a symptomatic or asymptomatic bloodstream infection that allows the pathogen to reach the bone. Worldwide incidence of haematogenous osteomyelitis is 1:1,000-20,000 people, with half of the cases occurring in children younger than 5 years (Popescu *et al*., 2020).

Generally, microorganisms will arrive at the metaphyses of long bones (*i.e.* femur or tibia), since these are highly vascularised. The lower fluid flow at the bone metaphysis allows the microorganism to establish an infection and cause local inflammation. In the haematogenous mouse infection models' studies reviewed, the inoculum volume used to establish the infection was between 100 and 150 µL and a dose between $10^6$ and $10^8$ CFU, with the inoculum administered by injection *via* the retro-orbital venous sinus, intravenously or *via* the lateral tail vein (Table 1; Fig. 6**a**). 33 % of the bone haematogenous infection studies evaluated the presence of infection in the femur, 40 % in the tibia and 20 % in both tibia and femur (Fig. 7**a**). In most of the haematogenous studies, no trauma or fracture was caused nor was a device inserted into the bones of the animals before the inoculation. There were 2 studies where a fracture or a trauma was caused before the inoculation of the infection (Chadha *et al*., 1999; Yoon *et al*., 1999) and in 1 study a haematogenous infection in a bone implant was studied (Wang *et al*., 2017c).

A haematogenous osteomyelitis model was developed to study the contribution of *S. aureus* Cna to the capacity of the bacteria to reach the bone from the bloodstream and cause an osteomyelitis (Elasri *et al*., 2002). The authors infected NIH Swiss mice with a 100 µL inoculum containing $10^8$ CFU of *S. aureus* UAMS-1 or its isogenic Cna mutant strain UAMS-237 injected *via* the lateral tail vein. Their results showed that the mutation of Cna limited the capacity of *S. aureus* to cause osteomyelitis through the haematogenous route. Another study with a similar set up (150 µL inoculum of $10^6$ CFU of *S. aureus* ATCC 53657 injected in the lateral tail vein) described a biphasic development of the bacterial infection. There was an acute phase of infection in the tibiae during the first 2 weeks followed by a chronic phase until the termination at 60 d (Horst *et al*., 2012).

Tuchscherr *et al*. (2017) studied the role of *sigB* in the development of a chronic osteomyelitis infection. They used a mouse model based on studies by Horst *et al.* (2012) and infected the animals with 150 µL of $10^6$ CFUs *via* the lateral tail vein. Mice were infected with *S. aureus* LS1, *S. aureus* LS1 with *sigB* deleted and *S. aureus* LS1 *sigB*-deleted strain complemented for this deletion. Their results demonstrated the importance of *sigB* to establish osteomyelitis through the haematogenous route (Tuchscherr *et al*., 2017).

Wang *et al*. (2017c) developed a well-described model to mimic a haematogenous infection with an implanted device. They used male C57BL/6 mice and inoculated *S. aureus* SAP231 intravenously through the retro-orbital sinus 21 d after the implantation of a pin in the bone. All mice challenged with either $10^6$ CFU or $5 \times 10^6$ CFU inoculum survived the bacterial challenge. An inoculum of $10^7$ CFU was too large and killed several animals. However, not all the inoculated mice developed the hematogenous implant infection because at 28 d post-inoculation there were no detectable CFU from the implants or surrounding tissues (Wang *et al*., 2017c).

In general, bone haematogenous infection models were successfully developed in the mouse and allowed for studying the essential bacterial features to establish an acute or chronic bone infection.

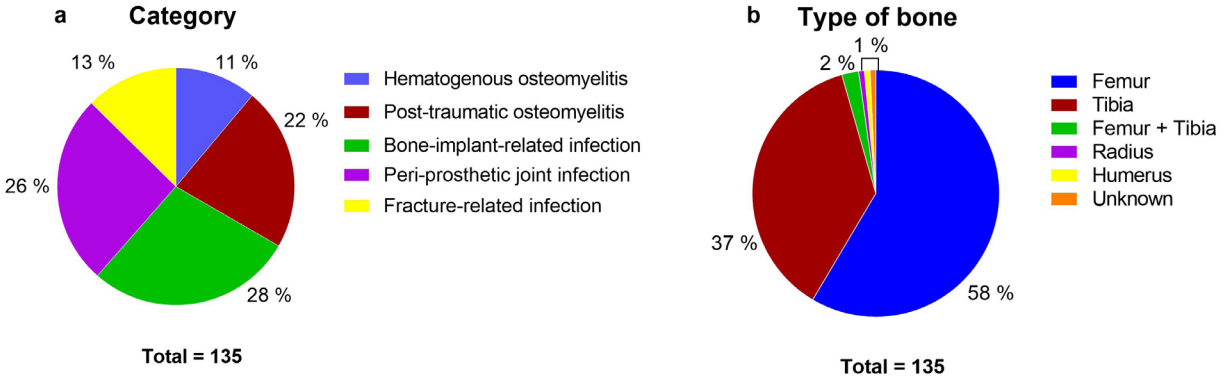


**Fig. 5. Classification of the osteomyelitis mouse models by (a) categories and by (b) type of bone infected**. 135 studies were included in the graphs.

*Post-traumatic osteomyelitis mouse models*

Osteomyelitis can occur after trauma even without the insertion of a fixation device (Table 2; Fig. 6**b**). The incidence of osteomyelitis following open fractures is reported to be 1-30 %, depending significantly on the grade of trauma and the type of treatment administered (Metsemakers *et al.*, 2015).

The post-traumatic osteomyelitis studies that have been included in this review have in common the creation of a unicortical bone defect and the local infection of the defect with 0.5 to 2 µL of bacterial inoculum containing $10^5$ to $10^8$ CFU as inoculum. Such a small volume of inoculum is recommended to prevent the diffusion of the inoculum to the contiguous tissues and to better mimic the real situation occurring in patients. The unicortical defect was a perforation only affecting one lateral side of the bone, with a size that ranged from 0.5 to 1.5 mm of diameter (Table 2, Fig. 6**b**). In 57 % of the post-traumatic osteomyelitis studies the defect was created in the mouse femur and in 43 % in the tibia (Fig. 7**b**).

The post-traumatic osteomyelitis mouse models were used to study different virulence factors involved in the pathogenesis of the osteomyelitis as described previously (Cassat *et al.*, 2013; Isogai *et al.*, 2020; Loughran *et al.*, 2016; Wilde *et al.*, 2015; Xiao *et al.*, 2017). The models were also used to study the effects of the immune response in clearing

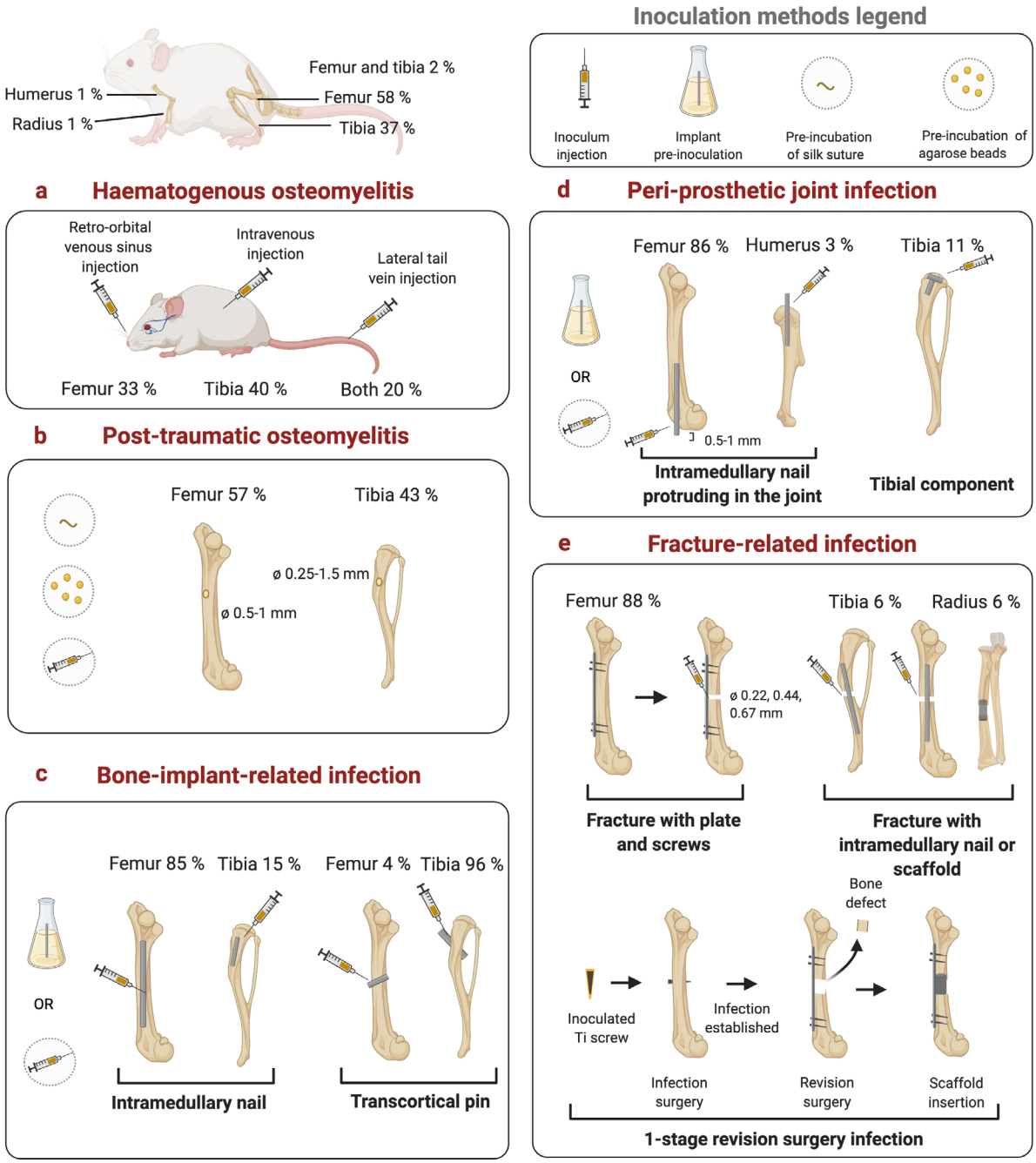


**Fig. 6. Schematic representation of mouse models to induce bone infections and osteomyelitis based on the results of the literature search.** (**a**) Haematogenous osteomyelitis, (**b**) post-traumatic osteomyelitis, (**c**) bone-implant-related infection, (**d**) PJI, (**e**) fracture-related infection. Ø: diameter.

the infection and in the repair of the bone damage (Chen *et al.*, 2017; Marriott *et al.*, 2004; Putnam *et al.*, 2019; Wagner *et al.*, 2019; Yoshii *et al.*, 2002b). For example, Marriot *et al.* (2004; 2005) developed a trauma-induced staphylococcal osteomyelitis model to study the inflammatory response of osteoblasts to infection. They created a bone defect in the bone cortex, inoculated with $10^3$ CFU of *S. aureus* UAMS-1 in agarose beads, and evaluated inflammatory mediators' levels for 4 d. An increase in the level of the cytokines IL-6 and MCP1 by the osteoblasts was measured in the animals infected with *S. aureus*. The positive recruitment of macrophages by the MCP1 to clear the infection also had the negative consequence of an increased inflammation with bone damage (Marriott *et al.*, 2004; 2005). An increase in the levels of IL-6 was also observed in a study where a silk suture, pre-inoculated with $10^5$ CFU of a clinical isolate of *S. aureus*, was inserted into the tibia of ICR mice (Yoshii *et al.*, 2002b). This resulted in a local elevated level of the cytokines IL-6 and IL-1β in the early phase of the infection related to the bone damage, which was followed by an increase in TNFα and IL-4 in a later phase of the infection (Yoshii *et al.*, 2002b). Putnam *et al.* (2019) studied the host immune pathways that contribute to bacterial immunity but also to bone destruction during *S. aureus* osteomyelitis. They created a bone defect in C5BL/6J wild type and

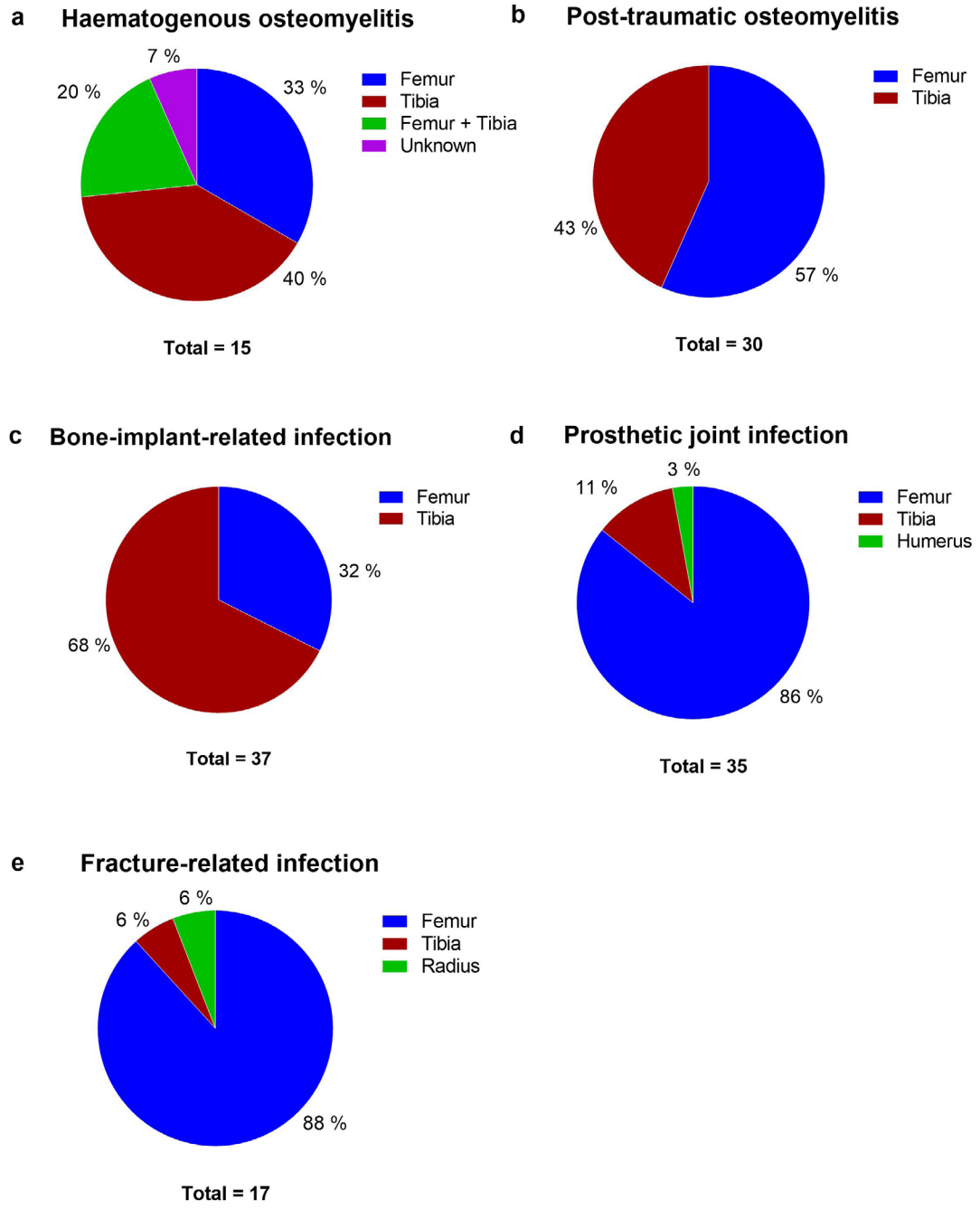


**Fig. 7. Type of bone infected (tibia, femur or both) in each category.** (**a**) Haematogenous osteomyelitis, (**b**) post-traumatic osteomyelitis, (**c**) bone-implant-related infection, (**d**) PJI, (**e**) fracture-related infection. 135 studies were included in the graphs.

in MyD88$^{-/-}$ and IL1r1$^{-/-}$ knock-out mice, infected them with a 2 μL inoculum containing $10^6$ CFU of *S. aureus* AH1263 strain and measured cytokine levels after 14 d. They discovered an essential role of IL-1R to control the local bacterial replication during osteomyelitis and IL-1R contribution to bone destruction. Specifically, they demonstrated that there is an increase in the numbers of osteoclasts residing on the bone surface during the infection (Putnam *et al*., 2019).

The post-traumatic osteomyelitis models were used to evaluate the efficacy of antimicrobial and anti-inflammatory strategies to prevent and treat both bone infection and inflammation (Funao *et al*., 2012; Lu *et al*., 2019; Takahashi *et al*., 2008; Wagner *et al*., 2016; Wu *et al*., 2018; Zhu *et al*., 2019). Funao *et al*. (2012) established a real-time, quantitative and reproducible osteomyelitis mouse model using the bioluminescent bacterial strain *S. aureus* Xen 29. They perforated the femur to simulate an osteotomy, injected a 1 μL inoculum containing $10^8$ CFU in the medullar cavity and followed the infection *in vivo* (Funao *et al*., 2012). Wagner *et al*. (2016) created a mouse model to analyse bone loss and regeneration following *S. aureus* bone infection and treatment. They inoculated C57BL/6 mice tibiae with 2 × $10^3$ CFU of *S. aureus* Rosenbach 1884 and, after 14 d, performed debridement and applied antibiotic therapy. The treatment group showed complete eradication of the bacteria, whereas the infection persisted in the control group (Wagner *et al*., 2016). Wu *et al.* (2018) used a post-traumatic osteomyelitis mouse model to evaluate the efficacy of the immune modulator baicalin to prevent bone destruction by regulating the toll-like receptor 2. They inoculated BALB/c male mice with 1 μL of $10^8$ CFU of *S. aureus* ATCC 43300 with or without baicalin and showed that baicalin reduced the destruction of the bone (Wu *et al*., 2018). Lu *et al*. (2019) developed a bone defect infection mouse model in ICR/JCL with 2 μL of $10^6$ CFU of *S. aureus* ATCC 6538 to evaluate the efficacy of intravenous injection of the antibiotic gentamicin combined with a photodynamic therapy as a treatment for osteomyelitis (Lu *et al*., 2019).

In conclusion, post-traumatic osteomyelitis mouse models can be used to elucidate the pathophysiology of the bone infection. They can be used to study the influence of the bacterial virulence factors or the influence of the infection in the immune system activation causing an increased bone damage.

*Bone-implant-related infection mouse models*

The presence of a foreign body, such as a bone implant, increases the risk of infection because the implant acts as a niche for bacterial colonisation and compromises the local immune response against the bacteria. An established bone-implant-related infection mouse model to study the pathophysiology of the bone implant infection is the intramedullary implant model (Table 3; Fig. 6**c**). This method basically consists of the implantation of a K-wire, a pin or a nail into the intramedullary canal of the femur or tibia, combined with a bacterial inoculum (Table 3, Fig. 6**c**). Other studies have described the transcortical insertion of a pin into the femur or tibia that in some cases was bent at both ends to increase the device stability (Jørgensen *et al*., 2014; Li *et al*., 2008; Prabhakara *et al*., 2011a). The bacterial inoculum was applied directly into the femoral or tibial insertion site to mimic a contamination during surgery (Funao *et al*., 2016). Alternatively, the device was pre-inoculated before insertion into the bone to mimic the contamination of the device (Jørgensen *et al*., 2014). In 68 % of the studies, the implant was inserted in the tibia of the animals and in 32 % in the femur (Fig. 7**c**). These bone-implant-related infection mouse models were used to study different pathophysiological mechanisms of osteomyelitis related to bone implants. For example, a recent study revealed that *S. aureus* bacteria can colonise very small spaces in the bone such as canaliculi and osteocyte lacunae of cortical bone, sites in the bone which are difficult for immune cells to reach (de Mesy Bentley *et al*., 2017). These models were also applied to study different pathways and aspects of the immune response to the infection and the implant (Prabhakara *et al*., 2011a; Prabhakara *et al*., 2011b).

The models were also extensively used to evaluate the efficacy of antimicrobial compounds administered either systemically (Jørgensen *et al*., 2016; Li *et al*., 2008) or locally at the site of infection (Crane *et al*., 2009; Funao *et al*., 2016; Wells *et al*., 2018; Zhang *et al*., 2019a). Novel strategies for preventing or treating infection, such as passive immunisation (Varrone *et al*., 2014), hyperbaric oxygen therapy (Jørgensen *et al*., 2017; Shandley *et al*., 2012) and antimicrobial peptides (Choe *et al*., 2015), were also evaluated using these models.

In conclusion, the bone implant infection models allow for the study of the different interactions that occur between implant, infection and immune response in the bone environment and can be used to evaluate the efficacy of antimicrobials administrated systemically or locally at the implant site. However, in these models there is no fracture nor device replacement to enable the study of the healing process in the presence of infection and implant. The fracture itself also influences the clearance of the infection. Hence, the model does not allow for studies on revision surgery with debridement and lavage or for evaluating antimicrobial devices used to treat infected bone tissue after removal of a contaminated device.

*Bone-implant-related infections in diabetic mouse models*

Diabetes is one of the most relevant risk factors in implant-related infection and its prevalence is growing worldwide (Berendt *et al*., 2008). Diabetes is a disease in which high blood glucose levels occur. It can be due to a loss of the insulin-producing β-cells in the pancreas islets, known as T1D, or to insulin resistance due to a glucose-enriched diet, known as T2D (Farnsworth *et al*., 2015). Both T1D

and T2D animal models are used to study diabetic complications, such as osteomyelitis, and their potential treatment.

Lovati *et al*. (2013) were the first to describe a diabetic bone-implant-related infection mouse model (Table 4). They compared the development of bone implant infection in the T1D diabetic mouse strain diabetic NOD/ShiLtJ and in non-diabetic CD1 mice (Lovati *et al*., 2013). Their results showed that the same bacterial inoculum of $10^3$ CFU of *S. aureus* ATCC 25923 induced bone-implant infection in the diabetic mice but not in the wild type mice. This animal model may be a useful tool for *in vivo* testing of treatment strategies in diabetic and non-diabetic individuals. Moreover, the authors showed the synergistic effects of the vasodilator PGE1 with an antibiotic, as a co-treatment for bone-implant infection in diabetic mice (Lovati *et al*., 2014).

Farnsworth *et al.* (2015) studied the risk factors of orthopaedic infections for diabetic patients by comparing the development of bone implant infection and adaptative immunity in T1D and T2D male C57BL/6J mice. The T1D model was induced using a toxic agent that selectively destroys the beta pancreatic cells (*i.e.* streptozotozin) eliminating the insulin production. The T2D model consisted of 5 week old mice that received a high-fat diet (60 % kcal). To confirm the hyperglycaemia, the glucose levels were measured at several time points. Then, the investigators inserted a surgical wire into the tibia of the animals that had already been inoculated with *S. aureus* Xen 36. Results showed that T2D mice had a more severe *S. aureus* osteomyelitis than T1D mice (Farnsworth *et al*., 2015).

*PJI mouse models*

PJI following total joint arthroplasty of the hip or knee, despite the low incidence of 1-2 %, is still associated with a large burden in orthopaedic surgery. The PJI mouse models' studies considered in the present review principally describe the insertion of a pin into the intramedullary canal that protrudes 0.5-1 mm into the joint (Table 5, Fig. 6**d**, Heim *et al*., 2014; Heim *et al*., 2015a; Kaur *et al*., 2016; Thompson *et al*., 2017; Thompson *et al*., 2018). To better mimic the PJI, other studies have developed the tibial component of the knee prosthesis and press-fitted this into the tibia, exposed to the joint space (Carli *et al*., 2017; Carli *et al*., 2018; Hernandez *et al*., 2019). In all the studies, the bacterial inoculum was pipetted or injected into the joint tissue or space to reproduce the principal clinical aetiology through intraoperative contamination (Table 5). 86 % of the studies inserted the device into the femur of the animals, 11 % into the tibia and 3 % into the humerus (Fig. 6**d**, 7**d**).

Bernthal *et al*. (2010) model provided real-time longitudinal tracking of the infection in a post-surgical joint for 10 d by using a bioluminescent *S. aureus* strain and monitoring the inflammation with the use of a mouse line that possesses fluorescent neutrophils, the LysEGFP knock-in mice. They showed a more acute joint infection when the mice were inoculated with $5 \times 10^3$ or $5 \times 10^4$ CFU *versus* a mild infection, resembling a chronic infection, following challenge with a bacterial inoculum of $5 \times 10^2$ CFU. Mice inoculated with 2 μL containing either $5 \times 10^3$ or $5 \times 10^4$ CFU developed an increased bacterial bioluminescent signal corresponding to increased bacterial numbers and marked swelling of the affected leg within 3 d, consistent with an acute joint infection. In contrast, mice inoculated with $5 \times 10^2$ CFU developed a low-grade infection, resembling more a chronic infection (Bernthal *et al*., 2010). This model was further used to compare infection development and biofilm formation with different *S. aureus* strains (Pribaz *et al*., 2012) or by extending the experiment to even 40-49 d to study a chronic infection (Niska *et al*., 2012a; Pribaz *et al*., 2012). Interestingly, the studies described a peak in bioluminescence for bacteria as well as neutrophils at 3 d, corresponding to the acute phase of the infection, and bioluminescence values decreasing over time, corresponding to the chronic phase of the infection. As previously mentioned, a decrease in luminescence does not necessarily correspond to a reduction in bacterial numbers but may well be associated with a lower metabolic activity of the bacteria in the later, chronic stages of infection (Pribaz *et al*., 2012). To provide deeper tissue penetration, a photoacoustic imaging system was applied to monitor the infection in this type of mouse model (Wang *et al*., 2017a). However, this method was only used to study a 4 d infection.

Sheppard *et al*. (2020) developed a mouse model with an implant in the humerus that was also protruding into the joint. The mouse humerus and femur have a similar diameter. In this model, two inoculum doses where evaluated: a lower inoculum of $10^3$ CFU that caused mild osteolysis and a higher inoculum of $10^4$ CFU that caused severe osteolysis and failure of the shoulder.

These models were also extensively used to evaluate the efficacy of antimicrobial compounds administered either systemically (Niska *et al*., 2013) or locally at the site of infection (Bernthal *et al*., 2010; Carli *et al*., 2017; Stavrakis *et al*., 2016; Stavrakis *et al*., 2019; Thompson *et al*., 2017). In a comparative study, local antibiotic administration was shown to be more efficacious than systemic administration (Young *et al*., 2015).

In summary, the PJI mouse models described in this section can reproduce the environment of the clinical condition by either incorporating the prosthetic device into the joint or protruding into joint and inoculating the infection into the joint. However, the small size of the mouse hampers the development of all the parts of the prosthetic device that are used for PJI human patients.

*Fracture-related infection mouse models*

A bone fracture is usually fixed using an intramedullary nail or a fixation plate with bone

screws. The presence of an infection will compromise the immune response and the regeneration of the bone. The incidence of an infection after the fixation of a fracture ranges from 1 % in closed fractures to 30 % in complex open tibial fractures (Metsemakers *et al*., 2015).

To mimic this clinical situation, fracture-related infection mouse models fix a fracture using a fixation plate or an intramedullary nail. In the studies that fix the fracture using a fixation plate and screws, the fixation plate is applied to the long bone with screws, followed by fracture or removal of a part of the bone and challenge with a bacterial inoculum (Table 6, Fig. 6**e**). All the studies using fixation plates apply surgical devices such as the "MouseFix" plate with 4 or 6 screw holes and/or surgical tools such as a Gigli saw to create a fracture size diameter of 0.22, 0.44 or 0.67 mm (RISystem, Davos, Switzerland). Alternatively, the studies that fix the fracture using an intramedullary nail, create the fracture first and then ream the bone pieces using a nail (Cahill *et al*., 2021; Johnson *et al*., 2018). 88 % of the studies analysed created the bone fracture in the femur, 6 % in the tibia and 6 % in the radius (Fig. 6**e**, 7**e**).

Rochford *et al*. (2016) used this type of model to study the immune response during healing in the presence of an infection. They pre-inoculated the fixation device, 20 min before surgery, with $10^5$ CFU/implant of *S. aureus* JAR 06.01.31. Sabaté-Bresco *et al.* (2017) used the same model and showed that stable fracture fixation led to better clearance of infection than unstable fixation. Moreover, the osteotomy gap had healed in the animals with the stable fixation by 30 d post-surgery (Sabaté Brescó *et al*., 2017).

In clinical practice, depending on the infection severity, there are different surgical approaches to treat an infection, such as one-stage or two-stage revision. A one-stage revision consists of one surgical intervention, with implant retraction, debridement and implantation of a new prosthesis. A two-stage revision consists of two surgical interventions: implant retraction, debridement and wound closure in the first stage surgery and, after several weeks, implantation of a new, cemented prosthesis during the second stage surgery. Moreover, a two-stage revision can also consist of implant removal with debridement and application of local antibiotics (spacers/beads) in the first stage and implant placement with antibiotic-loaded bone cement in the second stage.

Different parts of these revision-surgery approaches were mimicked in osteomyelitis mouse studies. For instance, the stage of revision surgery due to infection in the bone fracture fixation infection mouse model was first introduced by Windolf *et al.* (2013; 2014). The authors created a bone fracture fixation mouse model, with lavage and debridement of the infection at 7 and 14 d post-implantation and infection (Windolf *et al*., 2013). In a later study, they used this model to evaluate the treatment efficacy of a PMMA plate coated with the metallo-endopeptidase lysostaphin to prevent *S. aureus* infection (Windolf *et al*., 2014). The model was also used by others to evaluate the efficacy of other antimicrobial materials such as a calcium sulphate withgentamicin bone filler (Oezel *et al*., 2019) or hyperbaric oxygen therapy (Büren *et al*., 2019).

Other authors have developed models with hardware exchange to mimic one-stage revision surgery. For example, Inzana *et al*. (2015b) established a mid-diaphyseal femoral osteotomy repaired using a fixation device that was pre-inoculated with a collagen sheet containing *S. aureus* to initiate the infection. At 7 d post-infection, revision surgery with debridement and placement of an antibiotic-laden spacer was performed and, at 28 d post-infection, the efficacy of this procedure was evaluated. Yokogawa *et al.* (2018) established a similar model to investigate the synergy between systemic vancomycin treatment with immunotherapy. They pre-inoculated a bone screw with *S. aureus* and inserted it into the middle of the femur shaft to establish an infection.

Trombetta *et al.* (2019a) compared one- and two-stage revision surgery using a more complex *in vivo* model that more closely resembles the clinical situation. They pre-inoculated a bone screw with *S. aureus* Xen 36 and placed it in the middle of the femur for 7 d to establish an infection. Then, they removed the infected hardware and introduced a fixation device and a PMMA spacer with or without local antibiotic delivery. The delayed treatment of the infection, described in the studies above, is a relevant clinical feature that increases the challenge of efficient bacterial clearance.

Regarding the healing of the fracture, several authors have shown – using X-ray or μCT – a complete bone regeneration in the non-infected group when compared to an infected group of animals (Sabaté Brescó *et al*., 2017; Windolf *et al*., 2013; Windolf *et al*., 2014). Moreover, the bone healing was also observed after 28 d post-osteotomy in the treatment group infected (Windolf *et al*., 2014). Thus, the evaluation of bone healing indicates the progress in the eradication of the infection and osteomyelitis.

To summarise, fracture-related infection models allow the creation of procedures to study a wide spectrum of clinical situations and can be used to study new strategies for the prevention and treatment of osteomyelitis related to orthopaedic bone fixation devices.

## Advantages, limitations and conclusions

The advantages of the osteomyelitis mouse models are the similarity of their bone physiology to that of humans, their relatively low cost, the availability of well-defined inbred strains and molecular and immunological tools as well as the possibility of genetically modifying them.

Mouse models have proven to be adaptable to specific desired model conditions, evolving

from simpler models, such as the post-traumatic osteomyelitis (Funao *et al*., 2012), through the bone-implant infections (Li *et al*., 2008), until more complex models such as the fracture-related infection with hardware exchange (Trombetta *et al*., 2019a; Yokogawa *et al*., 2018). Thus, these *in vivo* mouse models can be applied to study a variety of research questions related to osteomyelitis infection.

Larger animal models such as rabbits, dogs or sheep show more similarities to humans than mouse in their bone microstructure, macrostructure and bone remodelling process (Muschler *et al*., 2010; Pearce *et al*., 2007; Wancket, 2015) and allow the use of implants of a size more closely resembling the actual implants used for humans. Moreover, larger animals such as dogs can tolerate multiple surgical procedures, allowing researchers to study some of the more complex procedures that are performed in humans (Patel *et al*., 2009). However, larger animals are more expensive, as is their maintenance, and they take longer to reach skeletal maturity than mice (Patel *et al*., 2009; Pearce *et al*., 2007).

The use of GM mouse strains and molecular tools allows performing detailed studies on pathways and cells involved in the different mechanisms and processes of a disease, such as the inflammatory response to infections and fractures as well as the healing process. For example, Bernthal *et al.* (2014) used a GM mouse strain with fluorescent neutrophils to follow *in vivo* the inflammatory response to the infection and the presence of the implant. GM mice were also very useful for creating an osteomyelitis diabetic mouse model (Farnsworth *et al*., 2015). Compared to larger animals, a wide range of mice GM lines is available, permitting the study of different aspects of osteomyelitis (Pearce *et al*., 2007).

Mouse models are also relevant to developing new preventive and treatment strategies to control infections. For example, antimicrobial devices might be a promising approach to reduce infections in orthopaedic surgery. Coatings of implants used for fracture stabilisation in rats or mice are less expensive than those used in large animals such as sheep or goats. In fact, many authors have well-described procedures to test the efficacy of antimicrobial coatings in osteomyelitis mouse models (Table 3-6). Such models can be used as a first step in the *in vivo* evaluation of *in vitro* results, to study the distribution of drugs in bones and other organs and to develop new antimicrobials for infection prevention. If the aim of using an antimicrobial device is to prevent an infection, it will be necessary to evaluate its *in vivo* antimicrobial efficacy for at least the first 10 d. But, if the antimicrobial device is meant to be used as a treatment, a longer evaluation will be necessary (Moriarty *et al*., 2019). In any case, an antimicrobial orthopaedic device must prove its antimicrobial efficacy against relevant Gram-positive and Gram-negative pathogens (such as multidrug-resistant bacteria), drug release, lack of inducing excessive inflammatory responses, prevention of bone tissue damage and support of bone healing. The antimicrobial efficacy should be determined by quantification of CFUs on the implant as well as in the bone tissue and surrounding soft tissue at relevant time points. Moreover, the inflammatory response to the device can be determined by measuring the cytokines in the tissue and performing immunohistology. Destruction of the bone tissue can be evaluated using imaging techniques such as μCT or MRI.

Most of the studies analysed established an infection using *S. aureus* clinical strains because *S. aureus* is one of the major osteomyelitis pathogens (Fig. 3**a**). However, it is also relevant to study more in depth the pathophysiology of other devastating bacterial and fungal species related to those that cause osteomyelitis – such as coagulase-negative staphylococcal and streptococcal species, *P. aeruginosa, C. acnes, A. baumannii, C. albicans* – or polymicrobial infections (Bemer *et al*., 2014; Kavanagh *et al*., 2018).

The mortality rate related to these osteomyelitis mouse models varied between studies principally due to the differences in the infective dose, the virulence of the bacterial strain and the type of surgical procedure. Part of the information related to the mortality rates was retrieved from the publications and another part by consulting the authors of studies where no details on mortality were published.

The type of inoculum administration and the infectious dose applied in the animals will directly affect the animal mortality rate. For example, the administration of a localised low inoculum is not expected to cause an invasive spread of the infection (Lloyd Miller, personal communication, 2021). However, if a high infective dose is locally inoculated into the joint or bone, it could cause an invasive haematogenous spread leading to sepsis and, consequently, to the death of the animals (Lloyd Miller, personal communication, 2021). Therefore, it is important to include dose-determining studies to find the proper inoculum to administer to the animals, depending on the final aim of the study.

The haematogenous models with associated sepsis had a high mortality rate of 20-50 % due to the highly infective doses administered that lead to the development of sepsis, infection of other organs or extreme weight loss that necessitated euthanasia (Horst *et al*., 2012; Lorena Tuchscherr, personal communication, 2021). The risk of sepsis development was also affected by the virulence of the bacterial strain used and the susceptibility of the mouse strain infected (Lorena Tuchscherr, personal communication, 2021). In the haematogenous implant study, 3 different bacterial inocula were used ($10^5$ to $10^7$ CFU), where only the largest bacterial inoculum caused a mortality rate of 10 % (Wang *et al*., 2017c).

The post-traumatic infection model, the bone implant infection model and the PJI model in some studies had a mortality rate ranging from 1 to 10 % due to anaesthesia complications during the surgical

procedure (Ford *et al*., 2020, Hernandez *et al*., 2019; Elysia Masters, personal communication, 2021; Tammy Kielian, personal communication, 2021). Other studies did not report any loss of animals with these types of mouse models (Alexandra Stavrakis, personal communication, 2021). In some studies, there was a range of animals used per group "such as 5-8 animals per group" (Ashbaugh *et al*., 2016), which was related to the numbers of animals available to undergo the surgical procedure on different days and not to the mortality rate (Lloyd Miller, personal communication, 2021).

The studies that used fracture-related infection models encountered more complications. In the models with a fracture and an intramedullary nail the mortality was ranging between 5 and 10 % and it was related to surgical complications (Cahill *et al*., 2021; Andres García, personal communication, 2021). In the models with a fracture fixed using a fixation plate, the mortality was related to intraoperative complications (ranging between 2 and 29 %) such as implant misplacement (Sabaté Brescó *et al*., 2017), anaesthesia fatality (Oezel *et al*., 2019; Sabaté Brescó *et al*., 2017; Ceylan Windolf, personal communication, 2021; Fintan Moriarty, personal communication, 2021) or cardiopulmonary instability (Oezel *et al*., 2019). The fatalities were also related to post-operative complications such as fixation device failure (Oezel *et al*., 2019; Sabaté Brescó *et al*., 2017; Ceylan Windolf, personal communication, 2021), fracture of the bone (Fintan Moriarty, personal communication, 2021), secondary infections (Sabaté Brescó *et al*., 2017) or device failure during revision surgery (Trombetta *et al*., 2019b). On the other hand, several other studies did not have any losses of animals (Büren *et al*., 2019; Inzana *et al*., 2015a; Inzana *et al*., 2015b).

Several authors concurred that once the surgical procedure and the infective dose were well-established and the personnel well trained, the mortality encountered was predominately related to the anaesthetics used during the procedure.

Other important features to study in more detail are the bacterial virulence factors related to the disease including the bacterial immune evasion mechanisms to avoid the clearance of the pathogens. The role of the immune response in osteomyelitis is very relevant for future studies considering the importance of the macrophages and neutrophils in the clearance of the infection and in the regeneration of the bone tissue. Understanding the cellular and molecular pathways involved in the recruitment, differentiation and activation of monocytes seems to be a central axis of research in the osteo-immunomodulation response. The mouse models can also be used to investigate how antimicrobial and anti-inflammatory drugs should be applied to the bone to prevent or treat the infection and orchestrate the inflammatory response to enhance the regeneration of the bone tissue.

Additional types of clinical osteomyelitis could also be mimicked using mouse models. For example, Röntgen *et al*. (2010) developed an external fracture fixation mouse model without infection. An infection could be established in this model to study its influence on bone healing with this type of fracture fixation device. Another clinical osteomyelitis model that could be established is the two-stages exchange of contaminated internal fixation hardware. However, the small size of the mouse makes it more challenging to perform multiple surgical procedures. Another interesting aspect for further study is the influence of the microbiome in the predisposition to osteomyelitis and how *e.g.* probiotics could help to reduce the effects of the disease (Hernandez *et al*., 2019). A bone infection could also be merged with other clinical models to try to reproduce models closer to the patient situation. For instance, Zhang *et al*. (2019b) developed a mouse fracture model using 20 to 28 months old mice presenting a *P. aeruginosa* infection in the endotracheal tube. This mimics a hospital-acquired infection due to the endotracheal tube, as occasionally present in patients with a fracture. The next step would be to inoculate the endotracheal tube to cause sepsis and study the ability of pathogens such as *S. aureus* to infect a bone fracture and how to prevent it using prophylaxis. However, it can be foreseen that establishing such a challenging model will be difficult.

The standardisation of the models is highly relevant for study results to be reproducible and comparable between laboratories and to achieve a better translation to the clinic (Coenye *et al*., 2018; Muschler *et al*., 2010). Ideally, standardised models would need to be developed but the wide variety of conditions used in the different models (as described in the present review) indicate that standardisation may be difficult. To allow for full understanding of differences between studies, it is vital to provide very clear and detailed descriptions of the models. For instance, the mouse strain used, animal age, gender, and weight should always be reported. The use of a well-defined bacterial strain, inoculum volume and dose as well as method of administration is also important. In this respect, guidelines defining the minimum study information that needs to be reported would be very useful tools to achieve these goals (Allkja *et al*., 2020; Moriarty *et al*., 2019).

In conclusion, the mouse is an excellent first step *in vivo* model to study the pathogenesis, inflammation and healing process of osteomyelitis with or without implanted medical devices and to evaluate novel prophylaxis and treatment strategies.

## Acknowledgements

Fig. 2,6 were created using BioRender.com. This research is part of the PRINT-AID consortium, which has received funding from the European Union's Horizon 2020 research and innovation program under the Marie Skłodowska-Curie grant agreement number 722467. The authors would like to thank Dr Lloyd Miller, Dr Lorena Tuchscherr, Elysia Masters,

Dr Tammy Kielian, Dr Alexandra Stavrakis, Dr Andres García, Dr Ceylan Windolf and Dr Fintan Moriarty for their personal input in the discussion about the mortality rate of the osteomyelitis mouse models.

## References

Adams S, Pacharinsak C (2015) Mouse anesthesia and analgesia. Curr Protoc Mouse Biol **5**: 51-63.

Aguilera-Correa JJ, Garcia-Casas A, Mediero A, Romera D, Mulero F, Cuevas-López I, Jiménez-Morales A, Esteban J (2020) A new antibiotic-loaded sol-gel can prevent bacterial prosthetic joint infection: from *in vitro* studies to an *in vivo* model. Front Microbiol **10**: 2935. DOI: 10.3389/fmicb.2019.02935.

Allkja J, Bjarnsholt T, Coenye T, Cos P, Fallarero A, Harrison JJ, Lopes SP, Oliver A, Pereira MO, Ramage G, Shirtliff ME, Stoodley P, Webb JS, Zaat SAJ, Goeres DM, Azevedo NF (2020) Minimum information guideline for spectrophotometric and fluorometric methods to assess biofilm formation in microplates. Biofilm **2**: 100010. DOI: 10.1016/j.bioflm.2019.100010.

Arciola CR, Campoccia D, Gamberini S, Baldassarri L, Montanaro L (2005a) Prevalence of *Cna*, *fnbA* and *fnbB* adhesin genes among *Staphylococcus aureus* isolates from orthopedic infections associated to different types of implant. FEMS Microbiol Lett **246**: 81-86.

Arciola CR, An YH, Campoccia D, Donati ME, Montanaro L (2005b) Etiology of implant orthopedic infections: a survey on 1027 clinical isolates. Int J Artif Organs **28**: 1091-1100.

Ashbaugh AG, Jiang X, Zheng J, Tsai AS, Kim WS, Thompson JM, Miller RJ, Shahbazian JH, Wang Y, Dillen CA, Ordonez AA, Chang YS, Jain SK, Jones LC, Sterling RS, Mao H-Q, Miller LS (2016) Polymeric nanofiber coating with tunable combinatorial antibiotic delivery prevents biofilm-associated infection *in vivo*. Proc Natl Acad Sci U S A **113**: E6919-E6928.

Ashman RB, Papadimitriou JM (1991) Chronic osteomyelitis as a consequence of systemic *Candida albicans* infection. Immunol Cell Biol **69**: 427-429.

Beamer WG, Donahue LR, Rosen CJ, Baylink DJ (1996) Genetic variability in adult bone density among inbred strains of mice. Bone **18**: 397-403.

Bemer P, Plouzeau C, Tande D, Leger J, Giraudeau B, Valentin AS, Jolivet-Gougeon A, Vincent P, Corvec S, Gibaud S, Juvin ME, Hery-Arnaud G, Lemarie C, Kempf M, Bret L, Quentin R, Coffre C, de Pinieux G, Bernard L, Burucoa C, the Centre de Référence des Infections Osteo-articulaires du Grand Ouest (CRIOGO) Study Team (2014) Evaluation of 16S rRNA gene PCR sensitivity and specificity for diagnosis of prosthetic joint infection: a prospective multicenter cross-sectional study. J Clin Microbiol **52**: 3583-3589.

Berendt AR, Peters EJG, Bakker K, Embil JM, Eneroth M, Hinchliffe RJ, Jeffcoate WJ, Lipsky BA, Senneville E, Teh J, Valk GD (2008) Diabetic foot osteomyelitis: a progress report on diagnosis and a systematic review of treatment. Diabetes Metab Res Rev **24**: S145-S161.

Bernthal NM, Pribaz JR, Stavrakis AI, Billi F, Cho JS, Ramos RI, Francis KP, Iwakura Y, Miller LS (2011) Protective role of IL-1β against post-arthroplasty *Staphylococcus aureus* infection. J Orthop Res **29**: 1621-1626.

Bernthal NM, Stavrakis AI, Billi F, Cho JS, Kremen TJ, Simon SI, Cheung AL, Finerman GA, Lieberman JR, Adams JS, Miller LS (2010) A mouse model of post-arthroplasty *Staphylococcus aureus* joint infection to evaluate *in vivo* the efficacy of antimicrobial implant coatings. PLoS One **5**: e12580. DOI: 10.1371/journal.pone.0012580.

Bernthal NM, Taylor BN, Meganck JA, Wang Y, Shahbazian JH, Niska JA, Francis KP, Miller LS (2014) Combined *in vivo* optical and μCT imaging to monitor infection, inflammation, and bone anatomy in an orthopaedic implant infection in mice. J Vis Exp: e51612. DOI:10.3791/51612.

Blevins JS, Elasri MO, Allmendinger SD, Beenken KE, Skinner RA, Thomas JR, Smeltzer MS (2003) Role of sarA in the pathogenesis of *Staphylococcus aureus* musculoskeletal infection. Infect Immun **71**: 516-523.

Boelens JJ, Dankert J, Murk JL, Weening JJ, van der Poll T, Dingemans KP, Koole L, Laman JD, Zaat SAJ (2000) Biomaterial-associated persistence of *Staphylococcus epidermidis* in pericatheter macrophages. J Infect Dis **181**: 1337-1349.

Boles LR, Awais R, Beenken KE, Smeltzer MS, Haggard WO, Jessica AJ (2018) Local delivery of amikacin and vancomycin from chitosan sponges prevent polymicrobial implant-associated biofilm. Mil Med **183**: 459-465.

Brodt MD, Ellis CB, Silva MJ (1999) Growing C57Bl/6 mice increase whole bone mechanical properties by increasing geometric and material properties. J Bone Miner Res **14**: 2159-2166.

Broekhuizen CAN, de Boer L, Schipper K, Jones CD, Quadir S, Feldman RG, Dankert J, Vandenbroucke-Grauls CMJE, Weening JJ, Zaat SAJ (2007) Peri-implant tissue is an important niche for *Staphylococcus epidermidis* in experimental biomaterial-associated infection in mice. Infect Immun **75**: 1129-1136.

Buitrago S, Martin TE, Tetens-Woodring J, Belicha-Villanueva A, Wilding GE (2008) Safety and efficacy of various combinations of injectable anesthetics in BALB/c Mice. J Am Assoc Lab Anim Sci **47**: 11-17.

Büren C, Hambüchen M, Windolf J, Lögters T, Windolf CD (2019) Histological score for degrees of severity in an implant-associated infection model in mice. Arch Orthop Trauma Surg **139**: 1235-1244.

Cahill SV, Kwon H, Back J, Lee I, Lee S, Alder KD, Hao Z, Yu KE, Dussik CM, Kyriakides TR, Lee FY (2021) Locally delivered adjuvant biofilm-penetrating antibiotics rescue impaired endochondral fracture healing caused by MRSA infection. J Orthop Res **39**: 402-414.

Carli AV, Bhimani S, Yang X, Shirley MB, de Mesy Bentley KL, Ross FP, Bostrom MPG (2017) Quantification of peri-implant bacterial load and *in vivo* biofilm formation in an innovative, clinically representative mouse model of periprosthetic joint infection. J Bone Joint Surg Am **99**: e25. DOI: 10.2106/JBJS.16.00815.

Carli AV, Bhimani S, Yang X, de Mesy Bentley KL, Ross FP, Bostrom MPG (2018) Vancomycin-loaded polymethylmethacrylate spacers fail to eradicate periprosthetic joint infection in a clinically representative mouse model. J Bone Joint Surg Am **100**: e76. DOI: 10.2106/JBJS.17.01100.

Cassat JE, Hammer ND, Campbell JP, Benson MA, Perrien DS, Mrak LN, Smeltzer MS, Torres VJ, Skaar EP (2013) A secreted bacterial protease tailors the *Staphylococcus aureus* virulence repertoire to modulate bone remodeling during osteomyelitis. Cell Host Microbe **13**: 759-772.

Chadha HS, Fitzgerald RH, Wiater P, Sud S, Nasser S, Wooley PH (1999) Experimental acute hematogenous osteomyelitis in mice. I. Histopathological and immunological findings. J Orthop Res **17**: 376-381.

Chen X, Jiao J, He X, Zhang J, Wang H, Xu Y, Jin T (2017) CHI3L1 regulation of inflammation and the effects on osteogenesis in a *Staphylococcus aureus* -induced murine model of osteomyelitis. FEBS J **284**: 1738-1747.

Choe H, Narayanan AS, Gandhi DA, Weinberg A, Marcus RE, Lee Z, Bonomo RA, Greenfield EM (2015) Immunomodulatory peptide IDR-1018 decreases implant infection and preserves osseointegration. Clin Orthop Relat Res **473**: 2898-2907.

Coenye T, Goeres D, Van Bambeke F, Bjarnsholt T (2018) Should standardized susceptibility testing for microbial biofilms be introduced in clinical practice? Clin Microbiol Infect **24**: 570-572.

Crabbé A, Jensen PØ, Bjarnsholt T, Coenye T (2019) Antimicrobial tolerance and metabolic adaptations in microbial biofilms. Trends Microbiol **27**: 850-863.

Crane DP, Gromov K, Li D, Søballe K, Wahnes C, Büchner H, Hilton MJ, O'Keefe RJ, Murray CK, Schwarz EM (2009) Efficacy of colistin-impregnated beads to prevent multidrug-resistant *A. baumannii* implant-associated osteomyelitis. J Orthop Res **27**: 1008-1015.

de Mesy Bentley KL, Trombetta R, Nishitani K, Bello-Irizarry SN, Ninomiya M, Zhang L, Chung HL, McGrath JL, Daiss JL, Awad HA, Kates SL, Schwarz EM (2017) Evidence of *Staphylococcus aureus* deformation, proliferation, and migration in canaliculi of live cortical bone in murine models of osteomyelitis: *S. aureus* in canaliculi of cortical bone in murine models of osteomyelitis. J Bone Miner Res **32**: 985-990.

Elasri MO, Thomas JR, Skinner RA, Blevins JS, Beenken KE, Nelson CL, Smelter MS (2002) *Staphylococcus aureus* collagen adhesin contributes to the pathogenesis of osteomyelitis. Bone **30**: 275-280.

Ellington JK, Harris M, Hudson MC, Vishin S, Webb LX, Sherertz R (2006) Intracellular *Staphylococcus aureus* and antibiotic resistance: implications for treatment of staphylococcal osteomyelitis. J Orthop Res **24**: 87-93.

Farnsworth CW, Schott EM, Benvie AM, Zukoski J, Kates SL, Schwarz EM, Gill SR, Zuscik MJ, Mooney RA (2018) Obesity/type 2 diabetes increases inflammation, periosteal reactive bone formation, and osteolysis during *Staphylococcus aureus* implant-associated bone infection. J Orthop Res **36**: 1614-1623.

Farnsworth CW, Schott EM, Jensen SE, Zukoski J, Benvie AM, Refaai MA, Kates SL, Schwarz EM, Zuscik MJ, Gill SR, Mooney RA (2017) Adaptive upregulation of clumping factor A (ClfA) by *Staphylococcus aureus* in the obese, type 2 diabetic host mediates increased virulence. Infect Immun **85**: e01005-16. DOI:10.1128/IAI.01005-16.

Farnsworth CW, Shehatou CT, Maynard R, Nishitani K, Kates SL, Zuscik MJ, Schwarz EM, Daiss JL, Mooney RA (2015) A humoral immune defect distinguishes the response to *Staphylococcus aureus* infections in mice with obesity and type 2 diabetes from that in mice with type 1 diabetes. Infect Immun **83**: 2264-2274.

Ferguson VL, Ayers RA, Bateman TA, Simske SJ (2003) Bone development and age-related bone loss in male C57BL/6J mice. Bone **33**: 387-398.

Ford CA, Spoonmore TJ, Gupta MK, Duvall CL, Guelcher SA, Cassat JE (2020) Diflunisal-loaded poly(propylene sulfide) nanoparticles decrease *S. aureus*-mediated bone destruction during osteomyelitis. J Orthop Res **39**: 426-437.

Funao H, Ishii K, Nagai S, Sasaki A, Hoshikawa T, Aizawa M, Okada Y, Chiba K, Koyasu S, Toyama Y, Matsumoto M (2012) Establishment of a real-time, quantitative, and reproducible mouse model of *Staphylococcus osteomyelitis* using bioluminescence imaging. Infect Immun **80**: 733-741.

Funao H, Nagai S, Sasaki A, Hoshikawa T, Tsuji T, Okada Y, Koyasu S, Toyama Y, Nakamura M, Aizawa M, Matsumoto M, Ishii K (2016) A novel hydroxyapatite film coated with ionic silver via inositol hexaphosphate chelation prevents implant-associated infection. Sci Rep **6**: 23238. DOI: 10.1038/srep23238.

Gargiulo S, Greco A, Gramanzini M, Esposito S, Affuso A, Brunetti A, Vesce G (2012) Mice anesthesia, analgesia, and care, part I: anesthetic considerations in preclinical research. ILAR J **53**: E55-69.

Gedbjerg N, LaRosa R, Hunter JG, Varrone JJ, Kates SL, Schwarz EM, Daiss JL (2013) Anti-glucosaminidase IgG in sera as a biomarker of host immunity against *Staphylococcus aureus* in orthopaedic surgery patients. J Bone Jointt Surg Am **95**: e171. DOI: 10.2106/JBJS.L.01654.

Guggenberger C, Wolz C, Morrissey JA, Heesemann J (2012) Two distinct coagulase-dependent barriers protect *Staphylococcus aureus* from neutrophils in a three dimensional *in vitro* infection

model. PLoS Pathog **8**: e1002434. DOI: 10.1371/journal.ppat.1002434.

Haffner-Luntzer M, Kovtun A, Rapp AE, Ignatius A (2016) Mouse models in bone fracture healing research. Curr Mol Biol Rep **2**: 101-111.

Harris MA, Beenken KE, Smeltzer MS, Haggard WO, Jennings AJ (2017) Phosphatidylcholine coatings deliver local antimicrobials and reduce infection in a murine model: a preliminary study. Clin Orthop Relat Res **475**: 1847-1853.

Hegde V, Dworsky EM, Stavrakis AI, Loftin AH, Zoller SD, Park HY, Richman S, Johansen D, Hu Y, Taylor JA, Hamad CD, Chun RF, Xi W, Adams JS, Bernthal NM (2017) Single-dose, preoperative vitamin-d supplementation decreases infection in a mouse model of periprosthetic joint infection. J Bone Joint Surg Am **99**: 1737-1744.

Heim CE, Vidlak D, Kielian T (2015a) Interleukin-10 production by myeloid-derived suppressor cells contributes to bacterial persistence during *Staphylococcus aureus* orthopedic biofilm infection. J Leukoc Biol **98**: 1003-1013.

Heim CE, Vidlak D, Scherr TD, Hartman CW, Garvin KL, Kielian T (2015b) IL-12 promotes myeloid-derived suppressor cell recruitment and bacterial persistence during *Staphylococcus aureus* orthopedic implant infection. J Immunol **194**: 3861-3872.

Heim CE, Vidlak D, Scherr TD, Kozel JA, Holzapfel M, Muirhead DE, Kielian T (2014) Myeloid-derived suppressor cells contribute to *Staphylococcus aureus* orthopedic biofilm infection. J Immunol **192**: 3778-3792.

Heim CE, West SC, Ali H, Kielian T (2018) Heterogeneity of Ly6G$^+$ Ly6C$^+$ myeloid-derived suppressor cell infiltrates during *Staphylococcus aureus* biofilm infection. Infect Immun **86**: e00684-18. DOI: 10.1128/IAI.00684-18.

Hernandez CJ, Yang X, Ji G, Niu Y, Sethuraman AS, Koressel J, Shirley M, Fields MW, Chyou S, Li TM, Luna M, Callahan RL, Ross FP, Lu TT, Brito IL, Carli AV, Bostrom MPG (2019) Disruption of the gut microbiome increases the risk of periprosthetic joint infection in mice. Clin Orthop Relat Res **477**: 2588-2598.

Histing T, Garcia P, Holstein JH, Klein M, Matthys R, Nuetzi R, Steck R, Laschke MW, Wehner T, Bindl R, Recknagel S, Stuermer EK, Vollmar B, Wildemann B, Lienau J, Willie B, Peters A, Ignatius A, Pohlemann T, Claes L, Menger MD (2011) Small animal bone healing models: standards, tips, and pitfalls results of a consensus meeting. Bone **49**: 591-599.

Hofstee MI, Riool M, Terjajevs I, Thompson K, Stoddart MJ, Richards RG, Zaat SAJ, Moriarty TF (2020) Three-dimensional *in vitro Staphylococcus aureus* abscess communities display antibiotic tolerance and protection from neutrophil clearance. Infect Immun **88**: e00293-20. DOI: 10.1128/IAI.00293-20.

Holstein JH, Garcia P, Histing T, Kristen A, Scheuer C, Menger MD, Pohlemann T (2009) Advances in the establishment of defined mouse models for the study of fracture healing and bone regeneration. J Orthop Trauma **23**: S31-S38.

Horst SA, Hoerr V, Beineke A, Kreis C, Tuchscherr L, Kalinka J, Lehne S, Schleicher I, Köhler G, Fuchs T, Raschke MJ, Rohde M, Peters G, Faber C, Löffler B, Medina E (2012) A novel mouse model of *Staphylococcus aureus* chronic osteomyelitis that closely mimics the human infection. Am J Pathol **181**: 1206-1214.

Hou Y, Qin H, Jiang N, Liu G, Wu H, Bai L, Yu B, Zhang X (2019) G-CSF partially mediates bone loss induced by *Staphylococcus aureus* infection in mice. Clin Sci **133**: 1297-1308.

Inzana JA, Trombetta R, Schwarz EM, Kates SL, Awad HA (2015a) 3D printed bioceramics for dual antibiotic delivery to treat implant-associated bone infection. Eur Cell Mater **30**: 232-247.

Inzana JA, Schwarz EM, Kates SL, Awad HA (2015b) A novel murine model of established Staphylococcal bone infection in the presence of a fracture fixation plate to study therapies utilizing antibiotic-laden spacers after revision surgery. Bone **72**: 128-136.

Ishikawa M, de Mesy Bentley KL, McEntire BJ, Bal BS, Schwarz EM, Xie C (2017) Surface topography of silicon nitride affects antimicrobial and osseointegrative properties of tibial implants in a murine model. J Biomed Mater Res A **105**: 3413-3421.

Isogai N, Shiono Y, Kuramoto T, Yoshioka K, Ishihama H, Funao H, Nakamura M, Matsumoto M, Ishii K (2020) Potential osteomyelitis biomarkers identified by plasma metabolome analysis in mice. Sci Rep **10**: 839. DOI:10.1038/s41598-020-57619-1.

Ji Z, Su J, Hou Y, Yao Z, Yu B, Zhang X (2020) EGFR/FAK and c-Src signalling pathways mediate the internalisation of *Stapylococcus aureus* by osteoblasts. Cell Microbiol **22**: e13240. DOI: 10.1111/cmi.13240.

Jiang Y, Wang S, Wu H, Qin H, Ren M, Lin J, Yu B (2019) Aspirin alleviates orthopedic implant-associated infection. Int J Mol Med **44**: 1281-1288.

Jilka RL (2013) The relevance of mouse models for investigating age-related bone loss in humans. J Gerontol A Biol Sci Med Sci **68**: 1209-1217.

Johansson A, Flock JI, Svensson O (2001) Collagen and fibronectin binding in experimental staphylococcal osteomyelitis. Clin Orthop Relat Res **382**: 241-246.

Johnson CT, Wroe JA, Agarwal R, Martin KE, Guldberg RE, Donlan RM, Westblade LF, García AJ (2018) Hydrogel delivery of lysostaphin eliminates orthopedic implant infection by *Staphylococcus aureus* and supports fracture healing. Proc Natl Acad Sci **115**: E4960-E4969.

Jørgensen NP, Hansen K, Andreasen C, Pedersen M, Fuursted K, Meyer R, Petersen E (2017) Hyperbaric oxygen therapy is ineffective as an adjuvant to daptomycin with rifampicin treatment in a murine model of *Staphylococcus aureus* in implant-associated

osteomyelitis. Microorganisms **5**: 21. DOI: 10.3390/microorganisms5020021.

Jørgensen NP, Meyer R, Dagnæs-Hansen F, Fuursted K, Petersen E (2014) A modified chronic infection model for testing treatment of *Staphylococcus aureus* biofilms on implants. PLoS One **9**: e103688. DOI: 10.1371/journal.pone.0103688.

Jørgensen NP, Skovdal SM, Meyer RL, Dagnæs-Hansen F, Fuursted K, Petersen E (2016) Rifampicin-containing combinations are superior to combinations of vancomycin, linezolid and daptomycin against *Staphylococcus aureus* biofilm infection *in vivo* and *in vitro*. Pathog Dis **74**: ftw019. DOI: 10.1093/femspd/ftw019.

Kaur S, Harjai K, Chhibber S (2016) *In vivo* assessment of phage and linezolid based implant coatings for treatment of methicillin resistant *S. aureus* (MRSA) mediated orthopaedic device related infections. PLoS One **11**: e0157626. DOI: 10.1371/journal.pone.0157626.

Kavanagh N, Ryan EJ, Widaa A, Sexton G, Fennell J, O'Rourke S, Cahill KC, Kearney CJ, O'Brien FJ, Kerrigan SW (2018) Staphylococcal osteomyelitis: disease progression, treatment challenges, and future directions. Clin Microbiol Rev **31**: e00084-17. DOI: 10.1128/CMR.00084-17.

Kohler T, Beyeler M, Webster D, Müller R (2005) Compartmental bone morphometry in the mouse femur: reproducibility and resolution dependence of microtomographic measurements. Calcif Tissue Int **77**: 281-290. DOI: 10.1007/s00223-005-0039-2.

Laperre K, Depypere M, van Gastel N, Torrekens S, Moermans K, Bogaerts R, Maes F, Carmeliet G (2011) Development of micro-CT protocols for *in vivo* follow-up of mouse bone architecture without major radiation side effects. Bone **49**: 613-622.

Lazzarini L, Overgaard KA, Conti E, Shirtliff ME (2006) Experimental osteomyelitis: what have we learned from animal studies about the systemic treatment of osteomyelitis? J Chemother **18**: 451-460.

Lee LY, Miyamoto YJ, McIntyre BW, Höök M, McCrea KW, McDevitt D, Brown EL (2002) The *Staphylococcus aureus* map protein is an immunomodulator that interferes with T cell-mediated responses. J Clin Invest **110**: 1461-1471.

Letson HL, Morris J, Biros E, Dobson GP (2019) Conventional and specific-pathogen free rats respond differently to anesthesia and surgical trauma. Sci Rep **9**: 9399. DOI: 10.1038/s41598-019-45871-z.

Lew DP, Waldvogel FA (2004) Osteomyelitis. Lancet **364**: 369-379.

Li D, Gromov K, Søballe K, Puzas JE, O'Keefe RJ, Awad H, Drissi H, Schwarz EM (2008) Quantitative mouse model of implant-associated osteomyelitis and the kinetics of microbial growth, osteolysis, and humoral immunity. J Orthop Res **26**: 96-105.

Lin Y, Su J, Wang Y, Xu D, Zhang X, Yu B (2021) mRNA transcriptome analysis of bone in a mouse model of implant-associated *Staphylococcus aureus* osteomyelitis. Infect Immun **89**: e00814-20. DOI: 10.1128/IAI.00814-20.

Lindsay SE, Lindsay HG, Kallet J, Weaver MR, Curran-Everett D, Crapo JD, Regan EA (2021) MnTE-2-PyP disrupts *Staphylococcus aureus* biofilms in a novel fracture model. J Orthop Res. DOI: 10.1002/jor.24967.

Loughran AJ, Gaddy D, Beenken KE, Meeker DG, Morello R, Zhao H, Byrum SD, Tackett AJ, Cassat JE, Smeltzer MS (2016) Impact of *sarA* and phenol-soluble modulins on the pathogenesis of osteomyelitis in diverse clinical isolates of *Staphylococcus aureus*. Infect Immun **84**: 2586-2594.

Lovati AB, Drago L, Monti L, De Vecchi E, Previdi S, Banfi G, Romanò CL (2013) Diabetic mouse model of orthopaedic implant-related *Staphylococcus aureus* infection. PLoS One **8**: e67628. DOI: 10.1371/journal.pone.0067628.

Lovati AB, Romanò CL, Monti L, Vassena C, Previdi S, Drago L (2014) Does PGE1 vasodilator prevent orthopaedic implant-related infection in diabetes? Preliminary results in a mouse model. PLoS One **9**: e94758. DOI: 10.1371/journal.pone.0094758.

Lu X, Chen R, Lv J, Xu W, Chen H, Ma Z, Huang S, Li S, Liu H, Hu J, Nie L (2019) High-resolution bimodal imaging and potent antibiotic/photodynamic synergistic therapy for osteomyelitis with a bacterial inflammation-specific versatile agent. Acta Biomater **99**: 363-372.

Lüthje FL, Jensen LK, Jensen HE, Skovgaard K (2020) The inflammatory response to bone infection - a review based on animal models and human patients. APMIS **128**: 275-286.

Mandell JB, Deslouches B, Montelaro RC, Shanks RMQ, Doi Y, Urish KL (2017) Elimination of antibiotic resistant surgical implant biofilms using an engineered cationic amphipathic peptide WLBU2. Sci Rep **7**: 18098. DOI: 10.1038/s41598-017-17780-6.

Marriott I, Gray DL, Rati DM, Fowler VG, Stryjewski ME, Levin LS, Hudson MC, Bost KL (2005) Osteoblasts produce monocyte chemoattractant protein-1 in a murine model of *Staphylococcus aureus* osteomyelitis and infected human bone tissue. Bone **37**: 504-512.

Marriott I, Gray DL, Tranguch SL, Fowler VG, Stryjewski M, Scott Levin L, Hudson MC, Bost KL (2004) Osteoblasts express the inflammatory cytokine interleukin-6 in a murine model of *Staphylococcus aureus* osteomyelitis and infected human bone tissue. Am J Pathol **164**: 1399-1406.

Masters EA, Hao SP, Kenney HM, Morita Y, Galloway CA, Mesy Bentley KL, Ricciardi BF, Boyce BF, Schwarz EM, Oh I (2021) Distinct vasculotropic *versus* osteotropic features of *S. agalactiae versus S. aureus* implant-associated bone infection in mice. J Orthop Res **39**: 389-401.

Masters EA, de Mesy Bentley KL, Gill AL, Hao SP, Galloway CA, Salminen AT, Guy DR, McGrath JL, Awad HA, Gill SR, Schwarz EM (2020) Identification of penicillin binding protein 4 (PBP4) as a critical factor for *Staphylococcus aureus* bone invasion during osteomyelitis in mice. PLoS Pathog **16**: e1008988.

Masters EA, Trombetta RP, de Mesy Bentley KL, Boyce BF, Gill AL, Gill SR, Nishitani K, Ishikawa M, Morita Y, Ito H, Bello-Irizarry SN, Ninomiya M, Brodell JD, Lee CC, Hao SP, Oh I, Xie C, Awad HA, Daiss JL, Owen JR, Kates SL, Schwarz EM, Muthukrishnan G (2019) Evolving concepts in bone infection: redefining "biofilm", "acute *vs*. chronic osteomyelitis", "the immune proteome" and "local antibiotic therapy". Bone Res **7**: 20. DOI: 10.1038/s41413-019-0061-z.

Mendoza Bertelli A, Delpino MV, Lattar S, Giai C, Llana MN, Sanjuan N, Cassat JE, Sordelli D, Gómez MI (2016) *Staphylococcus aureus* protein A enhances osteoclastogenesis *via* TNFR1 and EGFR signaling. Biochim Biophys Acta **1862**: 1975-1983.

Metsemakers WJ, Emanuel N, Cohen O, Reichart M, Potapova I, Schmid T, Segal D, Riool M, Kwakman PHS, de Boer L, de Breij A, Nibbering PH, Richards RG, Zaat SAJ, Moriarty TF (2015) A doxycycline-loaded polymer-lipid encapsulation matrix coating for the prevention of implant-related osteomyelitis due to doxycycline-resistant methicillin-resistant *Staphylococcus aureus*. J Control Release **209**: 47-56.

Mills LA, Simpson AHRW (2012) *In vivo* models of bone repair. J Bone Joint Surg Br **94**: 865-874.

Moriarty TF, Harris LG, Mooney RA, Wenke JC, Riool M, Zaat SAJ, Moter A, Schaer TP, Khanna N, Kuehl R, Alt V, Montali A, Liu J, Zeiter S, Busscher HJ, Grainger DW, Richards RG (2019) Recommendations for design and conduct of preclinical *in vivo* studies of orthopedic device-related infection. J Orthop Res **37**: 271-287.

Moriarty TF, Kuehl R, Coenye T, Metsemakers WJ, Morgenstern M, Schwarz EM, Riool M, Zaat SAJ, Khana N, Kates SL, Richards RG (2016) Orthopaedic device-related infection: current and future interventions for improved prevention and treatment. EFORT Open Rev **1**: 89-99.

Muschler GF, Raut VP, Patterson TE, Wenke JC, Hollinger JO (2010) The design and use of animal models for translational research in bone tissue engineering and regenerative medicine. Tissue Eng Part B Rev **16**: 123-145.

Nishitani K, Beck CA, Rosenberg AF, Kates SL, Schwarz EM, Daiss JL (2015a) A diagnostic serum antibody test for patients with *Staphylococcus aureus* osteomyelitis. Clin Orthop Relat Res **473**: 2735-2749.

Nishitani K, Sutipornpalangkul W, de Mesy Bentley KL, Varrone JJ, Bello-Irizarry SN, Ito H, Matsuda S, Kates SL, Daiss JL, Schwarz EM (2015b) Quantifying the natural history of biofilm formation *in vivo* during the establishment of chronic implant-associated *Staphylococcus aureus* osteomyelitis in mice to identify critical pathogen and host factors. J Orthop Res **33**: 1311-1319.

Niska JA, Meganck JA, Pribaz JR, Shahbazian JH, Lim E, Zhang N, Rice BW, Akin A, Ramos RI, Bernthal NM, Francis KP, Miller LS (2012a) Monitoring bacterial burden, inflammation and bone damage longitudinally using optical and μCT imaging in an orthopaedic implant infection in mice. PLoS One **7**: e47397. DOI: 10.1371/journal.pone.0047397.

Niska JA, Shahbazian JH, Ramos RI, Francis KP, Bernthal NM, Miller LS (2013) Vancomycin-rifampin combination therapy has enhanced efficacy against an experimental *Staphylococcus aureus* prosthetic joint infection. Antimicrob Agents Chemother **57**: 5080-5086.

Niska JA, Shahbazian JH, Ramos RI, Pribaz JR, Billi F, Francis KP, Miller LS (2012b) Daptomycin and tigecycline have broader effective dose ranges than vancomycin as prophylaxis against a *Staphylococcus aureus* surgical implant infection in mice. Antimicrob Agents Chemother **56**: 2590-2597.

Oezel L, Büren C, Scholz AO, Windolf J, Windolf CD (2019) Effect of antibiotic infused calcium sulfate/hydroxyapatite (CAS/HA) insets on implant-associated osteitis in a femur fracture model in mice. PLoS One **14**: e0213590. DOI: 10.1371/journal.pone.0213590.

O'Neill J (2014) Antimicrobial resistance. Tackling a crisis for the health and wealth of nations. Review on Antimicrobial Resistance. Wellcome Collection, London.

Patel M, Rojavin Y, Jamali A, Wasielewski S, Salgado C (2009) Animal models for the study of osteomyelitis. Semin Plast Surg **23**: 148-154.

Pearce AI, Richards RG, Milz S, Schneider E, Pearce SG (2007) Animal models for implant biomaterial research in bone: a review. Eur Cell Mater **13**: 1-10.

Peng KT, Chiang YC, Huang TY, Chen PC, Chang PJ, Lee CW (2019) Curcumin nanoparticles are a promising anti-bacterial and anti-inflammatory agent for treating periprosthetic joint infections. Int J Nanomedicine **14**: 469-481.

Peng KT, Hsieh CC, Huang TY, Chen PC, Shih HN, Lee MS, Chang PJ (2017) *Staphylococcus aureus* biofilm elicits the expansion, activation and polarization of myeloid-derived suppressor cells *in vivo* and *in vitro*. PLoS One **12**: e0183271. DOI: 10.1371/journal.pone.0183271.

Pickett JE, Thompson JM, Sadowska A, Tkaczyk C, Sellman BR, Minola A, Corti D, Lanzavecchia A, Miller LS, Thorek DL (2018) Molecularly specific detection of bacterial lipoteichoic acid for diagnosis of prosthetic joint infection of the bone. Bone Res **6**: 13. DOI: 10.1038/s41413-018-0014-y.

Popescu B, Tevanov I, Carp M, Ulici A (2020) Acute hematogenous osteomyelitis in pediatric patients: epidemiology and risk factors of a poor outcome. J Int Med Res **48**: 0300060520910889. DOI: 10.1177/0300060520910889.

Potter AD, Butrico CE, Ford CA, Curry JM, Trenary IA, Tummarakota SS, Hendrix AS, Young JD, Cassat JE (2020) Host nutrient milieu drives an essential role for aspartate biosynthesis during invasive *Staphylococcus aureus* infection. Proc Natl Acad Sci U S A **117**: 12394-12401.

Prabhakara R, Harro JM, Leid JG, Harris M, Shirtliff ME (2011a) Murine immune response to a

chronic *Staphylococcus aureus* biofilm infection. Infect Immun **79**: 1789-1796.

Prabhakara R, Harro JM, Leid JG, Keegan AD, Prior ML, Shirtliff ME (2011b) Suppression of the inflammatory immune response prevents the development of chronic biofilm infection due to methicillin-resistant *Staphylococcus aureus*. Infect Immun **79**: 5010-5018.

Pribaz JR, Bernthal NM, Billi F, Cho JS, Ramos RI, Guo Y, Cheung AL, Francis KP, Miller LS (2012) Mouse model of chronic post-arthroplasty infection: noninvasive *in vivo* bioluminescence imaging to monitor bacterial burden for long-term study. J Orthop Res **30**: 335-340.

Putnam NE, Fulbright LE, Curry JM, Ford CA, Petronglo JR, Hendrix AS, Cassat JE (2019) MyD88 and IL-1R signaling drive antibacterial immunity and osteoclast-driven bone loss during *Staphylococcus aureus* osteomyelitis. PLoS Pathog **15**: e1007744. DOI: 10.1371/journal.ppat.1007744.

Qadri S, Haik Y, Mensah-Brown E, Bashir G, Fernandez-Cabezudo MJ, al-Ramadi BK (2017) Metallic nanoparticles to eradicate bacterial bone infection. Nanomedicine **13**: 2241-2250.

Ramirez AM, Byrum SD, Beenken KE, Washam C, Edmondson RD, Mackintosh SG, Spencer HJ, Tackett AJ, Smeltzer MS (2020) Exploiting correlations between protein abundance and the functional status of *saeRS* and *sarA* to identify virulence factors of potential importance in the pathogenesis of *Staphylococcus aureus* osteomyelitis. ACS Infect Dis **6**: 237-249.

Reizner W, Hunter J, O'Malley N, Southgate R, Schwarz E, Kates S (2014) A systematic review of animal models for *Staphylococcus aureus* osteomyelitis. Eur Cell Mater **27**: 196-212.

Rochford ETJ, Sabaté Brescó M, Poulsson AHC, Kluge K, Zeiter S, Ziegler M, O'Mahony L, Richards RG, Moriarty TF (2019) Infection burden and immunological responses are equivalent for polymeric and metallic implant materials *in vitro* and in a murine model of fracture-related infection. J Biomed Mater Res B Appl Biomater **107**: 1095-1106.

Rochford ETJ, Sabaté Brescó M, Zeiter S, Kluge K, Poulsson A, Ziegler M, Richards RG, O'Mahony L, Moriarty TF (2016) Monitoring immune responses in a mouse model of fracture fixation with and without *Staphylococcus aureus* osteomyelitis. Bone **83**: 82-92.

Rom JS, Ramirez AM, Beenken KE, Sahukhal GS, Elasri MO, Smeltzer MS (2020) The Impacts of *msaABCR* on *sarA*-associated phenotypes are different in divergent clinical isolates of *Staphylococcus aureus*. Infect Immun **88**: e00530-19. DOI: 10.1128/IAI.00530-19.

Röntgen V, Blakytny R, Matthys R, Landauer M, Wehner T, Göckelmann M, Jermendy P, Amling M, Schinke T, Claes L, Ignatius A (2010) Fracture healing in mice under controlled rigid and flexible conditions using an adjustable external fixator. J Orthop Res **28**: 1456-1462.

Sabaté Brescó M, O'Mahony L, Zeiter S, Kluge K, Ziegler M, Berset C, Nehrbass D, Richards RG, Moriarty TF (2017) Influence of fracture stability on *Staphylococcus epidermidis* and *Staphylococcus aureus* infection in a murine femoral fracture model. Eur Cell Mater **34**: 321-340.

Sander G, Börner T, Kriegeskorte A, von Eiff C, Becker K, Mahabir E (2012) Catheter colonization and abscess formation due to *Staphylococcus epidermidis* with normal and small-colony-variant phenotype is mouse strain dependent. PLoS One **7**: e36602. DOI: 10.1371/journal.pone.0036602.

Scherr TD, Hanke ML, Huang O, James DBA, Horswill AR, Bayles KW, Fey PD, Torres VJ, Kielian T (2015) *Staphylococcus aureus* biofilms induce macrophage dysfunction through leukocidin AB and alpha-toxin. mBio **6**: e01021-15. DOI: 10.1128/mBio.01021-15.

Sellers RS, Clifford CB, Treuting PM, Brayton C (2012) Immunological variation between inbred laboratory mouse strains: points to consider in phenotyping genetically immunomodified mice. Vet Pathol **49**: 32-43.

Shandley S, Matthews KP, Cox J, Romano D, Abplanalp A, Kalns J (2012) Hyperbaric oxygen therapy in a mouse model of implant-associated osteomyelitis. J Orthop Res **30**: 203-208.

Sheppard WL, Mosich GM, Smith RA, Hamad CD, Park HY, Zoller SD, Trikha R, McCoy TK, Borthwell R, Hoang J, Truong N, Cevallos N, Clarkson S, Hori KR, van Dijl JM, Francis KP, Petrigliano FA, Bernthal NM (2020) Novel *in vivo* mouse model of shoulder implant infection. J Shoulder Elbow Surg **29**: 1412-1424.

Shiono Y, Ishii K, Nagai S, Kakinuma H, Sasaki A, Funao H, Kuramoto T, Yoshioka K, Ishihama H, Isogai N, Takeshima K, Tsuji T, Okada Y, Koyasu S, Nakamura M, Toyama Y, Aizawa M, Matsumoto M (2016) Delayed propionibacterium acnes surgical site infections occur only in the presence of an implant. Sci Rep **6**: 32758. DOI: 10.1038/srep32758.

Sosa BR, Niu Y, Turajane K, Staats K, Suhardi V, Carli A, Fischetti V, Bostrom M, Yang X (2020) 2020 John Charnley Award: the antimicrobial potential of bacteriophage-derived lysin in a murine debridement, antibiotics, and implant retention model of prosthetic joint infection. Bone Joint J **102-B**: 3-10.

Sottnik JL, U'Ren LW, Thamm DH, Withrow SJ, Dow SW (2010) Chronic bacterial osteomyelitis suppression of tumor growth requires innate immune responses. Cancer Immunol Immunother **59**: 367-378.

Spoonmore TJ, Ford CA, Curry JM, Guelcher SA, Cassat JE (2020) Concurrent local delivery of diflunisal limits bone destruction but fails to improve systemic vancomycin efficacy during *Staphylococcus aureus* osteomyelitis. Antimicrob Agents Chemother **64**: e00182-20. DOI: 10.1128/AAC.00182-20.

Stavrakis AI, Zhu S, Loftin AH, Weixian X, Niska J, Hegde V, Segura T, Bernthal NM (2019) Controlled release of vancomycin and tigecycline

from an orthopaedic implant coating prevents *Staphylococcus aureus* infection in an open fracture animal model. Biomed Res Int **2019**: 1638508. DOI: 10.1155/2019/1638508.

Stavrakis AI, Zhu S, Hegde V, Loftin AH, Ashbaugh AG, Niska JA, Miller LS, Segura T, Bernthal NM (2016) *In vivo* efficacy of a "smart" antimicrobial implant coating: J Bone Joint Surg Am **98**: 1183-1189.

Szafranska AK, Oxley APA, Chaves-Moreno D, Horst SA, Roßlenbroich S, Peters G, Goldmann O, Rohde M, Sinha B, Pieper DH, Löffler B, Jauregui R, Wos-Oxley ML, Medina E (2014) High-resolution transcriptomic analysis of the adaptive response of *Staphylococcus aureus* during acute and chronic phases of osteomyelitis. mBio **5**: e01775-14. DOI: 10.1128/mBio.01775-14.

Takahashi T, Yokogawa K, Sakura N, Nomura M, Kobayashi S, Miyamoto K (2008) Bone-targeting of quinolones conjugated with an acidic oligopeptide. Pharm Res **25**: 2881-2888.

Takao K, Miyakawa T (2015) Genomic responses in mouse models greatly mimic human inflammatory diseases. Proc Natl Acad Sci U S A **112**: 1167-1172.

Thompson JM, Miller RJ, Ashbaugh AG, Dillen CA, Pickett JE, Wang Y, Ortines RV, Sterling RS, Francis KP, Bernthal NM, Cohen TS, Tkaczyk C, Yu L, Stover CK, DiGiandomenico A, Sellman BR, Thorek DLJ, Miller LS (2018) Mouse model of Gram-negative prosthetic joint infection reveals therapeutic targets. JCI Insight **3**: e121737. DOI: 10.1172/jci.insight.121737.

Thompson JM, Saini V, Ashbaugh AG, Miller RJ, Ordonez AA, Ortines RV, Wang Y, Sterling RS, Jain SK, Miller LS (2017) Oral-only linezolid-rifampin is highly effective compared with other antibiotics for periprosthetic joint infection: study of a mouse model. J Bone Joint Surg Am **99**: 656-665.

Tomizawa T, Ishikawa M, Bello-Irizarry SN, Mesy Bentley KL, Ito H, Kates SL, Daiss JL, Beck C, Matsuda S, Schwarz EM, Nishitani K (2020) Biofilm producing *Staphylococcus epidermidis* (RP62A strain) inhibits osseous integration without osteolysis and histopathology in a murine septic implant model. J Orthop Res **38**: 852-860.

Trombetta RP, Ninomiya MJ, El-Atawneh IM, Knapp EK, de Mesy Bentley KL, Dunman PM, Schwarz EM, Kates SL, Awad HA (2019a) Calcium phosphate spacers for the local delivery of sitafloxacin and rifampin to treat orthopedic infections: efficacy and proof of concept in a mouse model of single-stage revision of device-associated osteomyelitis. Pharmaceutics **11**: 94. DOI: 10.3390/pharmaceutics11020094.

Trombetta RP, de Mesy Bentley KL, Schwarz EM, Kate SL, Awad HA (2019b) A murine femoral ostectomy model with hardware exchange to assess antibiotic-impregnated spacers for implant-associated osteomyelitis. Eur Cell Mater **37**: 431-444.

Tuchscherr L, Geraci J, Löffler B (2017) *Staphylococcus aureus* regulator sigma B is important to develop chronic infections in hematogenous murine osteomyelitis model. Pathogens **6**: 31. DOI: 10.3390/pathogens6030031.

Tuchscherr L, Kreis CA, Hoerr V, Flint L, Hachmeister M, Geraci J, Bremer-Streck S, Kiehntopf M, Medina E, Kribus M, Raschke M, Pletz M, Peters G, Löffler B (2016) *Staphylococcus aureus* develops increased resistance to antibiotics by forming dynamic small colony variants during chronic osteomyelitis. J Antimicrob Chemother **71**: 438-448.

Tuchscherr L, Pöllath C, Siegmund A, Deinhardt-Emmer S, Hoerr V, Svensson CM, Thilo Figge M, Monecke S, Löffler B (2019) Clinical *S. aureus* isolates vary in their virulence to promote adaptation to the host. Toxins **11**: 135. DOI: 10.3390/toxins11030135.

Tuohy JL, Fogle JE, Meichner K, Borst LB, Petty CS, Griffith EH, Osborne JA, Lascelles BDX (2018) Assessment of a novel nanoparticle hyperthermia therapy in a murine model of osteosarcoma. Vet Surg **47**: 1021-1030.

Valour F, Trouillet-Assant S, Riffard N, Tasse J, Flammier S, Rasigade JP, Chidiac C, Vandenesch F, Ferry T, Laurent F (2015) Antimicrobial activity against intraosteoblastic *Staphylococcus aureus*. Antimicrob Agents Chemother **59**: 2029-2036.

Varoga D, Tohidnezhad M, Paulsen F, Wruck CJ, Brandenburg L, Mentlein R, Lippross S, Hassenpflug J, Besch L, Müller M, Jürgens C, Seekamp A, Schmitt L, Pufe T (2008) The role of human beta-defensin-2 in bone. J Anat **213**: 749-757.

Varoga D, Wruck CJ, Tohidnezhad M, Brandenburg L, Paulsen F, Mentlein R, Seekamp A, Besch L, Pufe T (2009) Osteoblasts participate in the innate immunity of the bone by producing human beta defensin-3. Histochem Cell Biol **131**: 207-218.

Varrone JJ, de Mesy Bentley KL, Bello-Irizarry SN, Nishitani K, Mack S, Hunter JG, Kates SL, Daiss JL, Schwarz EM (2014) Passive immunization with anti-glucosaminidase monoclonal antibodies protects mice from implant-associated osteomyelitis by mediating opsonophagocytosis of *Staphylococcus aureus* megaclusters. J Orthop Res **32**: 1389-1396.

Vidlak D, Kielian T (2016) Infectious dose dictates the host response during *Staphylococcus aureus* orthopedic-implant biofilm infection. Infect Immun **84**: 1957-1965.

Vlasova AN, Takanashi S, Miyazaki A, Rajashekara G, Saif LJ (2019) How the gut microbiome regulates host immune responses to viral vaccines. Curr Opin Virol **37**: 16-25.

Wagner JM, Jaurich H, Wallner C, Abraham S, Becerikli M, Dadras M, Harati K, Duhan V, Khairnar V, Lehnhardt M, Behr B (2017) Diminished bone regeneration after debridement of posttraumatic osteomyelitis is accompanied by altered cytokine levels, elevated B cell activity, and increased osteoclast activity. J Orthop Res **35**: 2425-2434.

Wagner JM, Reinkemeier F, Dadras M, Wallner C, Huber J, Sogorski A, Sacher M, Schmidt S, Drysch M, Dittfeld S, Becerikli M, Becker K, Rauch N, Lehnhardt

M, Behr B (2020) Local Wnt3a treatment restores bone regeneration in large osseous defects after surgical debridement of osteomyelitis. J Mol Med **98**: 897-906.

Wagner JM, Reinkemeier F, Wallner C, Dadras M, Huber J, Schmidt SV, Drysch M, Dittfeld S, Jaurich H, Becerikli M, Becker K, Rauch N, Duhan V, Lehnhardt M, Behr B (2019) Adipose-derived stromal cells are capable of restoring bone regeneration after post-traumatic osteomyelitis and modulate B-cell response. Stem Cells Transl Med **8**: 1084-1091.

Wagner JM, Zöllner H, Wallner C, Ismer B, Schira J, Abraham S, Harati K, Lehnhardt M, Behr B (2016) Surgical debridement is superior to sole antibiotic therapy in a novel murine posttraumatic osteomyelitis model. PLoS One **11**: e0149389. DOI: 10.1371/journal.pone.0149389.

Walton KD, Lord A, Kendall LV, Dow SW (2014) Comparison of 3 real-time, quantitative murine models of staphylococcal biofilm infection by using *in vivo* bioluminescent imaging. Comp Med **64**: 25-33.

Wancket LM (2015) Animal models for evaluation of bone implants and devices: comparative bone structure and common model uses. Vet Pathol **52**: 842-850.

Wang Y, Thompson JM, Ashbaugh AG, Khodakivskyi P, Budin G, Sinisi R, Heinmiller A, van Oosten M, van Dijl JM, van Dam GM, Francis KP, Bernthal NM, Dubikovskaya EA, Miller LS (2017a) Preclinical evaluation of photoacoustic imaging as a novel noninvasive approach to detect an orthopaedic implant infection. J Am Acad Orthop Surg **25 Suppl 1**: S7-S12.

Wang Y, Wang J, Deng Z, Jin J, Jiang H, Meng J, Xu H, Zhao J, Sun G, Qian H (2017b) Chronic osteomyelitis increases the incidence of type 2 diabetes in humans and mice. Int J Biol Sci **13**: 1192-1202.

Wang Y, Ashbaugh AG, Dikeman DA, Zhang J, Ackerman NE, Kim SE, Falgons C, Ortines RV, Liu H, Joyce DP, Alphonse MP, Dillen CA, Thompson JM, Archer NK, Miller LS (2020a) Interleukin-1β and tumor necrosis factor are essential in controlling an experimental orthopedic implant-associated infection. J Orthop Res **38**: 1800-1809.

Wang Y, Cheng LI, Helfer DR, Ashbaugh AG, Miller RJ, Tzomides AJ, Thompson JM, Ortines RV, Tsai AS, Liu H, Dillen CA, Archer NK, Cohen TS, Tkaczyk C, Stover CK, Sellman BR, Miller LS (2017c) Mouse model of hematogenous implant-related *Staphylococcus aureus* biofilm infection reveals therapeutic targets. Proc Natl Acad Sci U S A **114**: E5094-E5102.

Wang Y, Dikeman D, Zhang J, Ackerman N, Kim S, Alphonse MP, Ortines RV, Liu H, Joyce DP, Dillen CA, Thompson JM, Thomas AA, Plaut RD, Miller LS, Archer NK (2021) CCR2 contributes to host defense against *Staphylococcus aureus* orthopedic implant-associated infections in mice. J Orthop Res. DOI: 10.1002/jor.25027.

Wang Y, Lin Y, Cheng C, Chen P, Zhang P, Wu H, Li K, Deng Y, Qian J, Zhang X, Yu B (2020b) NF-κB/TWIST1 mediates migration and phagocytosis of macrophages in the mice model of implant-associated *Staphylococcus aureus* osteomyelitis. Front Microbiol **11**: 1301. DOI: 10.3389/fmicb.2020.01301.

Mouse Genome Sequencing Consortium, Waterston RH, Lindblad-Toh K, Birney E, Rogers J, Abril JF, Agarwal P, Agarwala R, Ainscough R, Alexandersson M, An P, Antonarakis SE, Attwood J, Baertsch R, Bailey J, Barlow K, Beck S, Berry E, Birren B, Bloom T, Bork P, Botcherby M, Bray N, Brent MR, Brown DG, Brown SD, Bult C, Burton J, Butler J, Campbell RD, Carninci P, Cawley S, Chiaromonte F, Chinwalla T, Church DM, Clamp M, Clee C, Collins FS, Cook LL, Copley RR, Coulson A, Couronne O, Cuff J, Curwen V, Cutts T, Daly M, David R, Davies J, Delehaunty KD, Deri J, Dermitzakis ET, Dewey C, Dickens NJ, Diekhans M, Dodge S, Dubchak I, Dunn DM, Eddy SR, Elnitski L, Emes RD, Eswara P, Eyras E, Felsenfeld A, Fewell GA, Flicek P, Foley K, Frankel WN, Fulton LA, Fulton RS, Furey TS, Gage D, Gibbs RA, Glusman G, Gnerre S, Goldman N, Goodstadt L, Grafham D, Graves TA, Green ED, Gregory S, Guigó R, Guyer M, Hardison RC, Haussler D, Hayashizaki Y, Hillier LW, Hinrichs A, Hlavina W, Holzer T, Hsu F, Hua A, Hubbard T, Hunt A, Jackson I, Jaffe DB, Johnson LS, Jones M, Jones TA, Joy A, Kamal M, Karlsson EK, Karolchik D, Kasprzyk A, Kawai J, Keibler E, Kells C, Kent WJ, Kirby A, Kolbe DL, Korf I, Kucherlapati RS, Kulbokas EJ, Kulp D, Landers T, Leger JP, Leonard S, Letunic I, Levine R, Li J, Li M, Lloyd C, Lucas S, Ma B, Maglott DR, Mardis ER, Matthews L, Mauceli E, Mayer JH, McCarthy M, McCombie WR, McLaren S, McLay K, McPherson JD, Meldrim J, Meredith B, Mesirov JP, Miller W, Miner TL, Mongin E, Montgomery KT, Morgan M, Mott R, Mullikin JC, Muzny DM, Nash WE, Nelson JO, Nhan MN, Nicol R, Ning Z, Nusbaum C, O'Connor MJ, Okazaki Y, Oliver K, Overton-Larty E, Pachter L, Parra G, Pepin KH, Peterson J, Pevzner P, Plumb R, Pohl CS, Poliakov A, Ponce TC, Ponting CP, Potter S, Quail M, Reymond A, Roe BA, Roskin KM, Rubin EM, Rust AG, Santos R, Sapojnikov V, Schultz B, Schultz J, Schwartz MS, Schwartz S, Scott C, Seaman S, Searle S, Sharpe T, Sheridan A, Shownkeen R, Sims S, Singer JB, Slater G, Smit A, Smith DR, Spencer B, Stabenau A, Stange-Thomann N, Sugnet C, Suyama M, Tesler G, Thompson J, Torrents D, Trevaskis E, Tromp J, Ucla C, Ureta-Vidal A, Vinson JP, Von Niederhausern AC, Wade CM, Wall M, Weber RJ, Weiss RB, Wendl MC, West AP, Wetterstrand K, Wheeler R, Whelan S, Wierzbowski J, Willey D, Williams S, Wilson RK, Winter E, Worley KC, Wyman D, Yang S, Yang SP, Zdobnov EM, Zody MC, Lander ES (2002) Initial sequencing and comparative analysis of the mouse genome. Nature **420**: 520-562.

Wells CM, Beenken KE, Smeltzer MS, Courtney HS, Jennings JA, Haggard WO (2018) Ciprofloxacin and rifampin dual antibiotic-loaded biopolymer chitosan sponge for bacterial inhibition. Mil Med **183**: 433-444.

Wilde AD, Snyder DJ, Putnam NE, Valentino MD, Hammer ND, Lonergan ZR, Hinger SA, Aysanoa

EE, Blanchard C, Dunman PM, Wasserman GA, Chen J, Shopsin B, Gilmore MS, Skaar EP, Cassat JE (2015) Bacterial hypoxic responses revealed as critical determinants of the host-pathogen outcome by TnSeq analysis of *Staphylococcus aureus* invasive infection. PLoS Pathog **11**: e1005341. DOI: 10.1371/journal.ppat.1005341.

Windolf CD, Lögters T, Scholz M, Windolf J, Flohé S (2014) Lysostaphin-coated titan-implants preventing localized osteitis by *Staphylococcus aureus* in a mouse model. PLoS One **9**: e115940. DOI: 10.1371/journal.pone.0115940.

Windolf CD, Meng W, Lögters TT, MacKenzie CR, Windolf J, Flohé S (2013) Implant-associated localized osteitis in murine femur fracture by biofilm forming *Staphylococcus aureus*: a novel experimental model. J Orthop Res **31**: 2013-2020.

Wu T, Weng Z, Xu J, Wen G, Yu Y, Chai Y (2018) Baicalin alleviates osteomyelitis by regulating TLR2 in the murine model. Pathog Dis **76**. DOI: 10.1093/femspd/ftx123.

Xiao L, Li T, Ding M, Yang J, Rodríguez-Corrales J, LaConte SM, Nacey N, Weiss DB, Jin L, Dorn HC, Li X (2017) Detecting chronic post-traumatic osteomyelitis of mouse tibia *via* an IL-13R$\alpha$2 targeted metallofullerene magnetic resonance imaging probe. Bioconjug Chem **28**: 649-658.

Yamada KJ, Heim CE, Xi X, Attri KS, Wang D, Zhang W, Singh PK, Bronich TK, Kielian T (2020) Monocyte metabolic reprogramming promotes pro-inflammatory activity and *Staphylococcus aureus* biofilm clearance. PLoS Pathog **16**: e1008354. DOI: 10.1371/journal.ppat.1008354.

Yang D, Wijenayaka AR, Solomon LB, Pederson SM, Findlay DM, Kidd SP, Atkins GJ (2018) Novel insights into *Staphylococcus aureus* deep bone infections: the involvement of osteocytes. mBio **9**: e00415-00418. DOI: 10.1128/mBio.00415-18.

Yokogawa N, Ishikawa M, Nishitani K, Beck CA, Tsuchiya H, Mesfin A, Kates SL, Daiss JL, Xie C, Schwarz EM (2018) Immunotherapy synergizes with debridement and antibiotic therapy in a murine 1-stage exchange model of MRSA implant-associated osteomyelitis: J Orthop Res **36**: 1590-1598.

Yoon KS, Fitzgerald RH, Sud S, Song Z, Wooley PH (1999) Experimental acute hematogenous osteomyelitis in mice. II. Influence of *Staphylococcus aureus* infection on T-cell immunity. J Orthop Res **17**: 382-391.

Yoshii T (2002a) Inhibitory effect of roxithromycin on the local levels of bone-resorbing cytokines in an experimental model of murine osteomyelitis. J Antimicrob Chemother **50**: 289-292.

Yoshii T, Magara S, Miyai D, Nishimura H, Kuroki E, Furudoi S, Komori T, Ohbayashi C (2002b) Local levels of interleukin-1beta, -4, -6, and tumor necrosis factor alpha in an experimental model of murine osteomyelitis due to *Staphylococcus aureus*. Cytokine **19**: 59-65.

Young SW, Roberts T, Johnson S, Dalton JP, Coleman B, Wiles S (2015) Regional intraosseous administration of prophylactic antibiotics is more effective than systemic administration in a mouse model of TKA. Clin Orthop Relat Res **473**: 3573-3584.

Zhang B, Braun BM, Skelly JD, Ayers DC, Song J (2019a) Significant suppression of *Staphylococcus aureus* colonization on intramedullary Ti6Al4V implants surface-grafted with vancomycin-bearing polymer brushes. ACS Appl Mater Interfaces **11**: 28641-28647.

Zhang B, Skelly JD, Braun BM, Ayers DC, Song J (2020) Surface-grafted zwitterionic polymers improve the efficacy of a single antibiotic injection in suppressing *Staphylococcus aureus* periprosthetic infections. ACS Appl Bio Mater **3**: 5896-5904.

Zhang H, Chen C, He J, Zhang J, Liu Z, Sun T (2019b) Anti-PD-1 antibody administration following hip fracture surgery reverses immune dysfunction and decreases susceptibility to infection. Mediators Inflamm **2019**: 8492090. DOI: 10.1155/2019/8492090.

Zhu C, Wang J, Cheng T, Li Q, Shen H, Qin H, Cheng M, Zhang X (2014) The potential role of increasing the release of mouse β- defensin-14 in the treatment of osteomyelitis in mice: a primary study. PLoS One **9**: e86874. DOI: 10.1371/journal.pone.0086874.

Zhu X, Zhang K, Lu K, Shi T, Shen S, Chen X, Dong J, Gong W, Bao Z, Shi Y, Ma Y, Teng H, Jiang Q (2019) Inhibition of pyroptosis attenuates *Staphylococcus aureus*-induced bone injury in traumatic osteomyelitis. Ann Transl Med **7**: 170. DOI: 10.21037/atm.2019.03.40.

Zimmerli W, Trampuz A (2011) Implant-associated infection. In Biofilm Infect.. Editors: Bjarnsholt T, Østrup Jensen P, Moser C, Høiby N. pp: 69-90. New York, NY. Springer New York. DOI: 10.1007/978-1-4419-6084-9_5.

## Web References

**1.** https://www.webofknowledge.com [15.03.2021]
**2.** https://pubmed.ncbi.nlm.nih.gov/ [15.03.2021]

## Discussion with Reviewer

**Reviewer**: There is apparently a wide range of mouse models available. Would the field benefit from standardisation and a reduction to relatively fewer models allowing greater consistency? What may be the pros and cons of this approach?

**Authors**: This is a very good point to discuss. Indeed, in each osteomyelitis section, the infection has been performed differently and by using a different mouse line, age and gender, different bacterial strain, infectious dose and volume or different evaluation methods. All these variables need to be taken into consideration when the studies are compared. Standardisation could be applied both for *in vitro* and *in vivo* assays and would increase the reproducibility of studies between laboratories. Moreover, the

standardisation of the model and the evaluation methods could be used as a preclinical step to follow to evaluate the efficacy of antimicrobial preventive or treatment strategies (Coenye *et al.*, 2018). However, since there simply is a vast number of relevant clinical parameters that vary from study to study, in many cases, models will need to be tailored to the specific clinical situation. Then, to assess comparability of the models and study outcomes, minimum information guidelines are advised.

**Editor's note**: The Scientific Editor responsible for this paper was Fintan Moriarty.